



UNIVERSIDADE FEDERAL DO RIO GRANDE DO SUL



Programa de Pós-Graduação em Recursos Hídricos e Saneamento Ambiental

Tese de Doutorado

**ESPAÇO DE VIABILIDADE: UMA FERRAMENTA PARA O DESENVOLVIMENTO
DE NOVAS TECNOLOGIAS DE ENERGIAS RENOVÁVEIS**

Jones Souza da Silva

Porto Alegre
2021

Jones Souza da Silva

**ESPAÇO DE VIABILIDADE: UMA FERRAMENTA PARA O DESENVOLVIMENTO
DE NOVAS TECNOLOGIAS DE ENERGIAS RENOVÁVEIS**

Tese apresentada ao Programa de Pós-Graduação em Recursos Hídricos e Saneamento Ambiental do Instituto de Pesquisas Hidráulicas da Universidade Federal do Rio Grande do Sul, como requisito parcial à obtenção do título de **Doutor em Recursos Hídricos e Saneamento Ambiental**.

Orientador: Prof. Dr. Alexandre Beluco

Porto Alegre
2021

Souza da Silva, Jones
ESPAÇO DE VIABILIDADE: UMA FERRAMENTA PARA O
DESENVOLVIMENTO DE NOVAS TECNOLOGIAS DE ENERGIAS
RENOVÁVEIS / Jones Souza da Silva. -- 2021.
128 f.
Orientador: Alexandre Beluco.

Tese (Doutorado) -- Universidade Federal do Rio
Grande do Sul, Instituto de Pesquisas Hidráulicas,
Programa de Pós-Graduação em Recursos Hídricos e
Saneamento Ambiental, Porto Alegre, BR-RS, 2021.

1. Simulação computacional. 2. HOMER software. 3.
Sistemas híbridos de energia. 4. Geração e
armazenamento de energia. 5. Espaço de viabilidade. I.
Beluco, Alexandre, orient. II. Título.

Jones Souza da Silva

**ESPAÇO DE VIABILIDADE: UMA FERRAMENTA PARA O DESENVOLVIMENTO
DE NOVAS TECNOLOGIAS DE ENERGIAS RENOVÁVEIS**

Tese apresentada ao Programa de Pós-Graduação em Recursos Hídricos e Saneamento Ambiental do Instituto de Pesquisas Hidráulicas da Universidade Federal do Rio Grande do Sul, como requisito parcial à obtenção do título de **Doutor em Recursos Hídricos e Saneamento Ambiental**.

Aprovado em: Porto Alegre, 30 de dezembro de 2021.

Prof. Dr. Alexandre Beluco – IPH/UFRGS
Orientador

Prof. Dr. Alfonso Risso – IPH/UFRGS
Examinador

Profa. Dra. Andrea Fischer – IFSUL – Pelotas
Examinador

Prof. Dr. Elton Gimenez Rossini – UERGS
Examinador

Prof. Dr. José de Souza – Fundação Liberato
Examinador

Dedico esta pesquisa
aos meus pais.

AGRADECIMENTOS

Gostaria de agradecer aos amigos, que estiveram ao meu lado em todos os momentos, compartilhando sentimentos sinceros, verdadeiros, e me dando força para prosseguir. A ajuda de vocês foi essencial!

Um agradecimento muito especial aos queridos alunos, professores e ao povo de Cabo Verde, África, pela acolhida humana que tive durante o período de Doutorado Sanduíche, pela energia incrível, pelo aprendizado, pelas surpresas e pelas emoções grandiosas que deram um novo sentido ao meu Doutorado. Vivi momentos intensos e incríveis, que não podem ser expressos em palavras. Aos alunos e professores do curso de Agronomia Sócio-Ambiental da Escola de Ciências Agrárias e Ambientais – ECAA da Universidade de Cabo Verde – UniCV, em especial aos professores Vladmir e Arlindo, minha eterna gratidão!

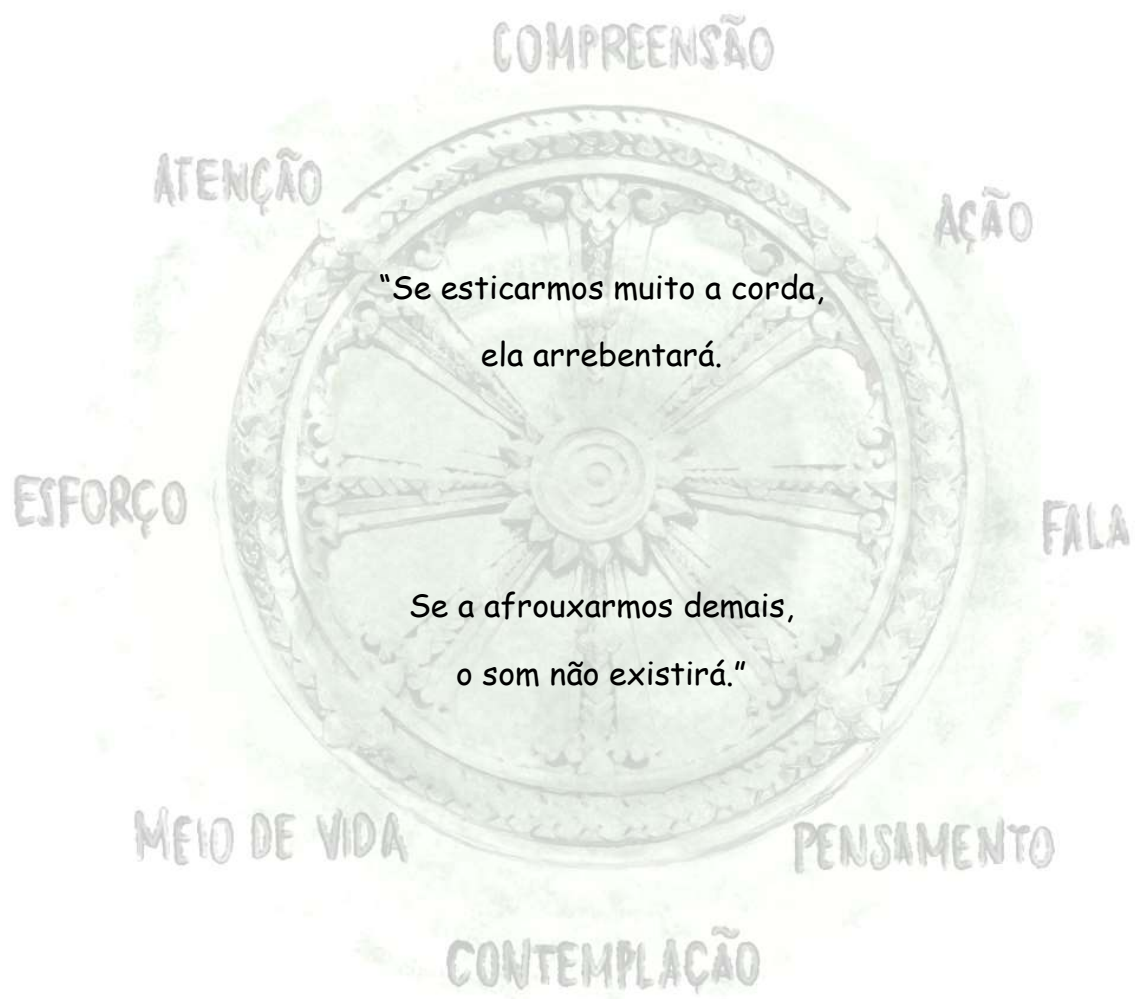
Ao professor José Barbosa, da Faculdade de Agronomia, e ao professor Fabio Beck, do Programa de Pós-Graduação em Desenvolvimento Rural (PGDR), muito obrigado pela confiança no meu trabalho junto à ECAA-UniCV, por toda a orientação cuidadosamente recebida, e pela oportunidade de ministrar disciplinas em Cabo Verde. Eu adorei a experiência!

Agradeço aos professores Masato, Nilza e Claudia pelo apoio, pelo aprendizado, pela orientação e por acreditarem em mim. A ajuda que recebi de vocês foi fundamental para a finalização desta etapa.

Agradeço ao meu orientador, Beluco, pela paciência, pela perseverança, por me receber novamente na orientação do Doutorado, e pelo grande auxílio na realização de um trabalho sintético, mas não menos importante. Sou também muito grato pela orientação e pelas nossas conversas, que aconteceram nos cafés Baden e Mattina na Jerônimo de Ornelas. Muito obrigado por me ajudar a finalizar este ciclo!

Agradeço a minha querida mãe, a dona Nina, pelas orações, e por toda a ajuda, principalmente na fase final do Doutorado. Sua força e seu amor incondicional foram as maiores motivações que eu poderia receber. Muito obrigado, Deus, por ter me presenteado com uma mãe maravilhosa, um ser de Luz!

E, a todos que, de certa forma, contribuíram para o meu crescimento acadêmico, profissional, moral e espiritual, o meu muito obrigado!



सिद्धार्थ गौतम

Fonte da ilustração: Índio San (2022).

RESUMO

O objetivo desta Tese é apresentar um espaço de viabilidade como uma meta a ser alcançada por pesquisadores e gestores durante o desenvolvimento de uma nova tecnologia de geração ou de armazenamento de energia. Para tanto, utilizou-se o programa HOMER para as simulações, que é um modelo projetado para simular sistemas de energia de pequeno porte, mas que permite, também, a simulação de modelos mais robustos. Primeiramente, é demonstrado um novo estudo de simulação de um sistema híbrido de geração de energia para o litoral Norte do Rio Grande do Sul, com novos custos da energia da rede de distribuição, apresentando o espaço de viabilidade para uma tecnologia genérica de geração de energia de ondas do mar, que ainda se encontra em processo de consolidação. Após, é detalhado o método utilizado para simulação de sistemas híbridos de energia na busca pelo espaço de viabilidade, que compreende um domínio composto por conjuntos de valores de parâmetros chaves, os quais devem ser definidos durante o desenvolvimento de qualquer tecnologia de energias renováveis. Finalmente, é apresentada uma nova aplicação do método proposto, em um novo estudo de sistema híbrido de geração e armazenamento de energia para a barragem de Laranjeiras, localizada em Canela/RS, e com espaço de viabilidade focado para uma tecnologia de armazenamento de energia sob a forma de ar comprimido. Os resultados indicaram que, para as condições consideradas nas simulações, usinas de ondas serão viáveis para a energia da rede variando entre US\$ 0,05/kWh e US\$ 0,15/kWh, se puderem ser implementadas com custos entre US\$ 616,01/kW e US\$ 2.865,37/kW, respectivamente para eficiências entre 20% e 40%. Esses valores são extremamente baixos, comparáveis aos valores para alternativas já consolidadas, como energia hidrelétrica e eólica. Já para o sistema que inclui a usina de armazenamento com ar comprimido, a solução considerada ótima operou com um custo de energia de US\$ 0,021/kWh e um custo de implementação de US\$ 3.023.688,00. Portanto, essa forma de armazenamento permitiu reduzir o custo presente líquido total e o custo da energia gerada pelo sistema.

Palavras-chave: simulação computacional; HOMER *software*; energia; geração; armazenamento; sistemas híbridos; ondas do mar; ar comprimido; complementaridade; espaço de viabilidade.

ABSTRACT

The aim of this thesis is to present a feasibility space as a goal to be achieved by researchers and managers during the development of a new energy generation or storage technology. For that, HOMER program was used for the simulations, which is a model designed to create and simulate small energy systems, but which also allows the simulation of more robust models. First, a new simulation study of a hybrid power generation system for the North coast of Rio Grande do Sul is demonstrated, with new energy costs from the distribution network, presenting the feasibility space for a generic sea wave power generation technology, which is still in the process of consolidation. Afterwards, the method used to simulate hybrid energy systems in the search for the feasibility space is detailed, which comprises a domain composed of sets of key parameter values, which must be defined during the development of any renewable energy technology. Finally, a new application of the proposed method is presented, in a new study of a hybrid energy generation and storage system for the Laranjeiras dam, located in Canela/RS, and with a feasibility space focused on an energy storage technology in the form of compressed air. The results indicated that, for the conditions considered in the simulations, wave plants will be viable for grid energy ranging from US\$ 0.05/kWh to US\$ 0.15/kWh, if they can be implemented with costs between US\$ 616.01/kW and US\$ 2,865.37/kW, respectively, for efficiencies between 20% and 40%. These values are extremely low, comparable to values for already established alternatives, such as hydroelectric and wind power. For the system that includes the compressed air storage plant, the solution considered optimal operated with an energy cost of US\$ 0.021/kWh and an implementation cost of US\$ 3,023,688.00. Therefore, this form of storage made it possible to reduce the total net present cost and the cost of energy generated by the system.

Keywords: computer simulation; HOMER software; energy; generation; storage; hybrid systems; sea waves; compressed air; complementarity; feasibility space.

SUMÁRIO

1. Introdução.....	14
2. Justificativa, hipótese e objetivos	18
2.1. Justificativa.....	18
2.2. Hipótese	19
2.3. Objetivos	19
2.3.1. Objetivo principal.....	19
2.3.2. Objetivos específicos	19
3. Organização da Tese	20
4. Metodologia.....	21
4.1. Áreas de estudo	21
4.1.1. Litoral Norte do Rio Grande do Sul	21
4.1.2. Barragem de Laranjeiras.....	24
4.2. O programa HOMER.....	30
4.2.1. A utilização do programa	31
4.2.2. O funcionamento do programa	31
4.2.3. Principais funções do modelo	32
4.3. Armazenamento de energia com ar comprimido.....	33
REFERÊNCIAS.....	47
5. Artigo 1	51
6. Artigo 2	73
7. Artigo 3	83
8. Conclusão geral	107
9. Recomendações.....	109
ANEXO A – HOMER.....	110
ANEXO B – CEEE	128

LISTA DE FIGURAS

Figura 1.1: Percentuais da oferta de energia por fonte no mundo em 2017.	15
Figura 1.2: Oferta interna de energia elétrica por fonte no Brasil em 2019.	16
Figura 4.1: Localização geográfica dos municípios do Litoral Norte do RS.	22
Figura 4.2: Localização geográfica da Barragem de Laranjeiras, da UHE Canastra, da Barragem de Canastra e da PCH Bugres, e delimitação da bacia hidrográfica da Barragem de Laranjeiras.	24
Figura 4.3: Perfil do Sistema Salto.	26
Figura 4.4: Anteprojeto com o esquema da Usina Transitória.	29
Figura 4.5: Relação conceitual entre simulação, otimização e análise de sensibilidade.	32
Figura 4.6: Vista aérea da usina de Huntorf, Alemanha.	33
Figura 4.7: Usina de Mcintosh, Alabama, Estados Unidos.	33
Figura 4.8: Esquema de uma planta CAES.	34
Figura 4.9: Esquema de produção e armazenamento de ar comprimido.	39
Figura 4.10: Dispositivos existentes no reservatório.	39
Figura 4.11: Esquema de funcionamento de uma turbina a gás padrão.	40
Figura 4.12: Esquema de funcionamento de um sistema CAES padrão.	40
Figura 4.13: Princípio de funcionamento de uma turbina a gás.	41
Figura 4.14: Visão geral do sistema D-CAES de 2 ^a geração.	42
Figura 4.15: Visão geral do sistema AA-CAES.	43
Figura 4.16: Visão geral do sistema I-CAES.	44
Figura 4.17: Estrutura flexível.	45
Figura 4.18: Esfera de concreto.	45
Figura 4.19: Armazenamento de energia com ar comprimido subaquático.	46

Artigos

Figure 5.1: Map showing the location of the municipalities on the coast of southern Brazil where demand for electricity was considered as a goal to be achieved in this study.	57
Figure 5.2: Map showing the location suggested for the ocean wave power plant in southern Brazil.	58
Figure 5.3: Hybrid system simulated with HOMER to meet the demand of municipalities shown in Figure 5.1, with contribution obtained from ocean wave energy.	60

Figure 5.4: Demand for electricity in the municipalities shown in Figure 5.1. Above, average demand over the months of the year. Below, instant demand over the days of the year	60
Figure 5.5: Wind resource available to wind farm in the system of Figure 5.3. Above, average wind speed over the months; below, instant wind speed over the days of the year.	61
Figure 5.6: Solar resource available to PV modules in the system of Figure 5.3. Above, average incident radiation on a horizontal surface over the months; below, instant radiation on a horizontal surface over the days of the year.....	61
Figure 5.7: Wave energy resource available to the power plant in the system of Figure 5.3. Above, average power available per meter of wave front. In the middle, average resource over the months and, below, instant resource over the days of the year, adapted for use by HOMER.	62
Figure 5.8: Optimization space for ocean wave power plant efficiency as a function of initial capital cost, corresponding to average wind speed of 7,62 m/s, wave resource equal to 12 kW/m and energy from the grid equal to USD\$ 0.10/kWh.	65
Figure 5.9: Cost of energy for ocean wave power plant efficiency as a function of initial capital cost, corresponding to average wind speed of 7,62 m/s, wave resource equal to 12 kW/m and energy from the grid equal to USD\$ 0.10/kWh.	66
Figure 5.10: Optimization space for power per unit length as a function of initial capital cost, corresponding to average wind speed of 7,62 m/s, ocean wave power plant efficiency equal to 30% and energy from the grid equal to USD\$ 0.10/kWh....	66
Figure 5.11: Upper limit of feasibility for the system of Figure 5.3, considering the initial capital cost of the hybrid system as a function of grid power price and ocean wave power plant efficiency, with wind speed equal to 7.62 m/s.....	67
Figure 5.12: Optimization space for wind speed against initial capital cost, corresponding to wave resource equal to 12 kW/m, ocean wave power plant efficiency equal to 30% and energy from the grid equal to USD\$ 0.10/kWh.	69
Figure 6.1: Flowchart showing the steps of the method.	76
Figure 6.2: Upper limit of feasibility for the system of Ref. [1], considering the initial capital cost of the hybrid system as a function of grid power price and efficiency of the ocean wave power plant, with average wind speed equal to 7.62 m/s.	79
Figure 7.1: a) Lateral view of the spillway, on the left; b) water surface near the dam, on the right.	87
Figure 7.2: Image of the Laranjeiras Dam and comparison of the dimensions of the PV panels placed on floating structures with the region near the dam.	87
Figure 7.3: Flow discharged by the Canastra Hydro Power Plant. Above, monthly minimum, average and maximum stream flow; below, the hourly distribution of stream flow throughout the year.	88
Figure 7.4: Solar radiation incident on a horizontal plane, obtained with HOMER, for the location of the Laranjeiras Dam Power Plant. Above, monthly minimum, average and maximum solar radiation; below, the hourly distribution of solar radiation throughout the year.	89

Figure 7.5: Schematic diagram of the hydro PV hybrid system proposed by Vasco <i>et al.</i> (2019b)	90
Figure 7.6: Areas and volumes as a function of height for the Laranjeiras dam.....	91
Figure 7.7: Configuration details of the rechargeable battery model, to simulate water reservoir.	91
Figure 7.8: Schematic diagram of the hydro PV hybrid system with hybrid storage in water reservoir and compressed air studied in this paper.	94
Figure 7.9: Efficiency as a function of the percentage of power supplied by the generator, simulating a compressed air turbine.....	95
Figure 7.10: Optimization space for the system of Figure 7.8.	98
Figure 7.11: Optimization results obtained by HOMER Legacy for the system of Figure 7.8, for grid sale capacity equal to 4400 kW (above) and 0 kW (below).....	99
Figure 7.12: Optimization results obtained by HOMER Legacy for the system of Figure 7.8, for grid sale capacity equal to 4400 kW (above) and 0 kW (below), with the non-mandatory use of the Laranjeiras reservoir as an energy store.	99
Figure 7.13: Upper limit of feasibility and feasibility space for the system of Figure 7.8, considering the initial capital cost of the hybrid system as a function of PV Capital Cost Multiplier and Hydro Capital Cost.....	100
Figure 7.14: Upper limit of feasibility and feasibility space for the system of Figure 7.8, considering the Total NPC of the hybrid system as a function of PV Capital Cost Multiplier and Hydro Capital Cost.	101

LISTA DE TABELAS

Tabela 1.1: Empreendimentos em operação no RS.....	17
Tabela 4.1: População permanente e média mensal da população flutuante estimada, por municípios/praias investigados, do Litoral Norte – fevereiro/2018.....	23
Tabela 4.2: Tipos de compressores.	37

Artigos

Table 5.1: Results delimiting the feasibility space for ocean wave power plants in southern Brazil.	68
Table 6.1: Results delimiting the feasibility space for ocean wave power plants in southern Brazil.	78
Table 7.1: Optimization variables for the simulations performed with HOMER Legacy.	96
Table 7.2: Sensitivity variables for the simulations performed with HOMER Legacy.	97
Table 7.3: Results for the construction of the feasibility space of Figure 7.13.....	100
Table 7.4: Results for the construction of the feasibility space of Figure 7.14.....	101

LISTA DE SIGLAS

AA-CAES – Advanced Adiabatic Compressed Air Energy Storage

ANEEL – Agência Nacional de Energia Elétrica

BEN – Balanço Energético Nacional

CEEE – Companhia Estadual de Geração e Transmissão de Energia Elétrica

CGH – Central Geradora Hidrelétrica

D-CAES – Diabatic Compressed Air Energy Storage

DNOS – Departamento Nacional de Obras de Saneamento

EOL – Central Geradora Eólica

FEE – Fundação de Economia e Estatística

IBGE – Instituto Brasileiro de Geografia e Estatística

I-CAES – Isothermal Compressed Air Energy Storage

NREL – U.S. National Renewable Energy Laboratory

PCH – Pequena Central Hidrelétrica

SIN – Sistema Interligado Nacional

SS-CAES – Small Scale Compressed Air Energy Storage

Tep – toneladas equivalentes de petróleo

UFV – Central Geradora Fotovoltaica

UHE – Usina Hidrelétrica

UTE – Central Geradora Termelétrica

1. Introdução

Um dos tópicos de maior importância na atualidade é a questão energética, pois a qualidade de vida de uma sociedade está intimamente ligada ao consumo de energia. O crescimento da demanda energética mundial, em virtude também da melhoria dos padrões de vida nos países em desenvolvimento, é motivo de preocupação com aspectos essenciais ligados à política e ao planejamento energético de todas as economias emergentes. Dentre esses fatores, podem ser citados a segurança no suprimento de energia, necessária para o desenvolvimento social e econômico de um país, e os custos ambientais para atender a esse aumento no consumo de energia (GOLDEMBERG; VILLANUEVA, 2003).

Essa crescente demanda de energia elétrica no mundo, aliada às questões ambientais, despertou a humanidade quanto à busca por fontes de produção de energia que causem um menor impacto ambiental. Diversos estudos estão sendo desenvolvidos sobre as chamadas energias renováveis no intuito de desenvolvimento de tecnologias mais sustentáveis.

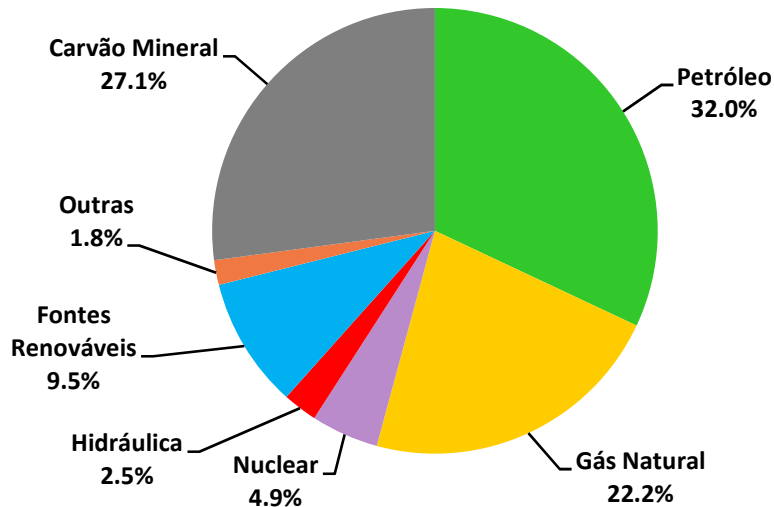
Energia renovável é a energia obtida através de fluxos contínuos e inesgotáveis de energia que ocorrem no meio ambiente, e energia não renovável é a energia obtida de armazenamentos finitos que existem no meio ambiente e que é liberada através da atuação humana. As energias solar, eólica, hídrica e a biomassa natural são exemplos de fontes naturalmente renováveis. Já o petróleo, o carvão mineral, o gás natural e o xisto betuminoso são exemplos de fontes não renováveis (TWIDELL e WEIR, 2006).

A utilização das energias renováveis torna-se ainda mais atraente do ponto de vista da complementariedade. As disponibilidades energéticas de uma ou mais fontes podem se complementar ao longo de uma região – complementariedade no espaço, ou as disponibilidades podem apresentar períodos em que se complementam ao longo do tempo em uma mesma região – complementariedade no tempo. A palavra complementariedade (ou complementaridade) pode ser interpretada, portanto, como a capacidade para servir de complemento (BELUCO et al., 2003).

Em determinadas regiões, por exemplo, períodos de seca podem diminuir e até mesmo comprometer a energia gerada por hidrelétricas. Porém, nessa mesma região, pode haver uma abundância de ventos e radiação solar. Assim, a utilização das energias eólica e solar pode suprir parte dessa diminuição da oferta energética. Esses sistemas formados por mais de uma fonte de energia são chamados de sistemas híbridos de energia, e o seu estudo é extremamente importante devido ao fato de que a falta de uma fonte pode ser suprida pela abundância de outra.

Segundo o Balanço Energético Nacional (BEN) de 2020, a oferta mundial de energia por fonte chegou a um total de 13.972×10^6 toneladas equivalentes de petróleo (tep) em 2017. Na Figura 1.1 é possível verificar os percentuais dessa oferta mundial. Apenas 12% da oferta de energia mundial (considerando-se, também, a energia hidráulica) é constituída por fontes renováveis, o que ainda é um percentual muito pequeno.

Figura 1.1: Percentuais da oferta de energia por fonte no mundo em 2017.

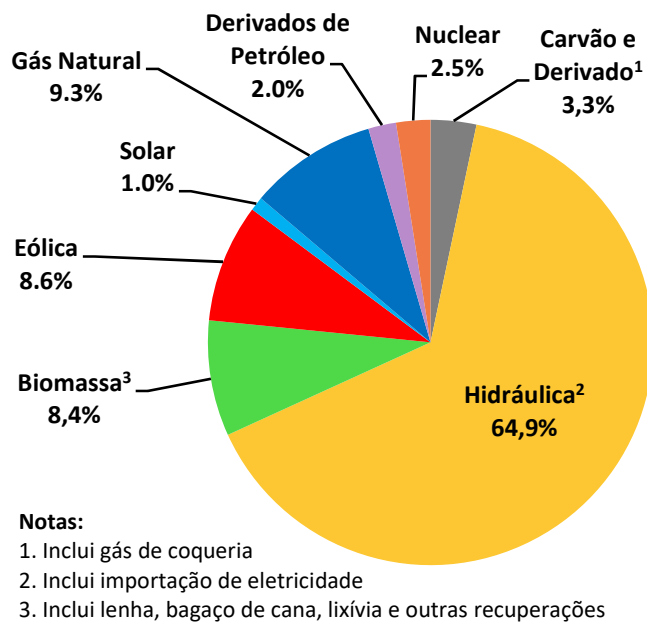


Fonte: BEN (2020).

O Brasil é conhecido mundialmente por possuir uma matriz de geração elétrica de origem predominantemente renovável, com destaque para a fonte hídrica, que corresponde a 64,9% da oferta interna do país. Ao total, as fontes renováveis representam aproximadamente 83% da oferta interna de energia no Brasil (Figura 1.2). A esse percentual, incluem-se também as importações, que essencialmente são de origem renovável. A geração de energia elétrica atingiu 626,3 TWh em 2019,

e as importações líquidas corresponderam a 25 TWh, totalizando uma oferta interna de energia elétrica no país de 651,3 TWh (BEN, 2020).

Figura 1.2: Oferta interna de energia elétrica por fonte no Brasil em 2019.



Fonte: BEN (2020).

O Rio Grande do Sul (RS) também possui uma matriz energética com predomínio de fontes renováveis. Conforme dados da Agência Nacional de Energia Elétrica (ANEEL) de 2021, 57,9% da capacidade instalada no estado correspondem à energia hidráulica, 19,16% correspondem à energia eólica, 0,05% à energia solar, e 22,89% à termeletricidade (usinas termelétricas movidas a combustível fóssil ou à biomassa). O estado possui um total de 357 empreendimentos em operação (Tabela 1.1), com uma potência outorgada total de 9.584.668,04 kW. Está prevista para os próximos anos uma adição de 1.548.784,95 kW na capacidade instalada do Estado, proveniente de seis empreendimentos atualmente em construção, e mais dezesseis que ainda não iniciaram sua construção (ANEEL, 2021).

Verifica-se que houve um grande avanço da diversificação das fontes no RS, com crescente presença de fontes alternativas de energia. Essa diversificação iniciou-se com a ampliação da utilização de gás natural e biomassa, e também, mais recentemente, com a expansão da energia eólica e com a instalação de novos empreendimentos de energia solar (Atlas Socioeconômico do RS, 2021).

Tabela 1.1: Empreendimentos em operação no RS.

Empreendimentos em Operação				
Fonte	Quantidade	Potência Outorgada (kW)	Potência Fiscalizada (kW)	% (P Fiscalizada)
CGH	62	60.091,95	60.091,95	0,63
PCH	53	674.097,30	672.857,30	7,02
UHE	17	4.815.020,00	4.815.325,00	50,25
EOL	81	1.835.891,98	1.835.891,98	19,16
UFV	12	4.618,61	4.618,61	0,05
UTE	132	2.194.948,20	2.193.520,20	22,89
Total	357	9.584.668,04	9.582.305,04	100

Legenda: CGH – Central Geradora Hidrelétrica; PCH – Pequena Central Hidrelétrica; UHE – Usina Hidrelétrica; EOL – Central Geradora Eólica; UFV – Central Geradora Fotovoltaica; UTE – Central Geradora Termelétrica.

Fonte: ANEEL (2021).

Uma integração de microusisas hidrelétricas com outras fontes renováveis torna o sistema híbrido mais eficiente e barato, pois elimina alguns dos problemas inerentes às energias renováveis quando utilizadas individualmente. Contudo, a combinação ótima dessas tecnologias é um problema complexo. Conforme a literatura especializada, existe ainda uma lacuna na pesquisa científica sobre sistemas híbridos formados por usinas hidrelétricas e outras usinas que utilizam fontes de energias renováveis (MASKEY; NESTMAN, 2000).

Além da lacuna referente ao estudo de sistemas híbridos de geração de energia renovável, o estudo desses sistemas (funcionando em conjunto com sistemas híbridos de armazenamento de energia) é muito raro na literatura especializada.

Assim, a contribuição desta Tese de doutorado será apontar alternativas de sistemas híbridos de geração e de armazenamento de energia, apresentando um espaço de viabilidade como um objetivo a ser alcançado durante a fase de desenvolvimento de uma nova tecnologia de geração ou de armazenamento de energia renovável.

2. Justificativa, hipótese e objetivos

2.1. Justificativa

Devido às questões ambientais, como a poluição gerada pelo uso do petróleo nas mais diversas aplicações, e também ao constante crescimento da população e à crescente demanda por energia, o uso de fontes renováveis se tornou a melhor solução no planejamento energético por serem energias mais limpas. Entretanto, as tecnologias de energias renováveis estão associadas à intermitência ou imprevisibilidade dos recursos. Assim, para que esse problema seja solucionado, é importante desenvolver novos sistemas de armazenamento de energia que sejam capazes de operar em conjunto com sistemas formados por tecnologias de geração de energias renováveis.

Porém, para que novas tecnologias de energias renováveis se tornem atrativas para investidores, é importante a construção de uma ferramenta que esteja relacionada às questões de viabilidade técnica e econômica da nova tecnologia de energia renovável e que possa ser utilizada para tomada de decisão por empresas e engenheiros. Essa tecnologia pode ser um empreendimento tanto de geração quanto de armazenamento de energia renovável. A literatura especializada carece de estudos de viabilidade de sistemas de geração combinados com sistemas de armazenamento, e a lacuna ainda é maior quando a questão a ser respondida é a viabilidade de uma tecnologia, que pode ser nova, em desenvolvimento, como as usinas de geração de energia de ondas do mar, ou já em um estado mais maduro, mas cuja eficiência ainda precisa ser melhorada, como é o caso do armazenamento de energia com ar comprimido.

Durante o desenvolvimento de tecnologias de energias renováveis, os limites que devem ser satisfeitos para se atingir viabilidade são ferramentas importantes para pesquisadores e gestores. O espaço de viabilidade, que é um conjunto de valores-chave de parâmetros de viabilidade que devem ser satisfeitos por dispositivos em desenvolvimento, é o foco principal desta Tese.

2.2. Hipótese

É possível estabelecer janelas de viabilidade compostas por conjuntos de valores de parâmetros de viabilidade para a definição de um espaço de viabilidade, que pode ser utilizado como uma ferramenta de tomada de decisão por gestores e investidores de novas tecnologias de energias renováveis.

2.3. Objetivos

2.3.1. Objetivo principal

O principal objetivo desta Tese é apresentar um espaço de viabilidade como uma ferramenta para ajudar gestores e investidores na tomada de decisão quanto à viabilidade técnica e econômica de desenvolvimento de uma nova tecnologia de energia renovável.

2.3.2. Objetivos específicos

Os objetivos específicos desta Tese são:

- apresentar o espaço de viabilidade para um dispositivo de geração de energia das ondas do mar para o litoral Norte do RS conectado a um sistema híbrido de geração de energia;
- propor um método para simulação de configurações de sistemas híbridos baseados em energias renováveis, incluindo os conceitos de construção de limites/janelas de viabilidade, que são valores indicativos, principalmente para tecnologias novas, do alvo a ser atingido pelo investidor para que uma nova tecnologia possa se tornar viável;
- definir o espaço de viabilidade para um sistema híbrido de geração de energia conectado a um sistema híbrido de armazenamento de energia composto pelo reservatório de água da barragem de Laranjeiras, Canela/RS, e um dispositivo de armazenamento de energia com ar comprimido.

3. Organização da Tese

Esta Tese será organizada na forma de três artigos, a saber:

Artigo 1: teve origem a partir da dissertação de mestrado, e contempla um estudo de um sistema híbrido de geração de energias renováveis para o litoral Norte do RS, interligado à rede de distribuição, composto por uma usina hipotética de ondas do mar, painéis fotovoltaicos e baterias, e a reprodução dos parques eólicos de Osório, que atende uma carga que representa a demanda do litoral Norte. O trabalho apresenta o gráfico de espaço de viabilidade para uma usina de geração de energia de ondas do mar. O artigo foi publicado em 29 de agosto de 2018 no periódico *Current Alternative Energy*, e deu origem ao Artigo 2 desta Tese.

Artigo 2: demonstra uma evolução de conceitos do método utilizado na dissertação de mestrado, e propõe o estabelecimento de um espaço de viabilidade como uma meta a ser alcançada durante o desenvolvimento de uma nova tecnologia de energia de aproveitamento de fontes renováveis. Portanto, o artigo foi uma evolução da dissertação, cujo método será aplicado na Tese de doutorado. Esse artigo foi publicado em 12 de junho de 2020 no periódico *MethodsX*, que é um periódico relativamente recente, e que deverá ter medição de fator de impacto brevemente, como todos os periódicos da *Elsevier*.

Artigo 3: trata de simulações de um sistema híbrido hidrelétrico fotovoltaico de geração de energia renovável, conectado à rede de distribuição, localizado na barragem de Laranjeiras, Canela/RS, e interligado a um sistema híbrido de armazenamento de energia composto pelo reservatório da barragem e por uma usina hipotética de ar comprimido instalada ao pé da barragem. Neste artigo, será apresentado o espaço de viabilidade para todo o sistema de energia, que foi projetado para atender a uma carga constante de 40 MWh/dia. Para tanto, será realizada uma adaptação no programa HOMER, ou seja, serão utilizados os componentes de Hidrogênio para simular armazenamento de energia com ar comprimido, pois o modelo não possui a opção de simulação de armazenamento com ar comprimido. É prevista a submissão do artigo para o periódico *Computational Water, Energy, and Environmental Engineering*.

4. Metodologia

4.1. Áreas de estudo

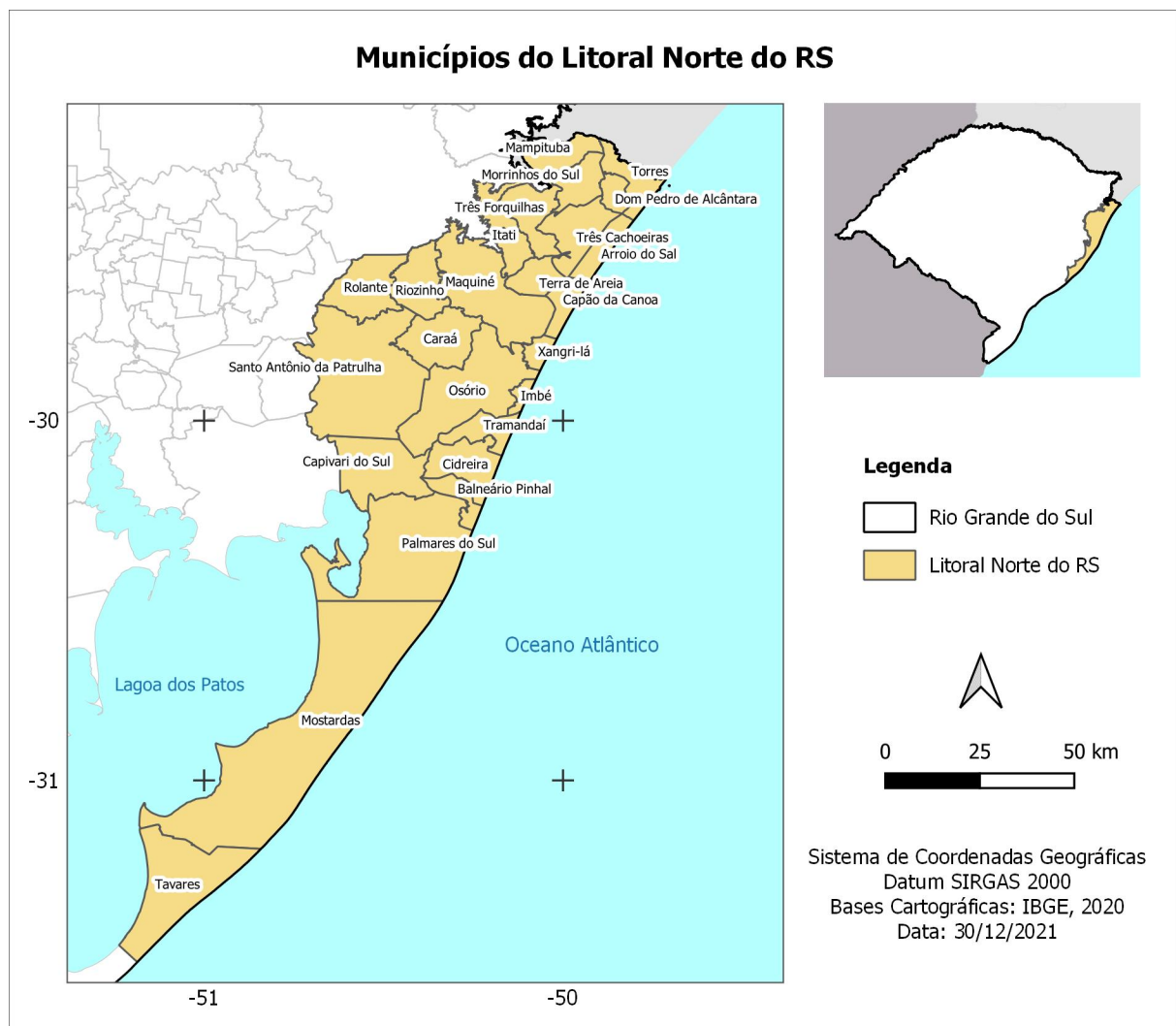
Esta Tese tem como foco duas áreas de estudo, a saber: Litoral Norte do Rio Grande do Sul e Barragem de Laranjeiras. A seguir, cada uma dessas áreas será detalhada.

4.1.1. Litoral Norte do Rio Grande do Sul

Essa área localiza-se na porção norte do litoral do RS, e será tratada nesta Tese apenas como Litoral Norte (Figura 4.1). A área em questão já foi estudada anteriormente por Beluco (2012) e também por Silva (2012). O primeiro autor apresentou três possíveis locais na Serra Geral para implantação de usinas reversíveis, que poderiam ser utilizadas para armazenar a energia excedente das usinas eólicas do litoral norte, bem como armazenar a energia proveniente de outras tecnologias que poderiam ser implantadas futuramente no litoral norte, como usinas de ondas. Já o segundo autor realizou um estudo de um sistema híbrido de energia conectado ao Sistema Interligado Nacional (SIN) com o objetivo de verificar a viabilidade de implantação de uma usina de ondas no litoral norte, que apresenta bom potencial para geração de energia de ondas do mar, conforme já apontado por Assis (2010).

O Litoral Norte possui uma população permanente estimada para 2021 de 432.843 habitantes segundo dados do Instituto Brasileiro de Geografia e Estatística (IBGE), o que representa, aproximadamente, 3,77% da população do RS (IBGE Cidades, 2021). Porém, durante os meses de verão, essa população tem um aumento muito expressivo devido aos veranistas e turistas provenientes, principalmente, de outras cidades do Estado, que caracterizam a população flutuante do litoral norte. Os municípios que integram o litoral norte são: Arroio do Sal, Balneário Pinhal, Capão da Canoa, Capivari do Sul, Caraá, Cidreira, Dom Pedro de Alcântara, Imbé, Itati, Mampituba, Maquiné, Morrinhos do Sul, Mostardas, Osório, Palmares do Sul, Riozinho, Rolante, Santo Antônio da Patrulha, Tavares, Terra de Areia, Torres, Tramandaí, Três Cachoeiras, Três Forquilhas e Xangri-lá.

Figura 4.1: Localização geográfica dos municípios do Litoral Norte do RS.



Um estudo da extinta Fundação de Economia e Estatística (FEE) do RS considerou como litoral norte apenas os oito municípios banhados pelo mar constantes da Tabela 4.1, além das praias de Quintão, Atlântida Sul e Santa Rita de Cássia pertencentes aos municípios de Palmares do Sul, Osório e Terra de Areia, respectivamente. O trabalho teve como objetivo realizar uma projeção da população do litoral norte para o mês de fevereiro de 2018, com o propósito de auxiliar os governos estadual e municipais quanto ao planejamento para o verão, como distribuição de recursos e deslocamento de policiais, e também o setor privado, pois, com uma estimativa da população, é possível prever a oferta de empregos no comércio, por exemplo. As estimativas de cada um dos municípios investigados incluem a população de todas as praias que estão contidas dentro da extensão da faixa de areia formada em cada município (FEE, 2021).

Tabela 4.1: População permanente e média mensal da população flutuante estimada, por municípios/praias investigados, do Litoral Norte – fevereiro/2018.

Município e/ou praia	População permanente	População flutuante*	População total*	Crescimento populacional (%) **
Capão da Canoa	51.721	58.541	110.262	113,2
Tramandaí	50.496	46.499	96.996	92,1
Torres	22.180	41.880	64.060	188,8
Imbé	39.870	23.768	63.638	59,6
Cidreira	14.712	27.766	42.478	188,7
Xangri-lá	14.547	26.671	41.218	183,3
Balneário Pinhal	12.735	23.269	36.004	182,7
Arroio do Sal	9.897	21.995	31.892	222,2
Quintão	3.559	18.339	21.899	515,2
Atlântida Sul	1.189	6.174	7.363	519,4
Santa Rita de Cássia	552	930	1.482	168,4
	221.460	295.832	517.292	133,6

* média mensal.

** pop. flutuante / pop. permanente

Fonte: FEE (2021).

A população flutuante foi calculada através de uma metodologia que utiliza o volume mensal de água medido por hidrômetros instalados e o número de domicílios de uso ocasional ou vagos, além da utilização dos Censos Demográficos. Como essas estimativas são para uma população média mensal, em dias de semana, esses números tendem a ser menores, e, nos finais de semana e feriados, tendem a ser mais elevados. Os dois balneários que apresentaram os maiores crescimentos médios da população em relação à população permanente foram Atlântida Sul, com um crescimento de 519,4%, e Quintão, cuja população teve um crescimento de 515,2% (FEE, 2021).

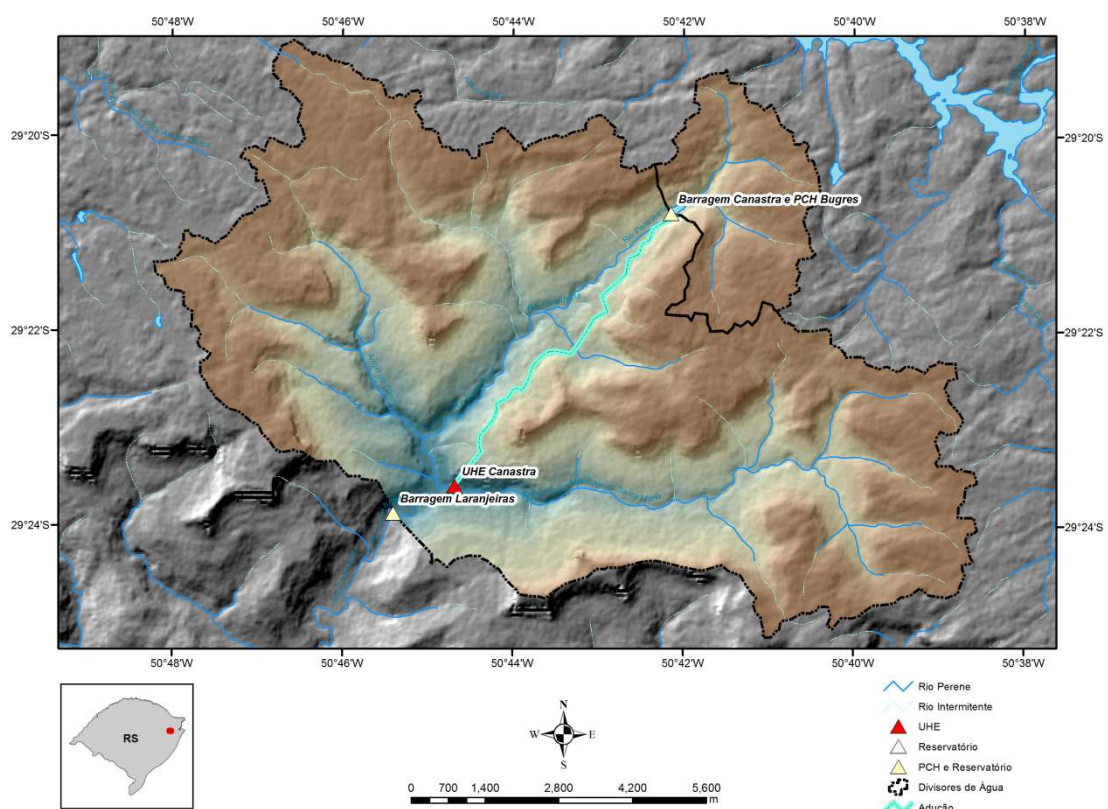
O primeiro artigo desta Tese envolve a área de estudo apresentada na Figura 4.1, composta por 25 municípios, e foi uma evolução da dissertação desenvolvida por Silva (2012). No artigo, a novidade apresentada é um espaço de viabilidade como um objetivo a ser alcançado para o desenvolvimento de tecnologias de geração de energia através das ondas do mar.

4.1.2. Barragem de Laranjeiras

A barragem de Laranjeiras localiza-se na cidade de Canela – RS, foi construída na década de 1960 pelo antigo Departamento Nacional de Obras de Saneamento (DNOS), e pertence à Companhia Estadual de Geração e Transmissão de Energia Elétrica (CEEE). A estrutura faz parte do Projeto da Central Hidrelétrica de Laranjeiras, que seria a terceira da série de usinas projetadas para o vale do rio Paranhana (o sistema que seria formado pelas três usinas foi chamado, na época, de Sistema Salto). A usina de Bugres, com potência instalada de 11,1 MW, entrou em operação em 1952, e a usina de Canastra, com potência de 42,5 MW, em 1956. Já a usina de Laranjeiras nunca foi construída.

Na Figura 4.2 é possível observar a localização geográfica da barragem de Laranjeiras, da bacia hidrográfica da barragem, e de algumas instalações que fazem parte de um sistema maior chamado de Sistema Salto.

Figura 4.2: Localização geográfica da Barragem de Laranjeiras, da UHE Canastra, da Barragem de Canastra e da PCH Bugres, e delimitação da bacia hidrográfica da Barragem de Laranjeiras.



Fonte: Laboratório de Água e Solo – IPH/UFRGS (2016).

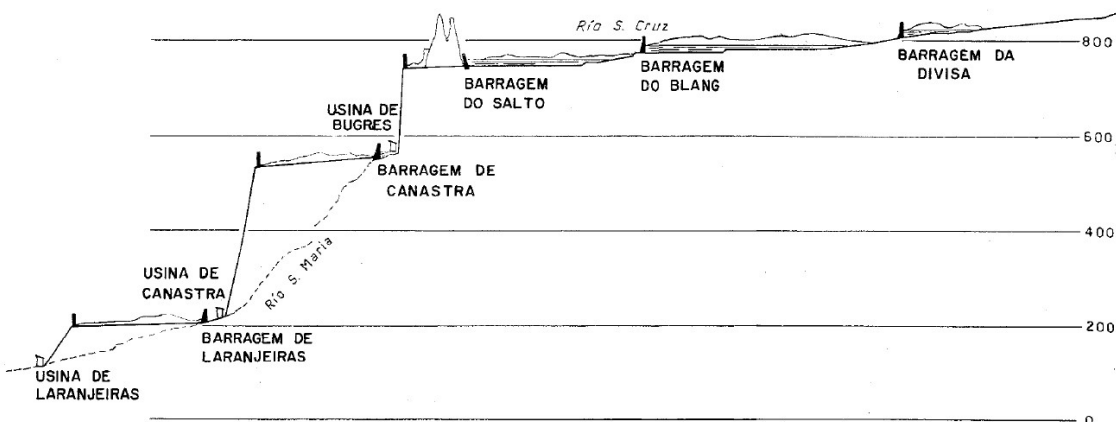
Uma das funções da barragem existente é a regularização das descargas provenientes da usina de Canastra. Assim, a barragem represa principalmente as descargas de Canastra, a qual é alimentada, principalmente, com águas provenientes do rio Santa Cruz, via transposição de bacias, e também represa as águas do rio Paranhana, que, na época de sua construção, se chamava rio Santa Maria.

Um perfil da barragem de Laranjeiras com sua altura, desde a fundação até o topo das ombreiras, pode ser observado no Anexo 2, que contém um projeto da CEEE de 1955 com os volumes acumulados e áreas inundadas em função de cotas para o reservatório da barragem.

Um perfil do Sistema Salto, constante em um dos anteprojetos de 1970 da CEEE, pode ser visto na Figura 4.3, o qual é composto pelas seguintes instalações:

- **Barragem da Divisa e Barragem do Blang:** seus reservatórios possuem apenas função de regularização da vazão do arroio Divisa e do rio Santa Cruz, respectivamente;
- **Barragem do Salto:** represa águas do rio Santa Cruz, e além de ter a função de regularização de vazão, fornece a vazão para a Usina de Bugres;
- **Usina de Bugres:** é alimentada pelas águas do reservatório do Salto através de transposição via túnel, galeria e conduto forçado, com queda de 180 m;
- **Barragem de Canastra:** o reservatório de Canastra regulariza a vazão do rio Paranhana e da vazão turbinada da Usina de Bugres, e fornece a vazão para a Usina de Canastra;
- **Usina de Canastra:** recebe a vazão da barragem de Canastra através de galeria e dois condutos forçados, com queda de 320 m;
- **Barragem de Laranjeiras:** possui função de regularização de vazão, principalmente pela vazão descarregada pela usina de Canastra;
- **Usina de Laranjeiras:** esta instalação nunca foi construída.

Figura 4.3: Perfil do Sistema Salto.



Fonte: CEEE, 1970.

Conforme projeto de 30 de novembro de 1955, fornecido pela CEEE, a barragem de Laranjeiras é do tipo gravidade, de concreto ciclópico, com fundação sobre rocha, e possui alinhamento reto. A sua altura máxima acima da fundação é de 28 m nos muros e de 26 m no vertedor, e o seu comprimento total, medido entre as extremidades das ombreiras, é de 226 m. As ombreiras esquerda e direita possuem 94 m e 32 m de comprimento, respectivamente, e ambas possuem largura de coroamento de 2m. A cota de coroamento das ombreiras, fixada em 212 m, garantiu uma boa margem de segurança com relação à descarga máxima de enchente. O vertedor, cuja crista coincide com a cota de 210 m, possui uma seção de 100 m de comprimento, flanqueado pelas ombreiras, que se estendem até as margens, e foi projetado de modo bastante extenso, visando diminuir a lâmina vertente da cheia máxima. O projeto do vertedor está baseado em uma descarga máxima de enchente de 200 m³/s, que corresponde à cota de represamento de 211 m na bacia de acumulação, e foi desenhado de forma a obter aderência perfeita ao perfil da lâmina vertente, evitando, assim, a formação de vácuo sob a lâmina para qualquer regime de descarga. O volume de acumulação total normal projetado do reservatório de Laranjeiras é de 1.180.000 m³, e o volume de acumulação útil diário é de 200.000 m³. A bacia hidrográfica da barragem de Laranjeiras possui aproximadamente 85 km² (CEEE, 1955).

Segundo reexame do projeto da Hidrelétrica de Laranjeiras, de agosto de 1970, elaborado pela empresa italiana ELC Electroconsult, a CEEE havia elaborado, em 1964, um projeto executivo das obras de adução do reservatório de Laranjeiras

até a casa de máquinas, onde seria instalada a usina de Laranjeiras. Essa primeira solução projetada para a Central Hidrelétrica de Laranjeiras seria construída a jusante da barragem, e corresponderia a uma instalação com potência máxima da ordem de 7,5 MW, com uma queda de cerca de 100 m, e adução com comprimento total de 5.900 m, formada essencialmente por um canal aberto de seção trapezoidal, revestido com concreto armado a meia encosta e com trechos de tubulações de concreto armado enterradas. Essa adução foi dimensionada para uma vazão de 10 m³/s (CEEE, 1970).

Além das informações do projeto de 1964, a CEEE repassou à empresa Electroconsult informações da vazão que seria descarregada no reservatório de Laranjeiras. A vazão média estimada descarregada da usina de Canastra no reservatório foi de 7 m³/s. Além disso, foi estimada uma contribuição adicional de 1 m³/s proveniente do arroio São Paulo. Assim, a vazão média total estimada e utilizada pela empresa italiana para o dimensionamento hidráulico das novas soluções para a usina de Laranjeiras foi de 8 m³/s. A empresa, então, realizou estudos para os casos de usinas de funcionamento em base e em ponta. A alternativa em base teve sua potência definida pela vazão regularizada disponível, e a alternativa para funcionamento em ponta teve a potência limitada pela capacidade disponível da linha de transmissão existente. Nas duas soluções, foi previsto uma adução de 5 a 6 km, um conduto forçado de aproximadamente 500 m, e uma queda estática de 100 m (CEEE, 1970).

Como a adução envolveu terrenos geologicamente pouco estáveis, formados por materiais de decomposição de basalto com fragmentos de rocha, com perceptível circulação de água de infiltração, a solução original da própria CEEE, composta por canal, foi descartada por motivo de insegurança hidrogeológica. Adotou-se, então, um esquema de adução em tubulação metálica para as instalações de base, e em túnel (galeria) tanto para as instalações de base e de ponta. Resumidamente, nesse reexame do projeto é possível encontrar soluções com diferentes configurações para a usina de Laranjeiras, conforme informações a seguir (CEEE, 1970):

- Usina de base com adução em tubulação metálica: vazão média de 8 m³/s, vazão máxima de 12 m³/s, queda estática de 100 m e potência instalada de 8 MW;

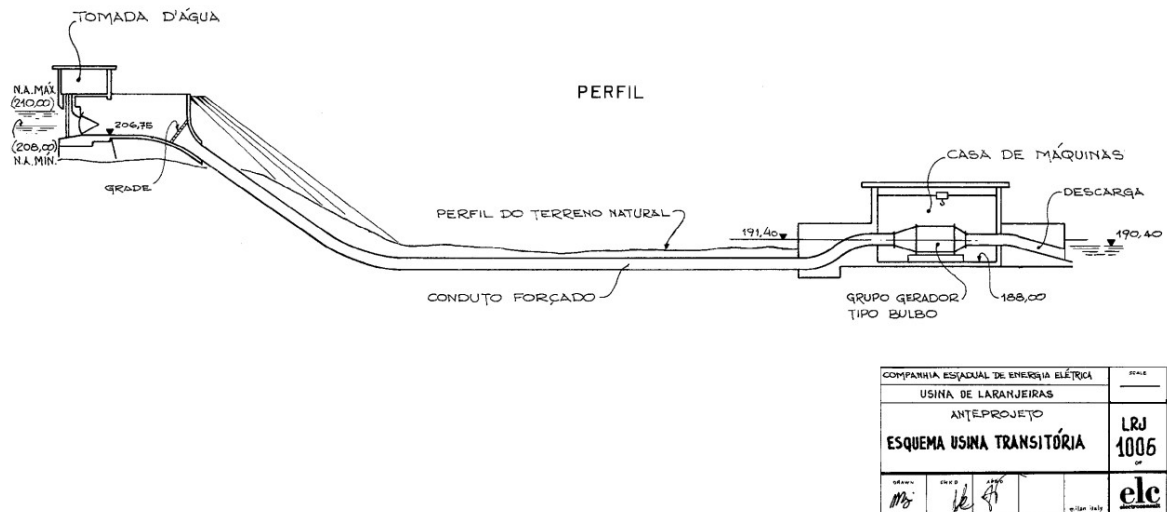
- Usina de base com adução em túnel: vazão média de 8 m³/s, vazão máxima de 12 m³/s, queda estática de 100 m e potência instalada de 8 MW;
- Usina de ponta: vazão média de 8 m³/s, vazão máxima de 38 m³/s, queda estática de 100 m e potência instalada de 25 MW;
- Usina transitória: pequeno grupo gerador com potência de 1.200 kW.

Na época em que foi realizado o reexame da usina de Laranjeiras, todas as soluções (de ponta e base) foram consideradas como alternativas antieconômicas, pois os custos de instalação e geração eram superiores até mesmo aos custos com usinas térmicas convencionais e a gás. Apenas a usina de caráter transitório foi considerada viável do ponto de vista técnico e econômico. Essa solução, em caráter transitório, seria instalada ao pé da barragem, e seria composta por um pequeno grupo gerador automático tipo bulbo, assíncrono, com potência aproximada de 1200 kW, e com capacidade garantida para gerar 8 GWh de energia. A turbina seria operada com carga constante, e a usina, do tipo automático, seria telecomandada da Usina de Canastra (CEEE, 1970).

Nesta Tese, realizar-se-á um estudo na área em questão a fim de se verificar a viabilidade de instalação no local de um sistema híbrido de geração de energias renováveis conectado a um sistema híbrido de armazenamento de energia. Esse estudo está detalhado no Artigo 3 desta Tese. Como ponto de partida e motivação para simulação de uma usina hidrelétrica hipotética a fio d'água, localizada ao pé da barragem de Laranjeiras, levou-se em consideração o esquema da Usina Transitória da Figura 4.4.

Dessa forma, pretende-se apresentar nesta Tese uma contribuição para que a energia potencial do reservatório da barragem possa ser aproveitada para geração de energia elétrica. Será proposto, então, um sistema híbrido de geração de energia conectado a um sistema híbrido de armazenamento de energia, que serão detalhados no artigo 3 desta pesquisa.

Figura 4.4: Anteprojeto com o esquema da Usina Transitória.



Fonte: CEEE, 1970.

Atualmente, a prática de esportes radicais e de aventura, como o *rafting*, é muito comum no reservatório e vertedor da barragem de Laranjeiras, ou seja, o local acabou se transformando em uma atração turística.

4.2. O programa HOMER

Desenvolvido pelo *U.S. National Renewable Energy Laboratory – NREL* (Laboratório Nacional de Energias Renováveis dos EUA), o *HOMER* é um modelo computacional utilizado para auxiliar no projeto de pequenas centrais de energia e para facilitar a comparação das tecnologias de geração de energia através de uma série de aplicações. O *HOMER* modela o comportamento físico de um sistema de energia e o seu custo de ciclo de vida, o qual comprehende o custo de instalação e operação do sistema ao longo de sua vida útil. O programa também permite ao usuário comparar diversas opções de projeto baseadas em suas características técnicas e econômicas, e também auxilia o projetista a entender e a quantificar os efeitos de incertezas ou de mudanças nos dados de entrada (LAMBERT *et al.*, 2006).

Um sistema de uma pequena central de energia é um sistema que gera energia, e possivelmente calor, para atender uma localidade próxima. Este sistema pode englobar qualquer combinação de tecnologia que gere e armazene energia, e pode ser um sistema interligado à rede de distribuição ou autônomo, isto é, separado de qualquer rede de transmissão elétrica. Apesar de o modelo ter sido projetado para pequenas centrais de energia, é possível simular também sistemas de médio e grande porte. O que vai determinar o tamanho máximo de cada componente do sistema que pode ser projetado na versão do *HOMER Legacy* são seus limites para cálculo, que só podem ser encontrados através de tentativa e erro, pois os fabricantes do modelo não informam a capacidade máxima de cada tecnologia que pode ser utilizada no programa.

Quando um sistema de energia é projetado, muitas decisões sobre a configuração do sistema devem ser tomadas, como a quantidade e o tamanho de cada componente que deve ser adotado, e os tipos de componentes que devem ser incluídos no projeto do sistema (painéis fotovoltaicos, turbinas eólicas, geradores, baterias etc.). O grande número de opções de tecnologia, e a variação tanto nos custos destas tecnologias, quanto na disponibilidade de recursos energéticos, tornam estas decisões bastante difíceis. Os algoritmos de análise de otimização e de sensibilidade do *HOMER* tornam mais fácil a avaliação das possíveis configurações do sistema, que podem ser muitas (SILVA; BELUCO, 2012).

4.2.1. A utilização do programa

Para usar o *HOMER*, é necessário alimentar o modelo com dados de entrada, os quais descrevem as opções de tecnologia, os custos de componentes e a disponibilidade de recursos energéticos. Essas entradas são utilizadas para simulação de diferentes configurações de sistema, ou combinações de componentes, e os resultados gerados podem ser visualizados através de uma lista de possíveis configurações, as quais são ordenadas pelo custo presente líquido. O programa também exibe os resultados de simulação em uma grande variedade de tabelas e gráficos, através dos quais é possível comparar e avaliar as configurações quanto aos seus aspectos econômicos e técnicos (SILVA; BELUCO, 2012).

As análises de sensibilidade do modelo podem ser utilizadas para se verificar o efeito que mudanças em fatores como disponibilidade de recursos e condições econômicas poderiam ter sobre o custo-benefício de diferentes configurações de sistema. Para realizar uma análise de sensibilidade, é preciso fornecer ao *software* valores de sensibilidade que descrevam uma série de disponibilidade de recursos e de custos de componentes. O modelo simula cada configuração de sistema com a série de valores dada. Os resultados de uma análise de sensibilidade podem ser usados para identificação dos fatores que possuem o maior impacto sobre o projeto e a operação de um sistema de energia.

4.2.2. O funcionamento do programa

O modelo simula a operação de um sistema efetuando cálculos do balanço de energia para cada uma das 8.760 horas do ano. Para cada hora, o programa compara a demanda elétrica e térmica com a energia que o sistema pode fornecer naquela hora, e calcula os fluxos de energia que entram e saem em cada componente do sistema. Para sistemas que incluem baterias, ou geradores movidos a combustível, o modelo também decide como operar os geradores em cada hora e se carrega ou descarrega as baterias (SILVA; BELUCO, 2012).

O programa realiza esses cálculos de balanço de energia para cada configuração de sistema desejado. Ele, então, determina se uma configuração é viável, ou seja, se ela pode atender a demanda elétrica nas condições que foram

especificadas pelo usuário, e estima o custo de instalação e operação do sistema durante a vida útil do projeto. Os cálculos de custo do sistema contabilizam custo de capital, custo de reposição, custos de operação e manutenção, custos com combustível, entre outros.

4.2.3. Principais funções do modelo

O HOMER executa as seguintes três principais funções:

- **simulação:** modelagem da performance de uma configuração de um sistema de uma micro central de energia em particular a cada hora do ano para determinar sua viabilidade técnica e seu custo de ciclo de vida;
- **otimização:** simulação de muitas configurações diferentes de sistemas na procura por aquela que satisfaça todas as restrições técnicas com o menor custo de ciclo de vida;
- **análise de sensibilidade:** execução de múltiplas otimizações sob uma série de premissas/suposições para avaliar os efeitos de incertezas ou mudanças nos dados de entrada do modelo (LAMBERT *et al.*, 2006).

Uma relação conceitual desses três principais processos do HOMER é apresentada na Figura 4.5. Essas etapas também são descritas em Bahramara *et al.* (2016).

Figura 4.5: Relação conceitual entre simulação, otimização e análise de sensibilidade.

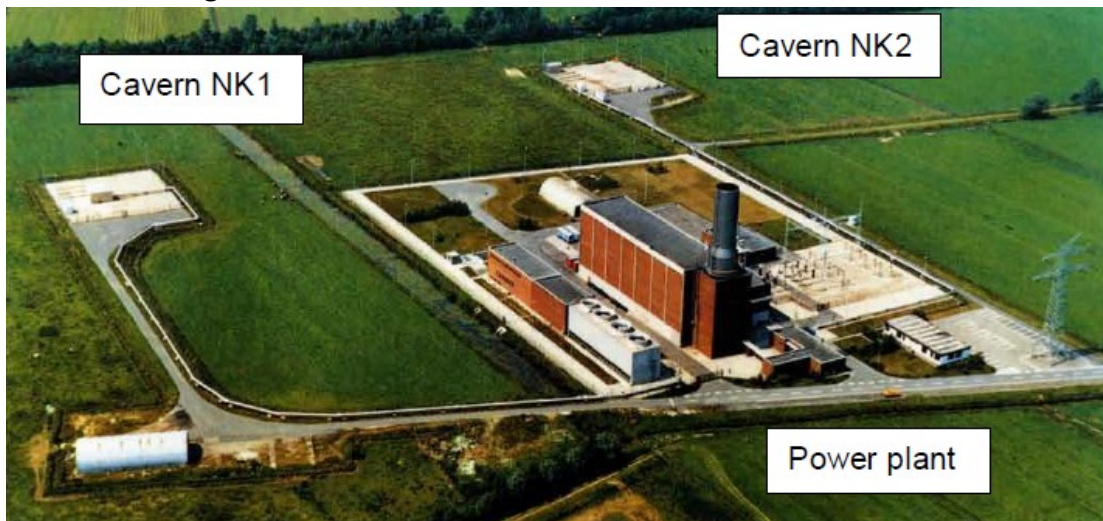


Fonte: Lambert *et al.* (2006).

4.3. Armazenamento de energia com ar comprimido

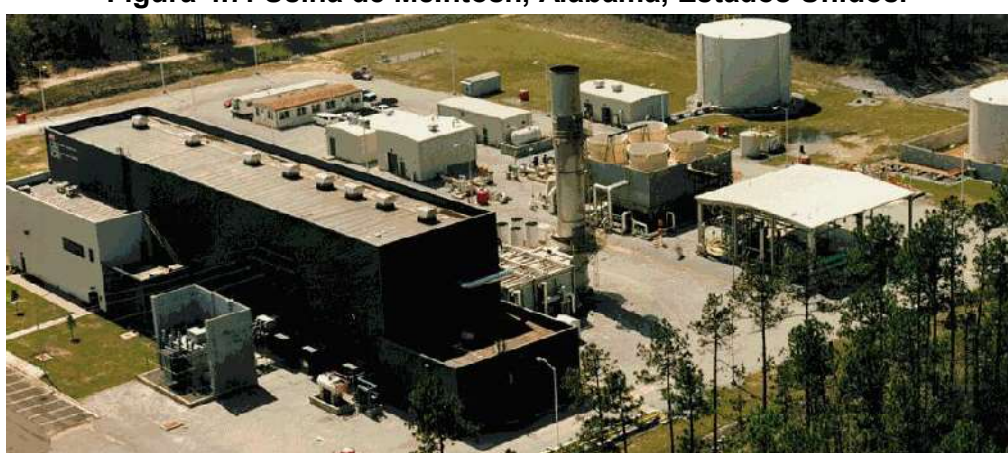
A utilização do armazenamento de energia sob a forma de ar comprimido como um complemento à rede de distribuição elétrica iniciou com a construção da usina de Huntorf (Figura 4.6), construída na Alemanha em 1978, com potência de 290 MW e eficiência de 41%. Uma segunda usina CAES, McIntosh (Figura 4.7), foi construída pela *Alabama Electric Cooperative*, nos Estados Unidos, e entrou em serviço em 1991, com capacidade de 110 MW e eficiência de 54% (BREEZE, 2018). Até o momento, essas foram as únicas usinas CAES de larga escala a entrarem em funcionamento no mundo.

Figura 4.6: Vista aérea da usina de Huntorf, Alemanha.



Fonte: Hoffeins e Mohmeyer (1986).

Figura 4.7: Usina de McIntosh, Alabama, Estados Unidos.

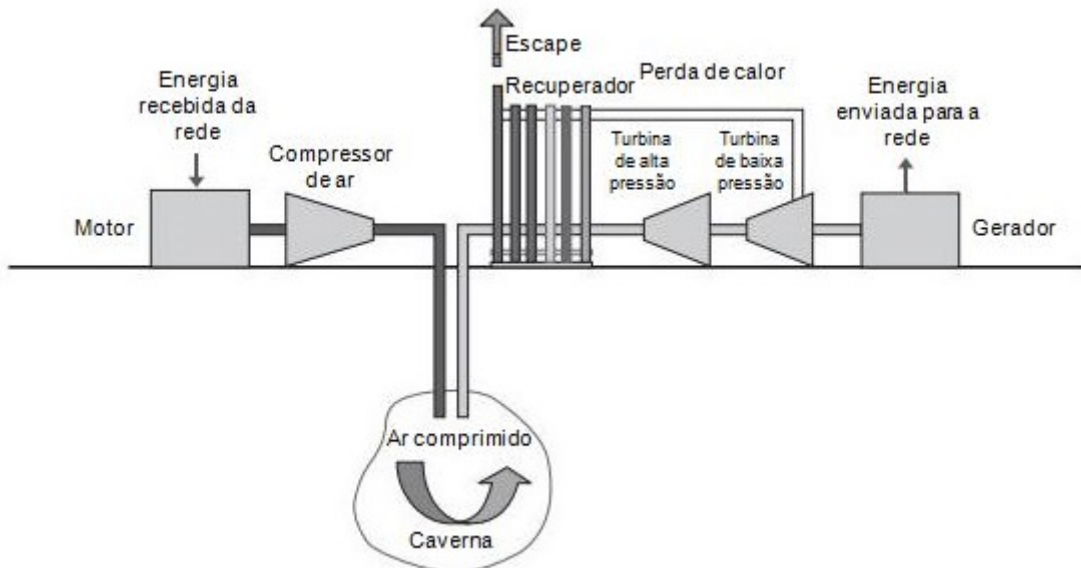


Fonte: Lee Layton (2012).

Baseada no ciclo da turbina a gás, uma planta CAES é relativamente simples de ser construída. No entanto, apesar de ser defendida por organizações, como a US Electric Power Research Institute, nenhum outro projeto comercial foi construído até então, embora vários outros tenham sido propostos. Mesmo assim, CAES continua a ser uma tecnologia muito interessante porque é o único sistema de armazenamento de energia em grande escala que pode ser construído além das tecnologias de armazenamento constituídas por usinas reversíveis. As plantas CAES individuais são geralmente menores do que as usinas reversíveis, mas os locais adequados para sua construção são muito mais fáceis de serem encontrados do que locais para usinas de armazenamento hidrelétrico. As melhores cavernas de armazenamento em grande escala para CAES possuem características geológicas subterrâneas, como os aquíferos, que podem armazenar grandes volumes de gás. Essas cavernas são amplamente distribuídas entre o globo e poderiam fornecer uma rede de armazenamento de energia em larga escala na maioria das nações (BREEZE, 2018).

Na Figura 4.8, há um esquema com os principais componentes de uma planta CAES.

Figura 4.8: Esquema de uma planta CAES.



Fonte: Traduzido de Breeze (2018).

Compressor

É um equipamento destinado ao armazenamento de ar comprimido. De acordo com o princípio de funcionamento, pode ser classificado em compressor dinâmico e de deslocamento positivo (BARROS *et al.*, 2015).

Compressor dinâmico: efetua o processo de compressão de maneira contínua, e pode ser denominado de compressor de fluxo axial ou radial (BARROS *et al.*, 2015; BOSCH, 2008).

- **compressor de fluxo axial:** máquina dinâmica constituída por uma turbina rotativa. O ar flui em direção axial através da turbina sofrendo aceleração e percorrendo uma trajetória constituída por lâminas estáticas fixadas na carcaça. Essas lâminas permitem que a energia cinética fornecida ao ar seja transformada em energia de pressão. Dessa forma, o ar é acelerado e depois comprimido. Características desse compressor: produz ar comprimido de forma uniforme e isento de óleo, é um equipamento sensível a variações de carga e é adequado a sistemas que demandam vazões elevadas.
- **compressor de fluxo radial:** máquina dinâmica que opera com altas rotações. O ar é dirigido para o centro de uma turbina através da rotação do rotor, que, combinada com a forma das pás, permite que o ar seja acelerado. Com a condução do ar através de um difusor, antes de alcançar a próxima lâmina, há um acréscimo de pressão. Assim, a energia cinética é convertida em pressão estática. Possui características iguais às do compressor de fluxo axial.

Compressor de deslocamento positivo ou volumétrico: opera através de rotação e do movimento alternado do pistão. Os tipos mais utilizados dessa categoria são: compressor de palheta, de parafuso, de lóbulo, de anel líquido, de pistão e de diafragma (BARROS *et al.*, 2015; BOSCH, 2008).

- **compressor de palhetas:** é constituído por um rotor com palhetas retangulares, que gira excentricamente em relação à carcaça. Possui baixo

ruído e dimensões reduzidas, porém alto custo de manutenção e baixa eficiência.

- **compressor de parafuso:** opera segundo a existência de dois rotores com o formato de parafusos, que giram em sentido contrário no interior de uma carcaça. Possui dimensões reduzidas e opera com fluxo de ar contínuo e baixa temperatura de compressão, para o caso de resfriamento por óleo.
- **compressor de lóbulo:** possui dois rotores que giram em sentido contrário, mantendo uma folga muito pequena no ponto de tangência entre si e com relação à carcaça. Possui baixo custo, pode suportar longa duração de funcionamento sem cuidados de manutenção, não necessita de lubrificação (assim, o ar é isento de óleo), é sensível à sujeira (pó e areia) e não possui pistão. Porém, é raramente empregado para fins industriais.
- **compressor de anel líquido:** compressor de deslocamento rotativo. Possui um eixo com lâminas radiais rígidas, que se deslocam no interior da carcaça excêntrica, fazendo com que o líquido de vedação gire. O anel líquido formado, usualmente constituído por água, veda as áreas de funcionamento entre as lâminas e a carcaça. Possui nível de ruído extremamente baixo, baixa sensibilidade contra sujeira, baixa eficiência, e apresenta um ar final isento de óleo.
- **compressor de pistão:** pode possuir vários cilindros através dos quais o ar é aspirado e comprimido com o acionamento automático de válvulas de admissão e descarga. Apesar de funcionar com excelente desempenho mecânico e permitir grande flexibilidade na produção de pressões e vazões, o compressor de pistão produz a vazão de ar comprimido em pulsos. Possui as seguintes características: baixa eficiência e alta pressão.
- **compressor de diafragma:** é um compressor de deslocamento oscilante, o qual utiliza eixos de ligação e diafragmas elásticos para compressão. Características: cilindro de grande diâmetro, movimento curto do diafragma, economia para o fornecimento de baixas pressões e pequenos volumes e geração de vácuo.

Os principais tipos de compressores existentes, relacionados aos parâmetros de pressão e vazão normalmente aplicados, encontram-se na Tabela 4.2.

Tabela 4.2: Tipos de compressores.

Tipo	Símbolo	Diagrama funcional	Pressão [bar]	Vol. do fluxo[m ³ /h]
Compressor de pistão tronco			10 (1 fase) 35 (2 fases)	120 600
Compressor de cabeçote cruzado			10 (1 fase) 35 (2 fases)	120 600
Compressor de diafragma			baixa	pequeno
Compressor s/ pistão				Uso limitado como gerador de gás
Compressor de palhetas			16	4.500
Compressor de anel líquido			10	
Compressor de parafuso			22	750
Compressor de lóbulos ou roots			1,6	1.200
Compressor de fluxo axial			10	200.000
Compressor de fluxo radial			10	200.000

Fonte: Bosch (2008).

Produção de ar comprimido

Conforme Gorgulho Júnior (2021a), o ar comprimido requer certa qualidade para que possa ser utilizado de forma adequada. Assim, o controle das seguintes variáveis é importante tanto na geração quanto na distribuição do ar comprimido:

- pressão requerida pelos equipamentos;
- vazão necessária para suprir a demanda;
- teor de água – quanto mais baixo melhor para evitar a oxidação dos componentes pneumáticos;
- teor de partículas sólidas – deve ser o mais baixo possível para que se evite a ocorrência de travamento das partes móveis dos componentes pneumáticos.
- teor de óleo – é adicionado em uma quantidade bem pequena ao equipamento pneumático para a correta lubrificação das partes móveis.

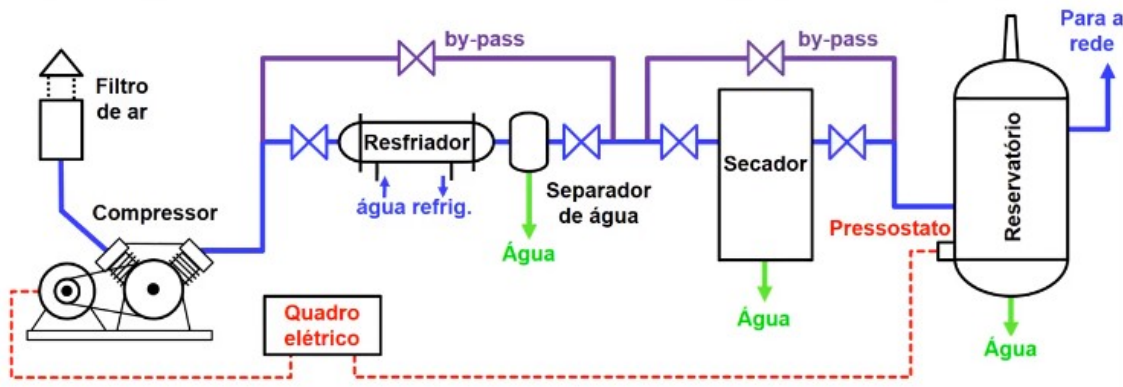
Os eventos que ocorrem na preparação do ar comprimido são:

- ao comprimir o ar, a sua temperatura se eleva;
- a água contida no ar devido à umidade relativa fica concentrada e transforma-se em vapor, sendo necessário o resfriamento do ar comprimido;
- ao resfriar o ar comprimido, o vapor se condensa, ou seja, se transforma em água, a qual precisa ser eliminada;
- ainda, podem estar presentes partículas sólidas como fragmentos de óleo do próprio compressor, partículas metálicas que se desprendem do compressor ou da tubulação, e também partículas que foram aspiradas pelo compressor, apesar da existência de um filtro em sua entrada. Essas partículas devem ser removidas para que o ar fique com qualidade (GORGULHO JÚNIOR, 2021a).

Componentes da produção de ar comprimido

Na Figura 4.9, a seguir, há um esquema com os componentes que fazem parte da produção e armazenamento de ar comprimido. Salienta-se que existem diversas outras configurações diferentes para um sistema de armazenamento a ar comprimido.

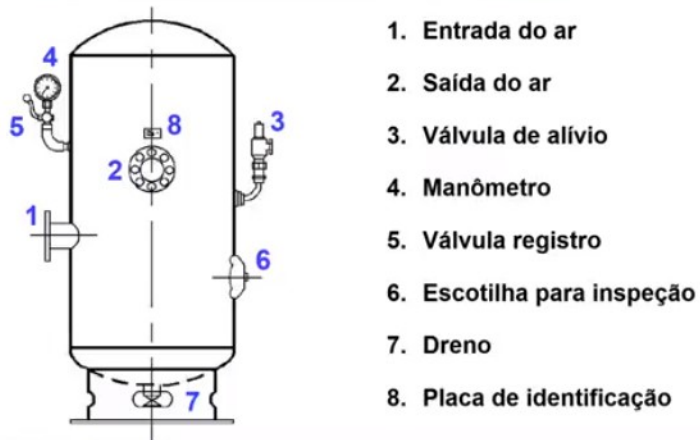
Figura 4.9: Esquema de produção e armazenamento de ar comprimido.



Fonte: Gorgulho Júnior (2021a).

Os dispositivos existentes em um reservatório de ar comprimido são listados na Figura 4.10.

Figura 4.10: Dispositivos existentes no reservatório.

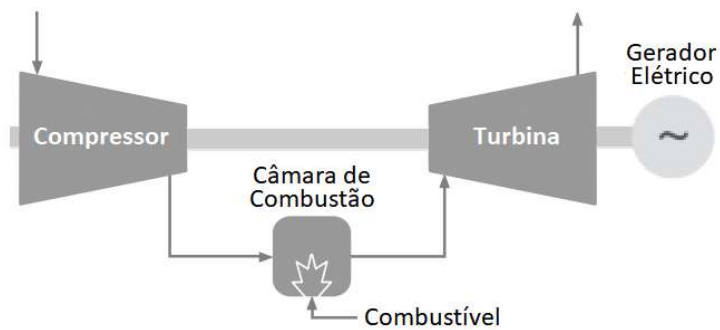


Fonte: Gorgulho Júnior (2021b).

Turbina a gás

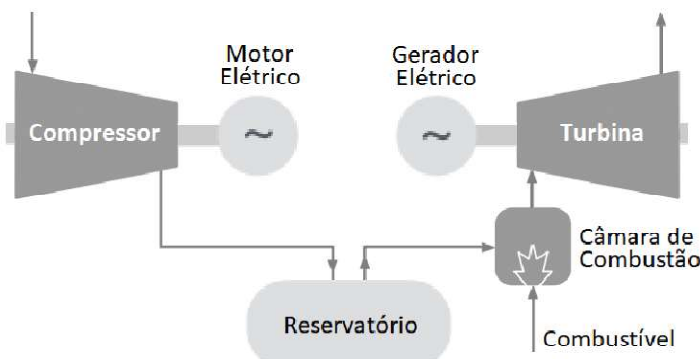
Um sistema de armazenamento de energia por ar comprimido opera de forma muito semelhante ao de uma turbina a gás convencional (Figura 4.11). A diferença é que em um sistema CAES as etapas de compressão e expansão ocorrem de forma separada e em momentos independentes (Figura 4.12).

Figura 4.11: Esquema de funcionamento de uma turbina a gás padrão.



Fonte: Altmann (2018).

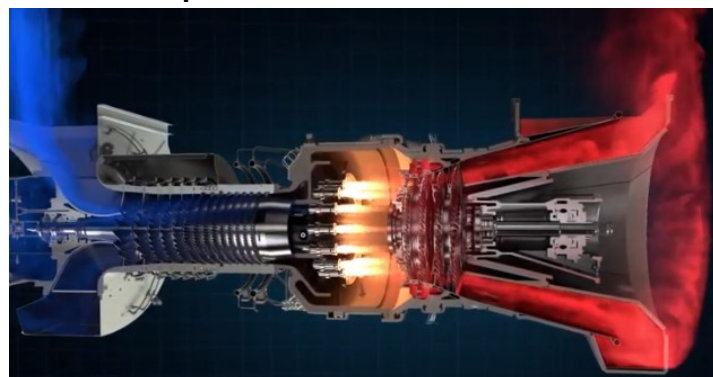
Figura 4.12: Esquema de funcionamento de um sistema CAES padrão.



Fonte: Altmann (2018).

Quanto ao funcionamento de uma turbina a gás, inicialmente, o ar entra através da admissão da turbina. Em seguida, o compressor aumenta a pressão do ar antes de entrar na câmara de combustão. Então, esse ar comprimido é misturado com o combustível e sofre ignição, criando uma expansão de gás quente. Finalmente, este gás quente aciona a turbina de potência e gera energia mecânica (Figura 4.13). As turbinas a gás são usadas para acionar geradores, gerando eletricidade e calor (cogeração) para universidades, hospitais, instalações industriais etc., e também acionam bombas que transportam líquidos (instalações de processamento). E, finalmente, acionam compressores que entregam gás natural para abastecer casas, prédios e indústrias em todo o mundo (SOLAR TURBINES, 2021).

Figura 4.13: Princípio de funcionamento de uma turbina a gás.



Fonte: Solar Turbines (2021).

Tecnologias de armazenamento de energia sob a forma de ar comprimido

A tecnologia de armazenamento de ar comprimido surgiu na década de 70, com a criação do sistema convencional *Diabatic Compressed Air Energy Storage (D-CAES)*. Com o passar dos anos, outras soluções com novas abordagens do ponto de vista termodinâmico passaram a ser estudadas, com introdução de etapas intermediárias para gerenciamento das trocas de calor, o que possibilitou um aumento de rendimento dos sistemas. Assim, surgiu a solução conhecida como *Advanced Adiabatic Compressed Air Energy Storage (AA-CAES)*, a qual consiste em um processo avançado de conservação e reaproveitamento do calor gerado durante o processo de compressão. Na tentativa de melhorar ainda mais esse sistema avançado, criou-se a solução *Isothermal Compressed Air Energy Storage (I-CAES)*, na qual a temperatura do fluido é mantida aproximadamente constante durante os processos de compressão e expansão (CLEARY *et al.*, 2015; ROGERS *et al.*, 2014; SALVADOR *et al.*, 2016).

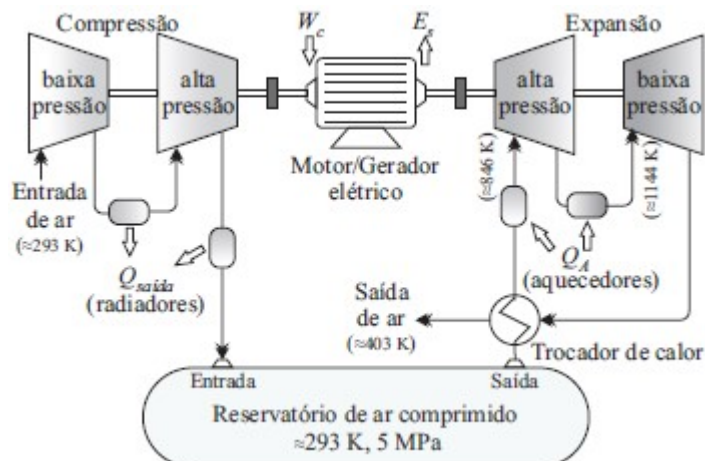
Além dos sistemas de grande porte mencionados anteriormente, existem sistemas de pequeno porte de armazenamento de energia sob a forma de ar comprimido chamados *Small Scale Compressed Air Energy Storage (SS-CAES)*, que são alternativas em algumas aplicações que normalmente utilizam baterias. Embora possuam vantagens do ponto de vista ecológico e de vida útil, quando comparados às baterias comerciais, sistemas de pequeno porte possuem menor densidade de energia e menor rendimento. Essas desvantagens têm desafiado os pesquisadores na busca pela elevação da eficiência no processo de expansão do ar (KOKAEW *et al.*, 2016; SALVADOR *et al.*, 2016).

Uma breve descrição dos sistemas de grande porte de armazenamento de ar comprimido é apresentada a seguir (SALVADOR *et al.*, 2016):

Sistemas D-CAES

Os sistemas diabáticos são classificados em sistemas de primeira e segunda geração. No sistema de primeira geração, o calor resultante do processo de compressão é transferido para a atmosfera, o que gera perdas de energia, e o ar é reaquecido, durante a expansão, através da queima de combustível, que pode ser gás natural ou óleo. O sistema de segunda geração funciona de maneira semelhante; entretanto, os processos de compressão e expansão são divididos em etapas, e parte da energia térmica contida no ar que sai da turbina é aproveitada para pré-aquecer o ar que deixa o reservatório de ar comprimido (Figura 4.14).

Figura 4.14: Visão geral do sistema D-CAES de 2^a geração.



Fonte: Rogers *et al.* (2014); adaptado por Salvador *et al.* (2016).

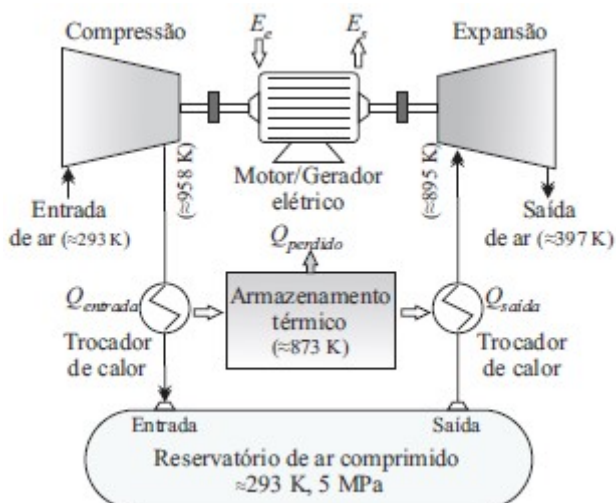
Apesar da inclusão do recuperador de calor no sistema D-CAES de segunda geração, ainda há a necessidade de queima de grande quantidade de combustível para a expansão do ar, com emissão de CO₂ para a atmosfera, o que é um aspecto negativo do ponto de vista ambiental, além de reduzir a eficiência do sistema, que pode atingir aproximadamente 54%. Esse rendimento é calculado em função da energia de saída (E_s) e a soma da energia elétrica (W_c) utilizada para compressão do ar com a energia (Q_A) adicionada ao processo na forma de calor.

Sistema AA-CAES

O sistema avançado adiabático¹ possui um arranjo que armazena o calor gerado durante o processo de compressão do ar, disponibilizando-o durante o processo de expansão para reduzir ou até mesmo eliminar o consumo de combustível utilizado para o aquecimento do ar na entrada da turbina (Figura 4.15).

As vantagens desse sistema são: a elevação da eficiência (em torno de 70%), e a redução da emissão de carbono, que é possível com a redução da utilização de combustível.

Figura 4.15: Visão geral do sistema AA-CAES.



Fonte: Rogers *et al.* (2014); adaptado por Salvador *et al.* (2016).

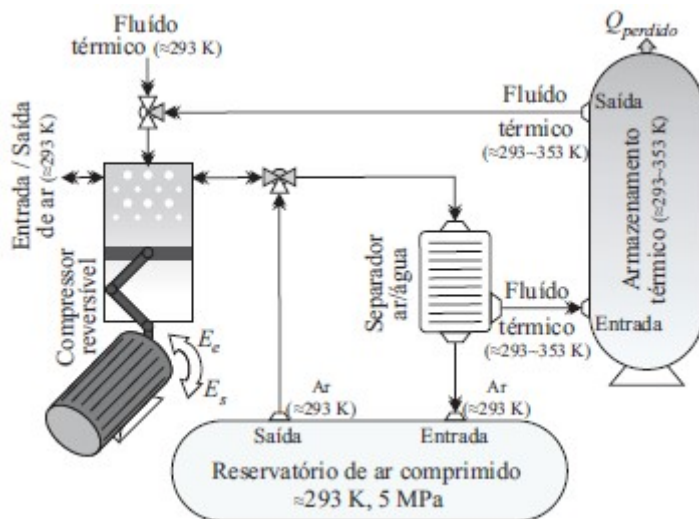
Sistema I-CAES

O sistema isotérmico² elimina a necessidade de armazenamento térmico em elevadas temperaturas e também a necessidade de queima de combustível. Esse sistema se aproxima do processo isotérmico de compressão/expansão ideal, ou seja, procura-se manter a temperatura constante dos processos por meio de métodos eficazes de troca de calor, atingindo-se eficiências na ordem de 75% (Figura 4.16).

¹ Processo adiabático: aquele que ocorre tão depressa, ou em um sistema tão bem isolado, que não há troca de calor entre o sistema e o ambiente (HALLIDAY *et al.*, 2016).

² Processo isotérmico: aquele no qual a temperatura do sistema permanece constante (LUIZ, 2013).

Figura 4.16: Visão geral do sistema I-CAES.



Fonte: Rogers *et al.* (2014); adaptado por Salvador *et al.* (2016).

Armazenamento com ar comprimido subaquático

Um sistema de armazenamento de ar a pressão constante também pode ser configurado usando uma forma de armazenamento subaquático. Nesse caso, o componente de armazenamento é um reservatório com parede expansível, que precisa estar localizado em certa profundidade no mar ou em um lago com grande profundidade. Quando o ar comprimido é bombeado para o acumulador, a pressão hidrostática da água controlará a pressão do gás, e, à medida que mais ar for bombeado, as paredes do reservatório de ar se expandirão para manter a pressão. A tecnologia do componente expansível (material) é a chave para a eficiência desse tipo de armazenamento CAES, e ainda se encontra em estudo (BREEZE, 2018).

Uma solução similar a um balão foi estudada por De Jong (2014). O dispositivo utilizado foi constituído por um material flexível (Figura 4.17), resistente à pressão exercida pelo ar comprimido. A vantagem da utilização desses balões submersos está ligada à redução dos custos com material, pois a pressão hidrostática permite que a massa estrutural do dispositivo seja muito reduzida.

Ainda com relação ao material, há estudos com estrutura composta por esfera de concreto (Figura 4.18). Tanto as estruturas flexíveis, quanto as de concreto podem ser ancoradas no fundo de lagos, mares ou oceanos.

Conforme Wang *et al.* (2019), os sistemas de armazenamento de energia subaquáticos podem atingir mais de 50% de eficiência.

Figura 4.17: Estrutura flexível.



Fonte: Energy Matters (2019).

Figura 4.18: Esfera de concreto.



Fonte: Energy Matters (2019).

Os principais componentes de um sistema de armazenamento de energia com ar comprimido subaquático podem ser verificados na Figura 4.19.

Figura 4.19: Armazenamento de energia com ar comprimido subaquático.



Fonte: Traduzido de Hydrostor (2018).

REFERÊNCIAS

ALTMANN, M. U. **Avaliação termodinâmica de um sistema de acumulação de energia por ar comprimido (CAES) frente a uma turbina a gás de ciclo aberto.** 2018. 27 f. Trabalho de diplomação (Graduação em Engenharia de Energia) – Escola de Engenharia. Universidade Federal do Rio Grande do Sul, Porto Alegre.

ANEEL. Agência Nacional de Energia Elétrica. **Sistema de Informações de Geração da ANEEL – SIGA.** Resumo Estadual. Capacidade Instalada do Rio Grande do Sul. Disponível em: <<https://bit.ly/2IGf4Q0>>. Acesso em: 03 dez. 2021.

ASSIS, L. E. **Avaliação e aproveitamento da energia de ondas oceânicas no litoral do Rio Grande do Sul.** 2010. 82 f. Dissertação (Mestrado em Recursos Hídricos e Saneamento Ambiental) – Programa de Pós-Graduação em Recursos Hídricos e Saneamento Ambiental. Universidade Federal do Rio Grande do Sul, Porto Alegre.

ATLAS SOCIOECONÔMICO DO RIO GRANDE DO SUL. Secretaria de Planejamento, Governança e Gestão. Departamento de Planejamento Governamental. 6. ed. Porto Alegre: SPGG, 2021. Disponível em: <<https://atlassocioeconomico.rs.gov.br/edicao>>. Acesso em: 18 set. 2021.

BAHRAMARA, S.; MOGHADDAM, M. P.; HAGHIFAM, M. R. Optimal planning of hybrid renewable energy systems using HOMER: A review. **Renewable and Sustainable Energy Reviews**, v. 62, p. 609-620, 2016.
<https://doi.org/10.1016/j.rser.2016.05.039>.

BARROS, B. F.; BORELLI, R.; GEDRA, R. L. **Eficiência energética:** técnicas de aproveitamento, gestão de recursos e fundamentos. São Paulo: Érica, 2015.

BELUCO, A. Três locais para implantação de usina hidrelétrica reversível ao sul dos Aparados da Serra, no Litoral Norte do RS. **Hydro & Hydro:** PCH Notícias & SHP NEWS, v. 1, n. 52, p. 32-37, 2012. Disponível em: <https://cerpch.unifei.edu.br/painel/assets/images/revistas/revista_5dcbf39fe9dec.pdf>. Acesso em: 16 jun. 2012.

BELUCO, A.; SOUZA, P. K.; KREZINGER, A. A complementaridade no tempo entre as energias hidrelétrica e fotovoltaica. **Revista Brasileira de Recursos Hídricos**, v. 8, n. 1, p. 99-109, 2003. <http://doi.org/10.21168/rbrh.v8n1.p99-109>.

BEN. **Balanço Energético Nacional 2020:** Ano base 2019. Ministério de Minas e Energia. Empresa de Pesquisa Energética. Rio de Janeiro: EPE, 2020. Disponível em: <<https://www.epe.gov.br/pt/publicacoes-dados-abertos/publicacoes/balanco-energetico-nacional-2020>>. Acesso em: 11 out. 2021.

BREEZE, P. Compressed Air Energy Storage. In: _____. **Power System Energy Storage Technologies**. Academic Press, 2018. Ch. 3, p. 23-31.

- <https://doi.org/10.1016/B978-0-12-812902-9.00003-1>.
- BOSCH. **Tecnologia de ar comprimido**. Campinas: Robert Bosch Limitada, 2008.
- CEEE. Comissão Estadual de Energia Elétrica. **Projeto Barragem Laranjeira**. 1955.
- CEEE. Companhia Estadual de Energia Elétrica. **Reexame do Projeto da Hidrelétrica de Laranjeiras**. Electroconsult – elc, ago. 1970.
- CLEARY, B.; DUFFY, A.; O'CONNOR, A.; CONLON, M.; FTHENAKIS, V. Assessing the Economic Benefits of Compressed Air Energy Storage for Mitigating Wind Curtailment. **IEEE Transactions on Sustainable Energy**, vol. 6, n. 3, p. 1021-1028, july 2015. <https://doi.org/10.1109/TSTE.2014.2376698>.
- De Jong, M. Commercial grid scaling of energy bags for underwater compressed air energy storage. **International Journal of Environmental Studies**, vol. 71, n. 6, p. 804-811, 2014. <https://doi.org/10.1080/00207233.2014.947726>.
- ENERGY MATTERS. A review of underwater compressed air storage. Disponível em: <<http://euanmearns.com/a-review-of-underwater-compressed-air-storage/>>. Acesso em: 14 jan. 2019.
- FEE. Fundação de Economia e Estatística. **Estimativas para a população flutuante do Litoral Norte do RS**. Disponível em: <<https://arquivofee.rs.gov.br/noticias/capao-da-canoa-e-o-municipio-com-maior-populacao-media-no-litoral-norte-durante-o-veraneio/>>. Acesso em: 17 nov. 2021.
- GOLDEMBERG, J.; VILLANUEVA, L. D. **Energia, Meio Ambiente & Desenvolvimento**. 2. ed. São Paulo: Edusp, 2003.
- GORGULHO JÚNIOR, J. H. C. Hidropneumática: produção do ar comprimido. Disponível em: <<https://www.youtube.com/watch?v=xzyVH-3QYKE>>. Acesso em: 27 ago. 2021a.
- GORGULHO JÚNIOR, J. H. C. Hidropneumática: componentes da produção de ar comprimido. Disponível em: <<https://www.youtube.com/watch?v=3HIIQux6zR0>>. Acesso em: 27 ago. 2021b.
- HALLIDAY, D.; RESNICK, R.; WALKER, J. **Fundamentos de Física**: gravitação, ondas e termodinâmica. Volume 2. 10. ed. Rio de Janeiro: LTC, 2016.
- HOFFEINS, H.; MOHMEYER, K. U. Operating experience with the Huntorf air-storage gas turbine power station. Switzerland, 1986.
- HYDROSTOR. Disponível em: <<https://www.hydrostor.ca/resources/Hydrostor-AECOM%202016-10.pdf>>. Acesso em: 18 mar. 2018.
- IBGE Cidades. Disponível em: <<https://cidades.ibge.gov.br/>>. Acesso em: 17 nov. 2021.

ÍNDIO SAN. Super interessante. Disponível em:
<https://super.abril.com.br/especiais/como-sidarta-gautama-se-tornou-buda/>.
 Acesso em: 15 ago. 2022.

KOKAEW, V.; SHARKH, S. M.; MOSHREFI-TORBATI M. Maximum Power Point Tracking of a Small-Scale Compressed Air Energy Storage System. **IEEE Transactions on Industrial Electronics**, v. 63, n. 2, p. 985-994, feb. 2016.
<https://doi.org/10.1109/TIE.2015.2477344>.

LAMBERT, T.; GILMAN, P.; LILIENTHAL, P. Micropower system modeling with HOMER. In: FARRET, F. A.; SIMÕES, M. G. (Eds.). **Integration of Alternative Sources of Energy**. Hoboken, New Jersey: John Wiley & Sons, Inc., 2006. Ch. 15, p. 379-418. <https://doi.org/10.1002/0471755621.ch15>.

LEE LAYTON, P. E. **Compressed air energy storage**. PDHonline Course E365 (4 PDH). VA, USA, 2012. Disponível em:
<https://pdhonline.com/courses/e365/e365content.pdf>. Acesso em: 26 ago. 2021.

LUIZ, A. M. **Termodinâmica: teoria & problemas**. Rio de Janeiro: LTC, 2013.

MASKEY, R. K.; NESTMAN, F. **Hydro Based Renewable Hybrid Power System for Rural Electrification**: A Concept Paper. Germany: Institute of Water Resources Management, University of Karlsruhe, 2000.

ROGERS, A.; HENDERSON, A.; WANG, X.; NEGNEVITSKY, M. Compressed Air Energy Storage: Thermodynamic and Economic Review. In: IEEE PES General Meeting: Conference & Exposition, 2014, National Harbor, MD, USA. **Proceedings...** IEEE, 2014. <https://doi.org/10.1109/PESGM.2014.6939098>.

SALVADOR, M. A.; LAZZARIN, T. B.; COELHO, R. F. Panorama das estratégias de armazenamento de energia sob forma de ar comprimido. **Eletrônica de Potência**, Campo Grande, v. 21, n. 3, p. 169-178, jul./set. 2016.
<http://doi.org/10.18618/REP.2016.3.2589>.

SILVA, J. S. **Viabilidade de geração de energia elétrica através de ondas oceânicas no litoral norte do Rio Grande do Sul**: estudo de um sistema híbrido de energias renováveis. 2012. 117 f. Dissertação (Mestrado em Recursos Hídricos e Saneamento Ambiental) – Instituto de Pesquisas Hidráulicas. Universidade Federal do Rio Grande do Sul, Porto Alegre.

SILVA, J. S. ; BELUCO, A. **Guia de Introdução para o HOMER Legacy – Versão 2.68**. Tradução. 2012. Disponível em:
https://www.homerenergy.com/pdf/HOMERGettingStarted_Portuguese.pdf. Acesso em: 31 mar. 2012.

SOLAR TURBINES. Gas Turbines. Disponível em:
https://www.solarturbines.com/en_US/products/gas-turbines.html. Acesso em: 16 ago. 2021.

TWIDELL, J.; WEIR, T. **Renewable Energy Resources**. Oxon: Taylor & Francis, 2006.

WANG, Z.; CARRIVEAU, R.; TING, D. S.-K.; XIONG, W.; WANG, Z. A review of marine renewable energy storage. **International Journal of Energy Research**, v. 43, n. 12, p. 1-43, 2019. <https://doi.org/10.1002/er.4444>.

5. Artigo 1

Characterization of a feasibility space for a new technology – a case study of wave energy in Southern Brazil

Jones S. Silva and Alexandre Beluco

Instituto de Pesquisas Hidráulicas (IPH), Universidade Federal do Rio Grande do Sul (UFRGS), Porto Alegre, RS, Brazil

Journal: Current Alternative Energy

Published on: 29 August, 2018

DOI: 10.2174/1570178615666180830102336

Abstract – Background: Currently there are several renewable resources in different stages of technological maturation. Among different alternatives, wave energy has some initiatives at an advanced stage of development and is one of the most promising alternatives. In the process of developing wave energy conversion devices, as well as developing other alternatives, the limits that must be satisfied to achieve feasibility would be a powerful tool for technology managers.

Method: This paper proposes a feasibility space as being the set of key parameter values for feasibility that must be satisfied by devices in development. This article also determines the feasibility space that must be satisfied in the current moment by devices for converting wave energy to the feasibility of a wave power plant in the southernmost coast of Brazil.

Results: The results indicate that, for the conditions considered in the simulations, wave power plants will be feasible for energy at USD\$ 0.05 / kWh, USD\$ 0.10 / kWh and USD\$ 0.15 / kWh, if they can be implemented with costs between USD\$ 616.01 / kW and USD\$ 2,865.37 / kW respectively for efficiencies between 20% and 40%. These values are extremely low, comparable to values for already mature alternatives such as hydropower and wind energy.

Conclusion: The definition of a feasibility space allows the establishment of an objective to be achieved so that generating plants based on renewable resources not yet exploited can become viable. This paper presented the feasibility space for the generation of energy from ocean waves on the southern coast of Brazil.

Keywords: computational simulation; feasibility space; hybrid systems; ocean wave energy; HOMER software; southern Brazil.

1. INTRODUCTION

Nowadays, among the so-called alternative energies, there are some that have achieved technical and economic maturity and continue to evolve and others that still have a long way to go before they become effectively viable alternatives. Among the mature alternatives are hydroelectric power, wind energy and various ways of harnessing solar energy. And there are several forms of energy that can be listed among those still in development, such as wave energy, current energy and tidal energy, energy in small temperature gradients, among others.

The celerity of the technological and economic development of alternative forms of energy depends on its eventual strategic importance, the pressure exerted by the demand for energy supplies and the specific demand for these new means to obtain energy supplies. A region with scarce resources will surely see its few resources being tapped faster. Likewise, a region with few resources or with its resources depleted and with increasing demands will also see its resources under great pressure to be used.

It is difficult to build a social and economic transition that leaves behind the unsustainable means to obtain energy supplies in favor of a society based at least mainly on renewable energies [1]. This process is obviously necessary and will occur very slowly. In this sense, it is necessary to provide tools for managers and governments to manage this necessary transition to sustainable path. This work is inserted in this point, contributing with a tool that offers a target to the technology developers.

The process of maturation of new energy forms, until they can be exploited with full technical and economic feasibility, can be guided by the determination of possible values for the variables influencing their feasibility. These possible values can be understood as a target to be attained, certainly varying over time, depending on the energy matrix and the demand for energy in which the developing resource should be inserted. This target must be based on accurate projections for the future moment when the energy from this new renewable resource will finally be available.

This goal can be understood as a feasibility space or a feasibility window, characterized by the ranges of variation of the parameters defining the technical and economic feasibility of a given power generation plant. The main variables to be

considered would be the initial costs for the installation of the generating plant and the cost of the energy generated by this plant, the total efficiency of the energy conversion process and the price contemporaneously practiced for the sale of energy by the power system to which the plant will be connected.

As an example, a new device for converting a certain type of energy resource into electricity. This new device will have its feasibility characterized by its initial cost per installed kW, the cost of the energy generated and its efficiency in the conversion of energy. The characterization of a feasibility space displays values of these parameters to which the new device will reach technical and economic feasibility. And this characterization of feasibility will obviously be connected to a particular historical moment and a specific power system.

The definition of a feasibility space and the appropriate characterization of its variation over the years required for the development of a new technology can be an important parameter for the establishment of new policies to encourage a transition to sustainable solutions [2]. In addition, since different technologies for the same purpose can be understood as competitors of the same economic niche [3, 4], the definition of a feasibility space can encourage competition among developing technologies, possibly leading to better technological results.

This article is devoted to wave energy which is a less developed alternative compared to other renewables but is still one of the most promising. Astariz and Iglesias [5] discuss the cost structure for the implementation of plants for the conversion of wave energy. A well-defined and well-known cost structure is a key asset for attracting investors. Kelly and Merritt [6] discuss the feasibility of hybrid systems and even consider the use of marine hydrokinetics in these systems, but wave energy has been showing consistent developments and may soon be considered as an important alternative.

This paper proposes the idea of a “feasibility space” for renewable energy resources that remain not exploited and determines the feasibility space for power generation from ocean waves on the southern coast of Brazil. The following sections discuss the power generation from ocean waves and the extent of this resource in southern Brazil. The subsequent sections discuss the characterization of a feasibility space and the approach adopted for the case study, with the application of HOMER software.

2. POWER GENERATION FROM OCEAN WAVES

The power P_{wav} [W] of a real plant with length L [m] parallel to the coast line and an overall performance of the plant equal to η_{wav} [1] is given by Equation (1), where ρ [kg/m³] is the density of sea water, g [m/s²] is the acceleration due to gravity, H_s [m] is the significant wave height and T_e [s] is the wave period. Twidell and Weir [7] and Sorensen [8] discuss this concept.

$$P_{\text{wav}} = \frac{\rho \cdot g^2}{64\pi} \cdot H_s^2 \cdot T_e \cdot L \cdot \eta_{\text{wav}} \quad (1)$$

Aside from places with an obvious energy resource, one of the biggest obstacles to the exploitation of the energy of ocean waves is the lack of available data. There are indirect [9] or expeditious measurements, but the monitoring of the characteristics of ocean waves over the years is the best tool for an accurate assessment of the available energy.

As this alternative presents the same difficulties as other renewable resources due to less permanence over time, the exploitation of wave energy can be carried out with better efficiency if its complementarity [10, 11] with other energy resources is identified. Obviously, the installation and operation of equipment in the marine environment present additional difficulties.

The technologies currently under development for wave power generation can be divided into eight categories: attenuators, point absorbers, oscillating water columns, oscillating wave surge converters, overtopping devices, submerged pressure differential devices, bulge wave devices and rotating mass devices. Unfortunately, there are still no fully viable devices.

The attenuators and bulge wave devices ride the waves. The attenuators consist of two floats connected by a joint, placed parallel to the direction of the waves. The energy is generated from the relative motion of the two floats. The bulge wave devices consist of rubber tubes filled with water, moored to the seabed, pierced by moving water. Water entering one end causes pressure variations along the length of the tubes. These pressure variations drive low-pressure turbines at the other end, where water returns to the sea.

Point absorbers and submerged pressure differential devices are trapped in the bottom and move vertically along the waves. The point absorbers consist of floats placed on the surface of the water, while the submerged pressure differential devices float at intermediate depths, taking advantage of the pressure variations induced by the movement of the waves. Variations in the motion of these floating structures, both on the surface and submerged, pump fluid in a system that converts energy into electricity.

Oscillating wave surge converters basically consist of a swinging arm, such as a pendulum, mounted to a hinged joint, moving in response to the movement of the water along the waves on the surface. It is quite suitable for the conversion of energy on continental shelves near the coast.

Rotating mass devices consist of semi-sphere shaped floats, with a shaft and an eccentric mass placed to rotate in the lowest part inside the structure. The movement of the waves causes the movement of the float and the rotation of this mass, which thus drives an energy converter.

Overtopping devices capture the water as the waves break over the edges of an artificial reservoir. Water entering this reservoir can be designed to cause an energy concentration effect. The water in this reservoir then returns to the sea through a low-head hydraulic turbine.

The oscillating water column devices are partially submerged hollow structures. The structure is open to the sea below the waterline, sealing a column of air at the top of a water column. The waves cause the water column to rise and fall, which in turn compresses and decompresses the air column. This trapped air column is allowed to flow into and out of the atmosphere through a turbine, which has the ability to rotate in one direction regardless of the direction of the airflow. This turbine drives an electric generator.

3. ENERGY FROM OCEAN WAVES ALONG THE SOUTHERN COAST OF BRAZIL

This study considers the results used by Assis [12] and revised by Silva [13] to evaluate the energy resource of ocean waves along the southern coast of Brazil. The

results indicate a mean power of 12.01 kW/m, with extremes of 6.98 kW/m and 16.51 kW/m, relatively low compared to potentials elsewhere in the world [5] but sufficient to contribute to the generation of energy from renewable resources in the region, together with existing hydroelectric plants and wind farms.

These values were obtained from measurements made in Tramandaí [14], but as discussed in Assis [12], these results can be extrapolated to the stretch of coast from Laguna [15] to the mouth of Chui river [16]. This stretch of the coast has very similar characteristics along its entire length. A region with a coastline with no points for mooring vessels, called "neutral fields" at the time of Portuguese and Spanish occupation. Obviously, the implementation of energy conversion devices will require study of the impacts on sediment deposition along the region.

The section that is located to the south of Quintão beach [17] to the historic city of São José do Norte [18], at the mouth of the Patos Lagoon, approximately 240 km long, has very small population and very few economic activities and it can be identified as the ideal area for the installation of an ocean wave power plant. It is obvious that studies on the coastal dynamics in the region with the implementation of energy conversion devices is absolutely necessary.

Figure 5.1 shows a map of municipalities in this region, whose demand for electricity is considered in the simulations with HOMER. Figure 5.2 shows a suggestion of location for a first wave power plant to be installed in the region. This work has not been performed on a specific technology for wave energy conversion, but it works generically with any technology that is selected for this purpose.

Figure 5.1: Map showing the location of the municipalities on the coast of southern Brazil where demand for electricity was considered as a goal to be achieved in this study.

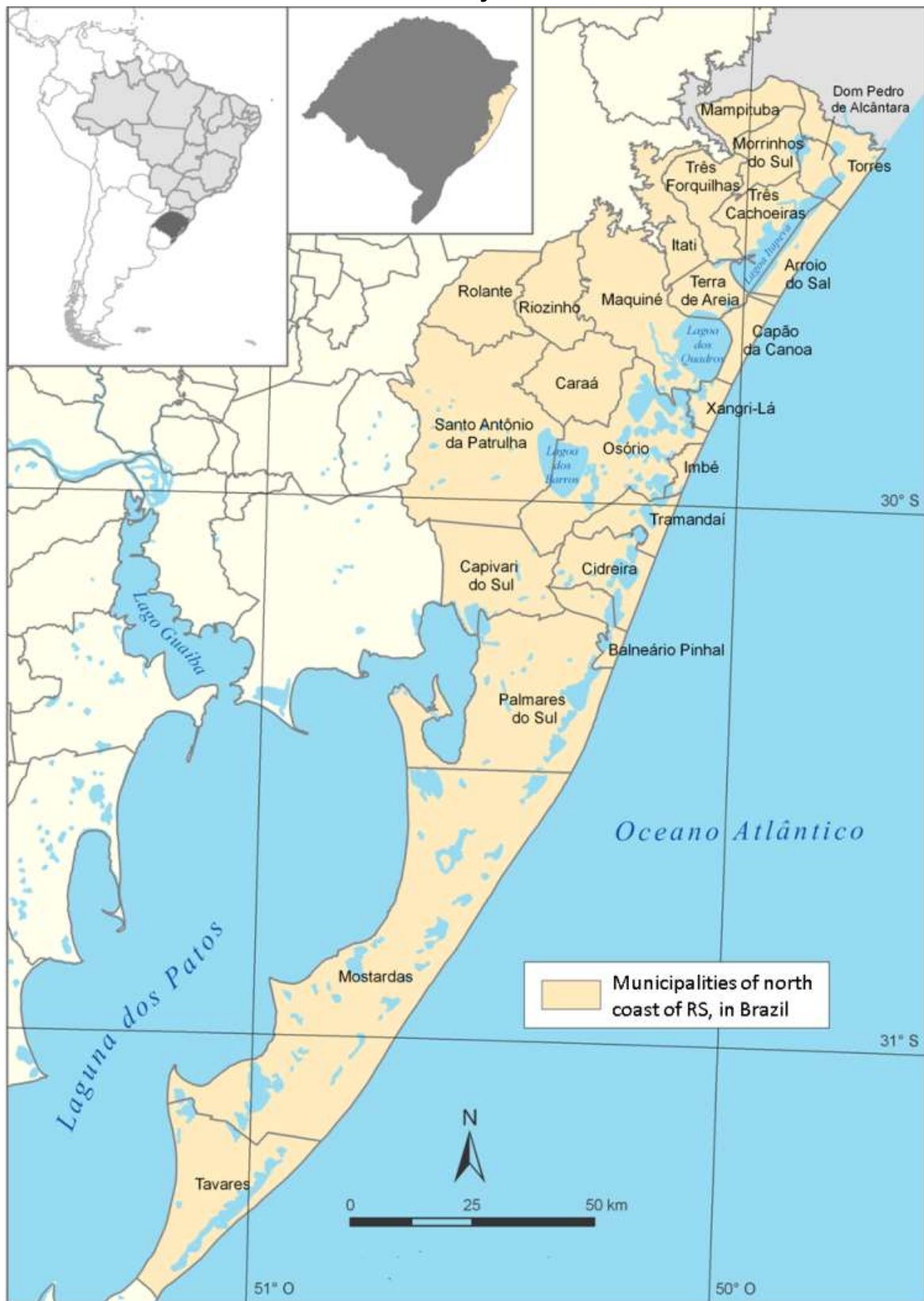
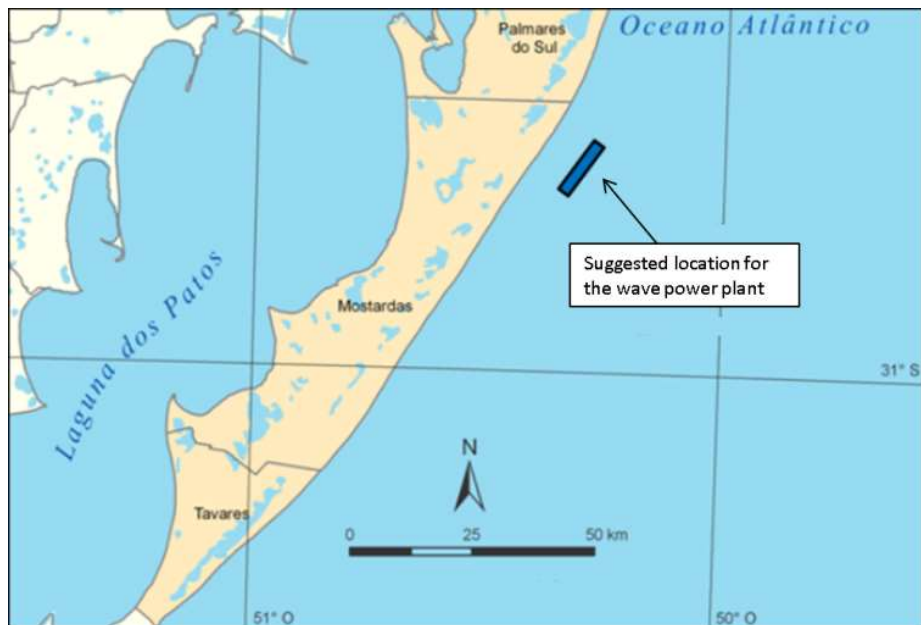


Figure 5.2: Map showing the location suggested for the ocean wave power plant in southern Brazil.



4. CHARACTERIZATION OF A FEASIBILITY SPACE FOR THIS CASE

A feasibility space will be defined in this context as a range of values for the variables considered important for the feasibility of a given project. Thus, the characterization of a feasibility space will show a goal to engineers and entrepreneurs interested in the implementation of a power plant based on a technology that is under development. Most importantly, this characterization should be a key tool for technology managers to set long-term goals for the maturation of devices for converting renewable energies.

As a set of values that establish the limits to the feasibility of a given project, a feasibility space is a set of data that is a function of time. Global and regional economic scenarios, financial constraints, technological developments, environmental issues and even climate change can decisively influence and pressure a feasibility space. The demand profile and its variation over time, consumer expectations for better quality of energy supplies and other investments for power generation in the energy system, among other factors, also influence a feasibility space.

The cost of energy supplied by the grid, the initial cost for the implementation of the ocean wave power plant and the cost of energy supplied by this plant, in addition to the efficiency of the energy conversion device, were the parameters

considered in this study. Specifically, USD\$ 0.05 / kWh, USD\$ 0.10 / kWh and USD\$ 0.15/ kWh were considered for the cost of energy supplied by the grid and 20%, 25%, 30%, 35% and 40% for the efficiency of the energy conversion device, with the corresponding values of the other two parameters determined from this study.

5. SIMULATIONS WITH HOMER

HOMER is a well known simulation software initially developed by the National Renewable Energy Laboratory (Department of Energy, USA) and now freely distributed by HOMER Energy in its Legacy version [19], which also offers more advanced versions of this software. HOMER simulates hybrid systems, usually with small dimensions, over a determined period of analysis at intervals of 1 hour, and presents the results corresponding to one year of operation of this system. HOMER runs simulations to perform optimization calculations and sensitivity analysis [20, 21].

For this study, initial data were inserted into HOMER in order to simulate the system of Figure 5.3, considering the region shown in Figure 5.1. Figure 5.4 shows the demand for electricity from the municipalities of the region; above, average demand over the months of the year and, below, instant demand over the days of the year. This demand will be considered as serviced by wind farms, by small photovoltaic systems connected to the grid and by the wave power plant that is the focus of this study.

The simulations consider the operation of a hybrid PV wind system where the wind component simulates the wind farms installed in the municipality of Osório and the PV component considers the possibility of PV panels distributed throughout the region. Figure 5.5 and Figure 5.6 show respectively the wind and solar resources available to the components of the system of Figure 5.3.

In the simulations, HOMER was able to choose between four total power possibilities generated with PV panels. These possibilities were 0 kW, 2000 kW, 4000 kW and 6000 kW and the most frequent values were 0 kW and 6000 kW. The systems containing PV modules, then distributed in the region where the system is operating, will have a certain amount of systems with much lower power, in the order of a few hundred kW, until reaching this total value.

Figure 5.3: Hybrid system simulated with HOMER to meet the demand of municipalities shown in Figure 5.1, with contribution obtained from ocean wave energy.

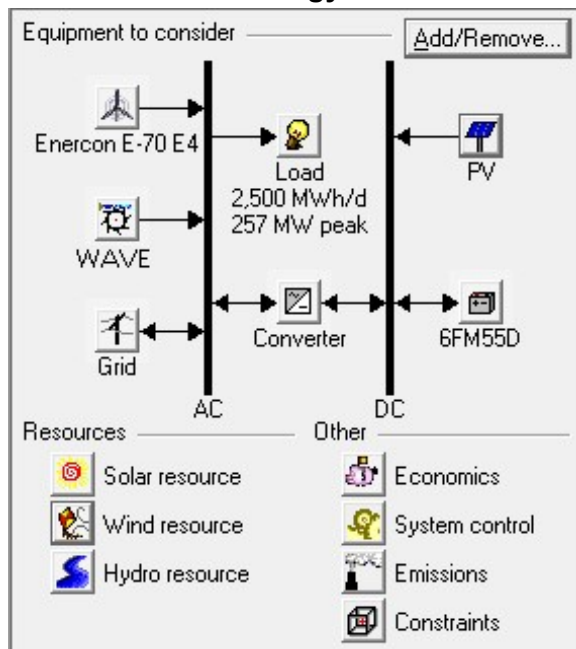


Figure 5.4: Demand for electricity in the municipalities shown in Figure 5.1. Above, average demand over the months of the year. Below, instant demand over the days of the year.

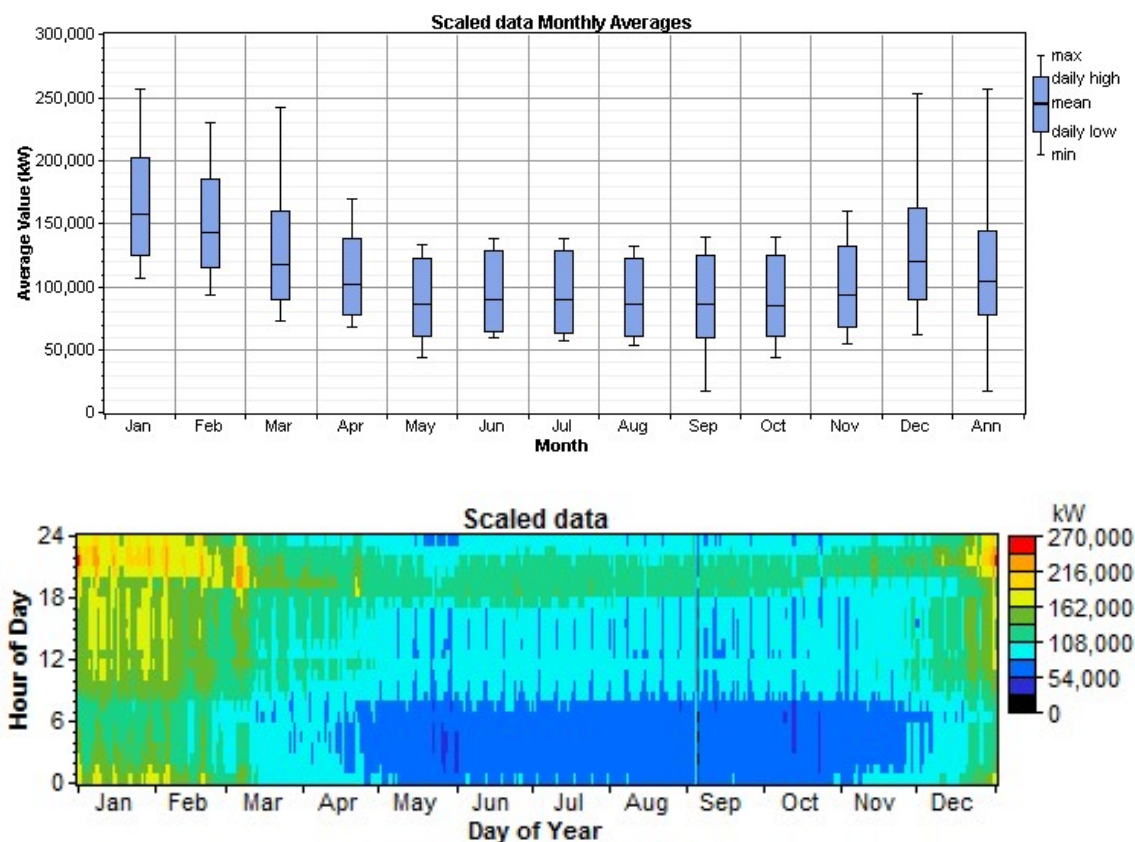


Figure 5.5: Wind resource available to wind farm in the system of Figure 5.3. Above, average wind speed over the months; below, instant wind speed over the days of the year.

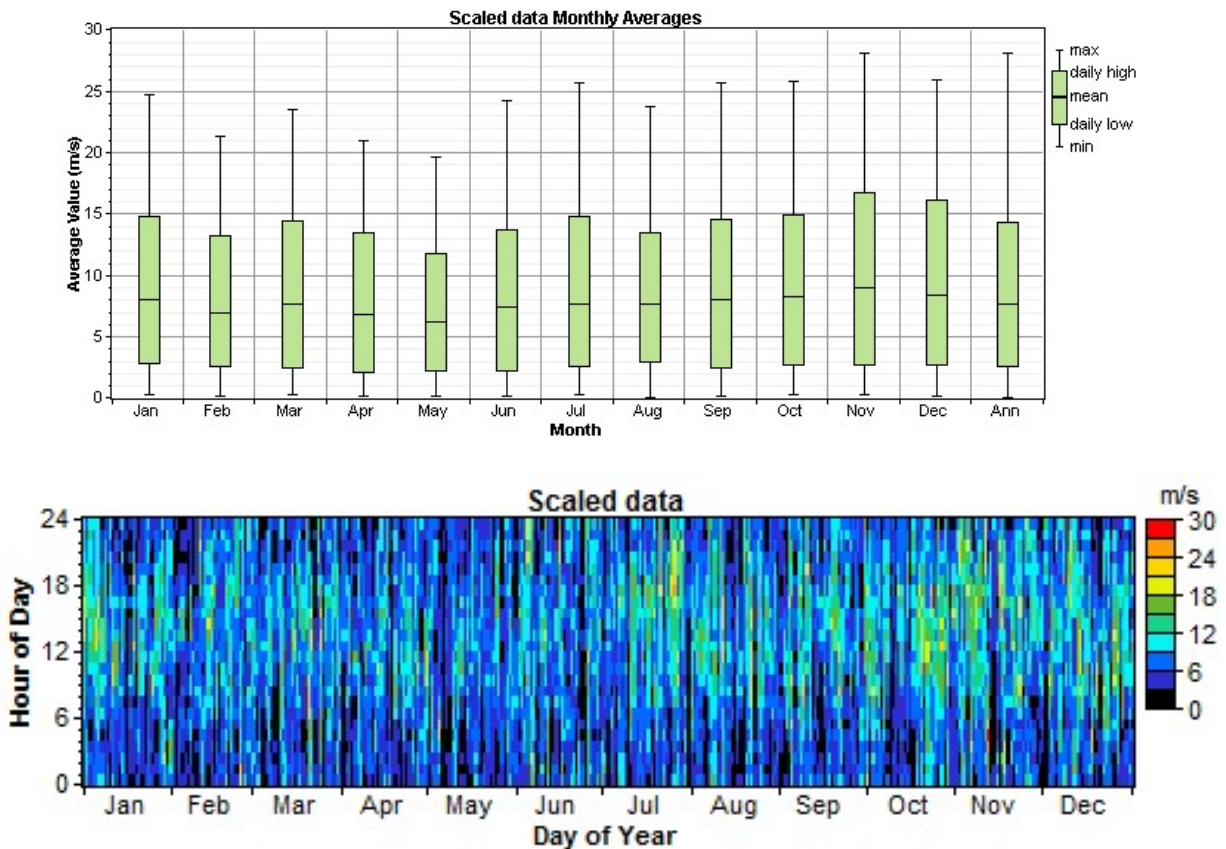
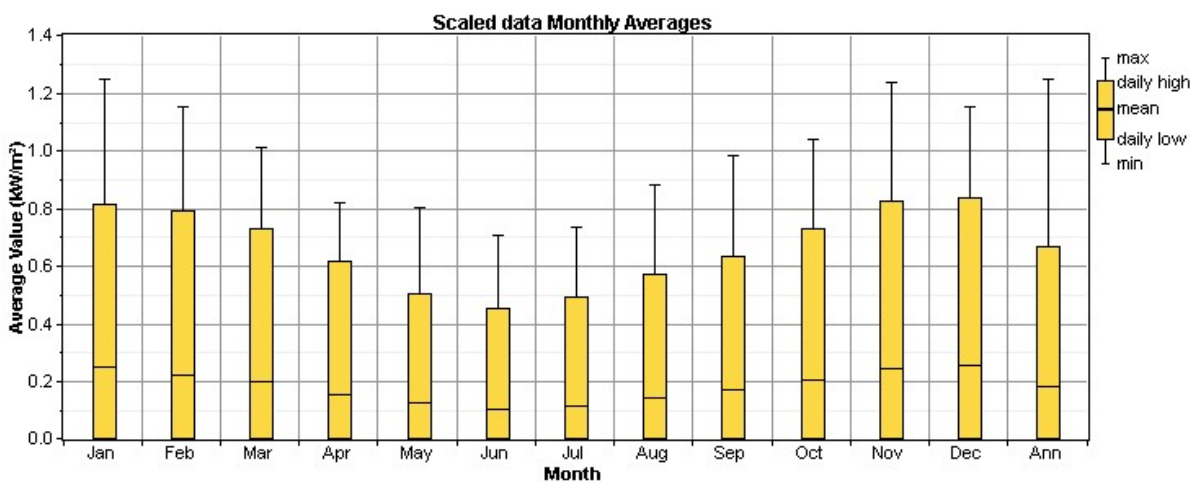
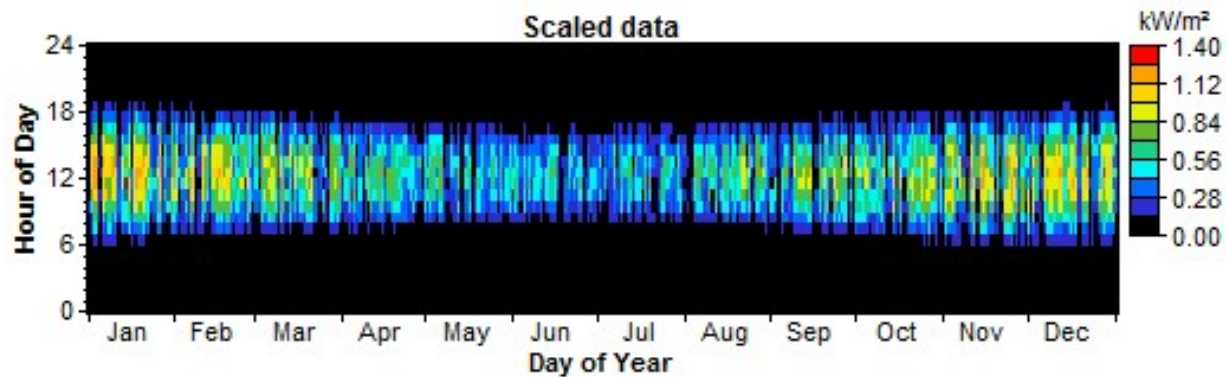


Figure 5.6: Solar resource available to PV modules in the system of Figure 5.3. Above, average incident radiation on a horizontal surface over the months; below, instant radiation on a horizontal surface over the days of the year.

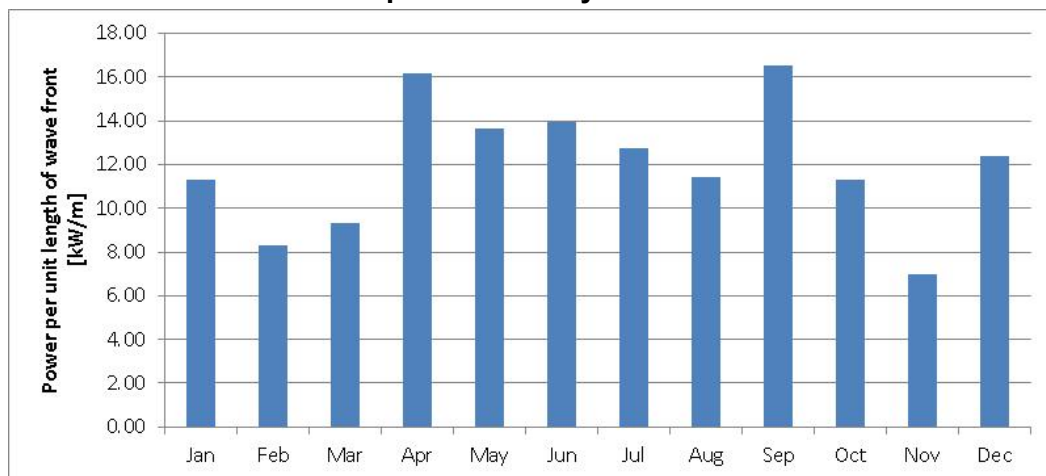


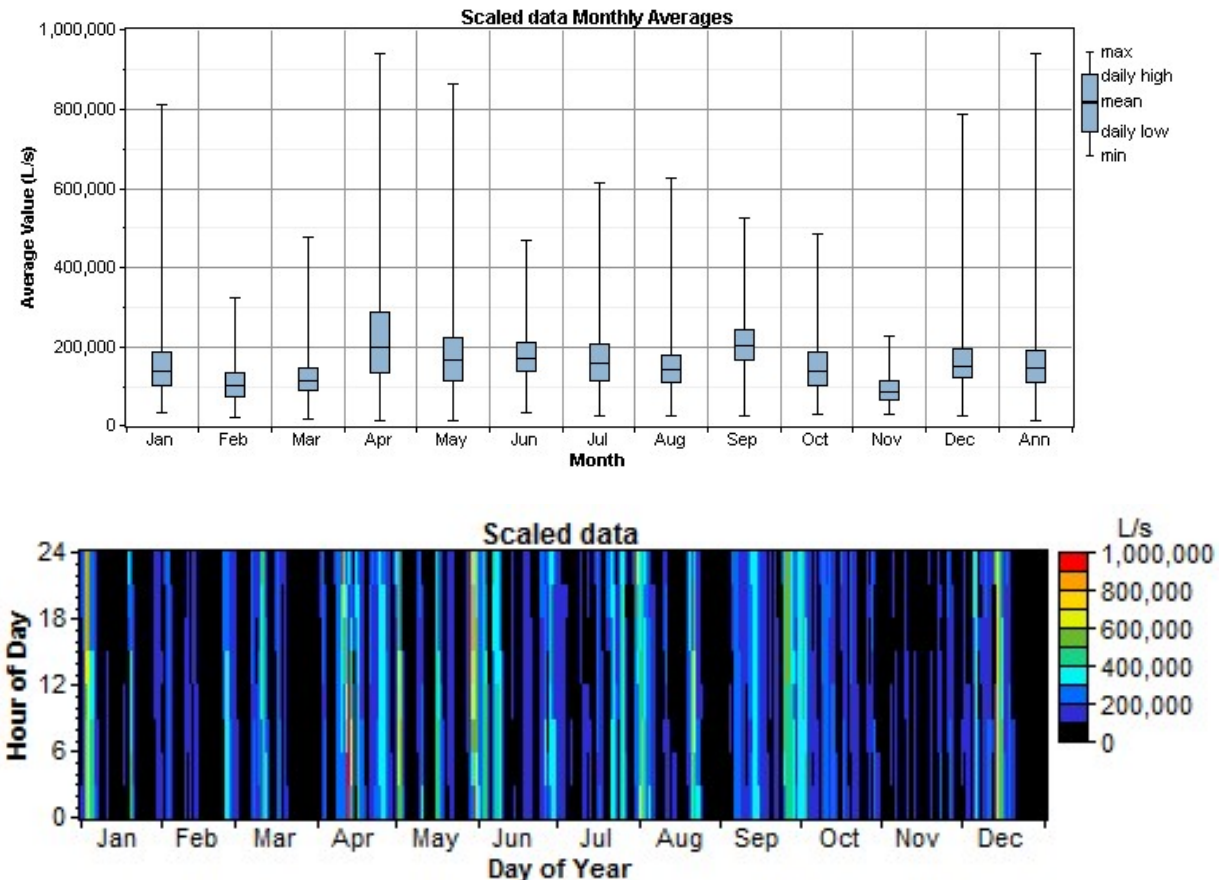


The wind turbines considered are Enercon E-70 E4, exactly the turbines operating at the wind farm installed in Osório. These turbines have a maximum capacity of 2000 kW, with towers with a height of 98 meters and with rotors with a diameter of 71 meters, operating in Osório with capacity factor of 34%. The simulations considered the possibility of 0 turbines, 25 turbines, 50 turbines and 75 turbines, with 75 turbines actually operating.

The “hydro” component of the system of Figure 5.3 is inserted to simulate the wave power plant, as described by Ref. [22]. Figure 5.7 shows the energy available for conversion into electricity. In this figure, above, average power available per meter of wave front is shown. In the middle, average resource over the months and, below, instant resource over the days of the year, both adapted for use by HOMER.

Figure 5.7: Wave energy resource available to the power plant in the system of Figure 5.3. Above, average power available per meter of wave front. In the middle, average resource over the months and, below, instant resource over the days of the year, adapted for use by HOMER.





The system includes an AC and a DC bus bars, with the first receiving supplies of wind generators and wave power plant and the second receiving PV generators. The electrical load is connected to the AC bus and battery bank to the DC bus, with the energy flow in both directions between the two buses made possible by converter devices.

The batteries considered in the simulations are batteries of the automotive type, with capacity of 55 Ah and voltage of 12 V, also for polarization of the PV modules. The simulations were performed with the possibilities of 0 batteries, 8,000 batteries, 16,000 batteries and 32,000 batteries, and the value selected in all simulations was the second one. This battery bank has a capacity of 2,048 MWh, equivalent to approximately 80% of the average daily consumption.

Simulations were performed for the following values for the optimization variables: 0 kW, 2,000 kW, 4,000 kW, 8,000 kW and 16,000 kW for PV modules; 0, 25, 50 and 75 wind turbines; 0, 2,000, 4,000, 8,000, 16,000 and 32,000 batteries; 0 kW, 10,000 kW and 20,000 kW for the converter capacity; 400,000 kW for the purchase capacity from the grid, when considered.

Simulations were performed for the following values for the sensitivity inputs: 5.5 m/s, 6.5 m/s, 7.5 m/s, 8.5 m/s and 9.5 m/s for the scaled annual average velocity of the wind, in addition to simulations for 7.62 m/s; USD\$ 50,000,000, USD\$ 150,000,000, USD\$ 250,000,000, USD\$ 350,000,000 and USD\$ 450,000,000 for initial capital cost, USD\$ 40,000,000, USD\$ 120,000,000, USD\$ 200,000,000, USD\$ 280,000,000 and USD\$ 360,000,000 for replacement cost and USD\$ 2,500,000, USD\$ 7,500,000, USD\$ 12,500,000, USD\$ 17,500,000 and USD\$ 22,500,000 for operating and maintenance costs of wave energy power plant, these latter two linked to the first; USD\$ 0.05 / kWh, USD\$ 0.10 / kWh and USD\$ 0.15 / kWh for the price of the purchased energy; 20%, 25%, 30%, 35% and 40% for the efficiency of the wave energy power plant; 10 kW/m, 11 kW/m, 12 kW/m, 13 kW/m, 14 kW/m and 15 kW/m for ocean wave power per unit length.

A set of 360 simulations, with 2250 different values for the variables of sensitivity, were performed. The results are presented and discussed in the next section.

6. RESULTS AND DISCUSSION

Three sets of simulations were performed, corresponding to energy purchased from the grid with costs equal to USD\$ 0.05/kWh, USD\$ 0.10/kWh and USD\$ 0.15/kWh. The results corresponding to the simulations for energy purchased by USD\$ 0.10/kWh will be presented below, followed by graphs showing the results for these three sets of simulations. Results of sensitivity analysis applied to the efficiency of the ocean wave power plant as a function of the initial capital cost, the total capacity of the plant as a function of the initial capital cost and different values of wind speed against initial capital cost will be presented.

Figure 5.8 shows the optimization space for ocean wave power plant efficiency as a function of the initial capital cost, corresponding to average wind speed of 7,62 m/s, wave resource equal to 12 kW/m and energy from the grid equal to USD\$ 0.10/kWh. This optimization space indicates two kinds of system as a solution with a clear boundary between them. To the left of a sloping straight line, solutions indicate hybrid systems with wind and waves contribution, with connection to the grid. To the right, the solutions do not include wave energy contribution.

Figure 5.8: Optimization space for ocean wave power plant efficiency as a function of initial capital cost, corresponding to average wind speed of 7,62 m/s, wave resource equal to 12 kW/m and energy from the grid equal to USD\$ 0.10/kWh.

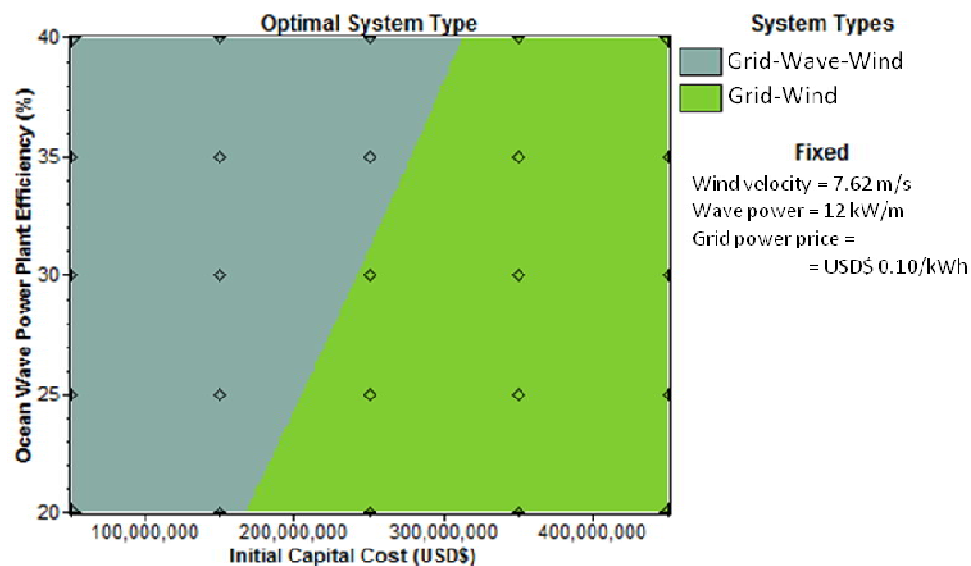


Figure 5.9 shows the cost of energy generated by the system being studied corresponding to the points of the optimization space of the Figure 5.8. The values for the cost of energy are between USD\$ 0.055/kWh and USD\$ 0.095/kWh, lying approximately between USD\$ 0.085/kWh and USD\$ 0.090/kWh on the limit of feasibility of solutions including wave energy contribution. These values obtained for the cost of energy generated by the system of Figure 5.3 are close to the values of the cost of energy purchased from the grid considered in the simulations.

Figure 5.10 shows the optimization space for ocean wave power per unit length as a function of the initial capital cost, corresponding to average wind speed of 7,62 m/s, ocean wave power plant efficiency equal to 30% and energy from the grid equal to USD\$ 0.10/kWh. This optimization space also indicates a clear boundary between two kinds of hybrid system. As in Figure 5.8, to the left solutions indicate hybrid systems with wave energy contribution and to the right solutions do not include wave energy contribution.

Figure 5.9: Cost of energy for ocean wave power plant efficiency as a function of initial capital cost, corresponding to average wind speed of 7,62 m/s, wave resource equal to 12 kW/m and energy from the grid equal to USD\$ 0.10/kWh.

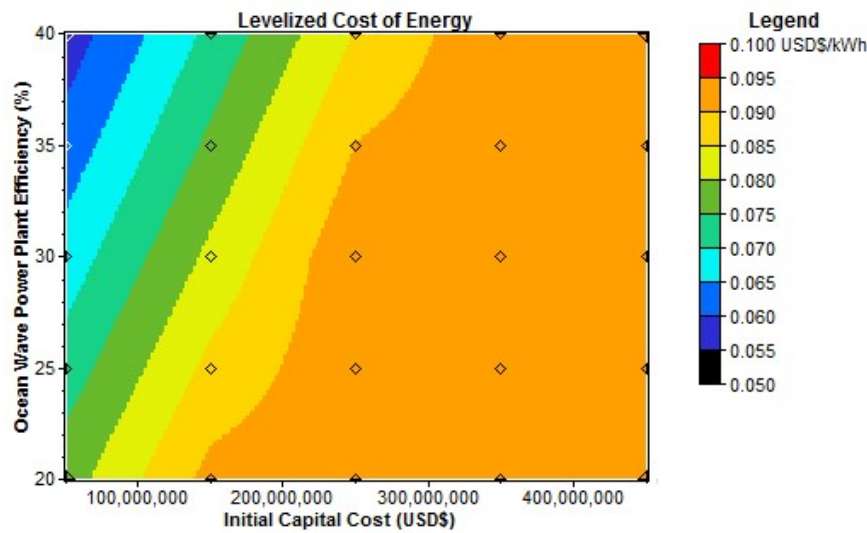


Figure 5.10: Optimization space for power per unit length as a function of initial capital cost, corresponding to average wind speed of 7,62 m/s, ocean wave power plant efficiency equal to 30% and energy from the grid equal to USD\$ 0.10/kWh.

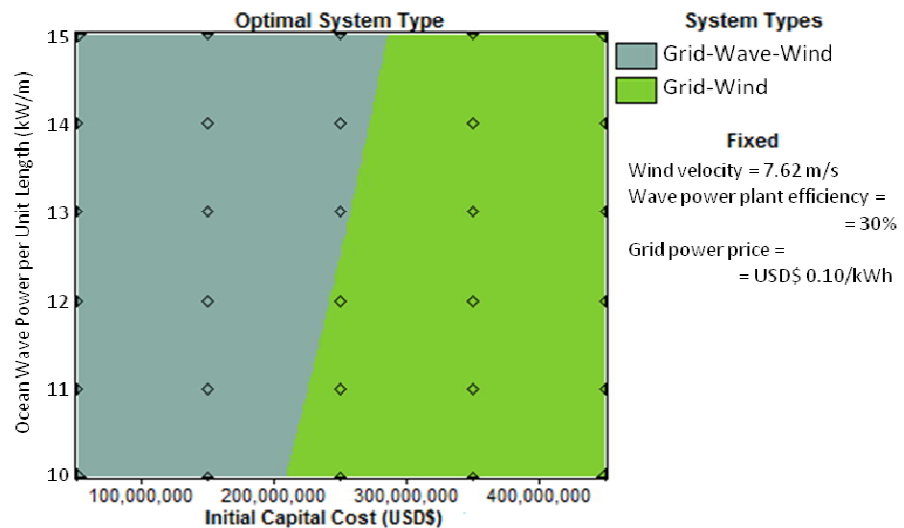
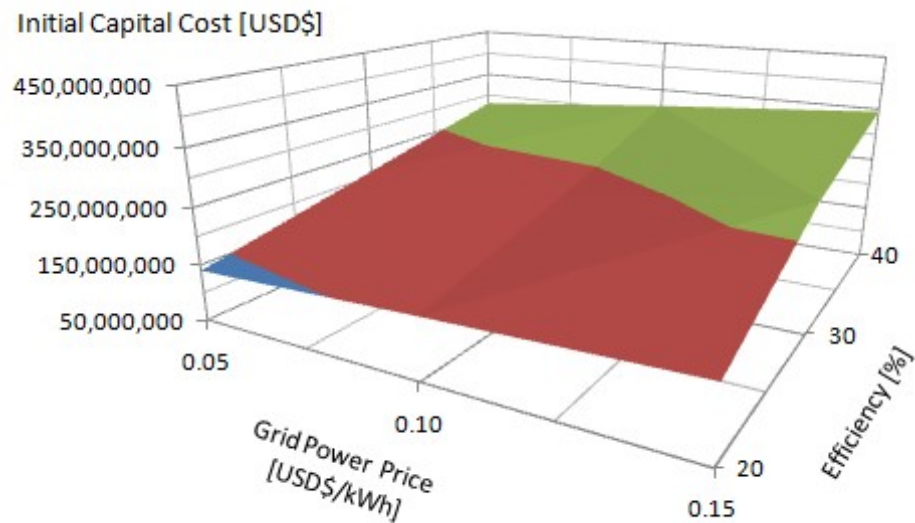


Figure 5.11 shows the influence of the cost of energy purchased from the grid on the boundary lines appearing in Figure 5.8 and Figure 5.10. A line in the center corresponds to the cost of energy equal to USD\$ 0.10/kWh and reproduces the results of Figure 5.8 and Figure 5.10. The line on the left shows the results corresponding to the cost of energy of USD\$ 0.05 per kWh and the line on the right shows the results corresponding to USD \$ 0.15 per kWh.

Figure 5.11: Upper limit of feasibility for the system of Figure 5.3, considering the initial capital cost of the hybrid system as a function of grid power price and ocean wave power plant efficiency, with wind speed equal to 7.62 m/s.



It is important to note that the colors in this figure do not identify different systems or different leveled costs, as in the previous figures. In this figure, the three colors differentiate systems costing less than USD\$ 150,000,000, systems with costs between USD\$ 150,000,000 and USD\$ 250,000,000 and systems with costs greater than USD\$ 250,000,000.

Table 5.1 gathers the results shown in the previous figures corresponding to the energy cost from the grid (in this table, COEg) equal to USD\$ 0.10/kWh and also shows similar results for USD\$ 0.05/kWh and USD\$ 0.15/kWh, not shown in figures. This table shows that wave power plants will be feasible, for energy at USD\$ 0.05 / kWh, if they can be implemented with costs between USD\$ 616.01 / kW and USD\$ 1,301.65 / kW respectively for efficiencies (in this table, Eff) between 20% and 40%. For energy at USD\$ 0.10 / kWh, these costs are equal to USD\$ 1,109.84 / kW and USD\$ 2,079.48 / kW, and for USD\$ 0.15 / kWh, they are equal to USD\$ 1,552.70 / kW and USD\$ 2,865.37 / kW.

These values are extremely low, comparable to values for already mature alternatives such as hydropower and wind energy, which may be due to the values adopted for the energy cost of the grid and to the efficiencies projected for the energy conversion devices. These two parameters, one external and the other internal to the project, are very important for the feasibility of any power generation project. The values adopted for the energy price can be considered low, but they are close to the

values practiced in Brazil and their relation with the final results show a tendency of its influence on the feasibility of the system being studied.

Table 5.1: Results delimiting the feasibility space for ocean wave power plants in southern Brazil.

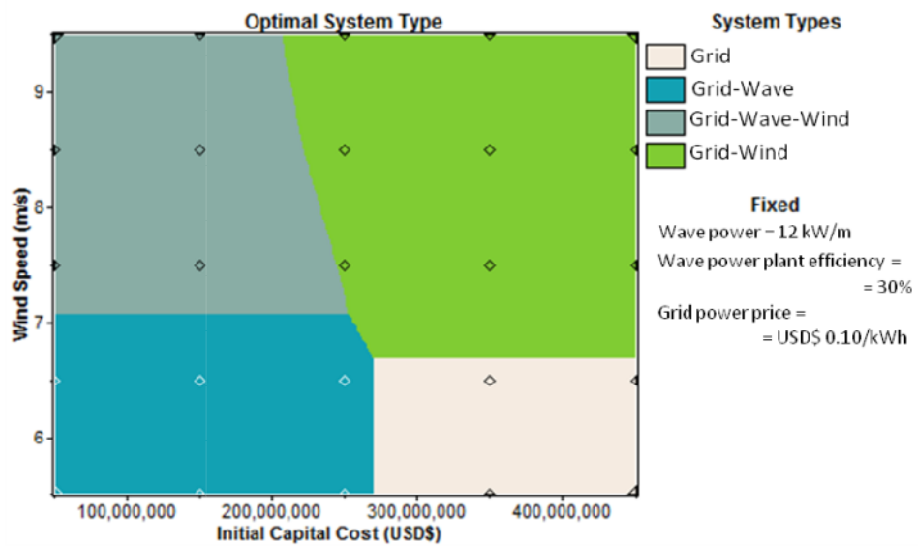
COE [USD\$]	Eff. [%]	Limit of feasibility		COEg [USD\$]
		[USD\$]	[USD\$/kW]	
0.15	40	429,805,626.60	2,865.37	0.120
	30	335,401,534.53	2,236.01	0.118
	20	232,905,370.84	1,552.70	0.118
0.10	40	311,922,569.29	2,079.48	0.094
	30	241,871,975.36	1,612.48	0.093
	20	166,476,022.88	1,109.84	0.093
0.05	40	195,247,807.46	1,301.65	0.048
	30	135,148,356.91	900.99	0.048
	20	92,401,361.27	616.01	0.047

Legend: COE is the cost of grid energy, Eff is the efficiency and COEg is the cost of energy generated.

Figure 5.12 shows the optimization space for different values of wind speed against initial capital cost, corresponding to wave resource equal to 12 kW/m, ocean wave power plant efficiency equal to 30% and energy from the grid equal to USD\$ 0.10/kWh. A section of this optimization space at a wind speed of 7.62 m/s corresponds to the results shown in Figure 5.8 for ocean wave power plant efficiency equal to 30% and in Figure 5.9 for power per unit length equal to 12 kW per meter.

This graph shows a higher number of solutions compared to the previous graphs. Solutions with only connection to the grid correspond to the lower wind speeds and systems with higher initial costs. Solutions with wave energy contribution and connection to the grid correspond to the lower wind speeds and systems with lower initial costs. Wind speeds exceeding 7.62 m/s show results quite similar to the previous figures. The two areas on the left are composed of solutions including wave energy contribution.

Figure 5.12: Optimization space for wind speed against initial capital cost, corresponding to wave resource equal to 12 kW/m, ocean wave power plant efficiency equal to 30% and energy from the grid equal to USD\$ 0.10/kWh.



CONCLUSION

This paper proposed the determination of a time-dependent feasibility space for renewable energy resources still under development as a tool for technology managers. This article also established a feasibility space for power generation from ocean waves on the southernmost coast of Brazil, with simulations with well-known HOMER software. The results indicate that, for the conditions considered in the simulations, wave power plants will be feasible, for energy at USD\$ 0.05 / kWh, if they can be implemented with costs between USD\$ 616.01 / kW and USD\$ 1,301.65 / kW respectively for efficiencies between 20% and 40%. For energy at USD\$ 0.10 / kWh, these costs are equal to USD\$ 1,109.84 / kW and USD\$ 2,079.48 / kW, and for USD\$ 0.15 / kWh, they are equal to USD\$ 1,552.70 / kW and USD\$ 2,865.37 / kW.

CONSENT FOR PUBLICATION

Not applicable.

CONFLICT OF INTEREST

The authors declare no conflict of interest, financial or otherwise.

ACKNOWLEDGEMENTS

This work was developed as a part of research activities on renewable energy developed at the Instituto de Pesquisas Hidráulicas, Universidade Federal do Rio Grande do Sul. The authors acknowledge the support received by the institution. The last author acknowledges the financial support received from CNPq for his research work (proc. n. 309021/2014-6).

REFERENCES

- [1] DANGERMAN, A. T. C. J.; SCHELLNHUBER, H. J. Energy systems transformation. **Proceedings of the National Academy of Sciences**, United States of America, v. 110, n. 7, p. E549-E558, 2013. <https://doi.org/10.1073/pnas.1219791110>.
- [2] van den BERGH , J. C. J. M. Policies to enhance economic feasibility of a sustainable energy transition. **Proceedings of the National Academy of Sciences**, United States of America, v. 110, n. 7, p. 2436-2437, 2013. <https://doi.org/10.1073/pnas.1221894110>.
- [3] ARTHUR, W. B. Competing technologies, increasing returns and lock-in by historical events. **The Economic Journal**, v. 99, n. 394, p. 116-131, 1989. <https://doi.org/10.2307/2234208>.
- [4] GEELS, F. W. Technological transitions as evolutionary reconfiguration processes: a multi-level perspective and a case-study. **Research Policy**, v. 31, n. 8-9, p. 1257-1274, 2002. [https://doi.org/10.1016/S0048-7333\(02\)00062-8](https://doi.org/10.1016/S0048-7333(02)00062-8).
- [5] ASTARIZ, S.; IGLESIAS, G. The economics of wave energy: a review. **Renewable and Sustainable Energy Reviews**, v. 45, p. 397-408, 2015. <https://doi.org/10.1016/j.rser.2015.01.061>.
- [6] KELLY, A. C.; MERRITT, J. A. Hybrid systems: a review of current and future feasibility. **The Electricity Journal**, v. 27, n. 9, p. 97-104, 2014. <https://doi.org/10.1016/j.tej.2014.10.008>.
- [7] TWIDELL, J.; WEIR, T. **Renewable Energy Resources**. 3. ed. London: Routledge, 2015. <https://doi.org/10.4324/9781315766416>.
- [8] SØRENSEN, B. **Renewable Energy: Physics, Engineering, Environmental Impacts, Economics & Planning**. 4. ed. Boston: Academic Press, 2011. <https://doi.org/10.1016/C2009-0-30432-8>.
- [9] GODDIJN-MURPHY, L.; MÍGUEZ, B. M.; MCILVENNY , J.; GLEIZON, P. Wave energy resource assessment with AltiKa satellite altimetry: a case study at a wave energy site. **Geophysical Research Letters**, v. 42, n. 13, p. 5452-5459, 2015. <https://doi.org/10.1002/2015GL064490>.
- [10] BELUCO, A.; SOUZA, P. K.; KRENZINGER, A. A dimensionless index evaluating the time complementarity between solar and hydraulic energies. **Renewable Energy**, v. 33, n. 10, p. 2157-2165, 2008. <https://doi.org/10.1016/j.renene.2008.01.019>.
- [11] BELUCO, A.; SOUZA, P. K.; KRENZINGER, A. A method to evaluate the effect of complementarity in time between hydro and solar energy on the performance

- of hybrid hydro PV generating plants. **Renewable Energy**, v. 45, p. 24-30, 2012. <https://doi.org/10.1016/j.renene.2012.01.096>.
- [12] ASSIS, L. E.; BELUCO, A.; ALMEIDA, L. E. B. On the wave energy potential along the southern coast of Brazil. **International Journal of Energy and Environment**, v. 5, n. 1, p. 59-66, 2014. <http://doi.org/10.5935/2076-2909.20140002>.
- [13] SILVA , J. S. **Feasibility of power generation from ocean waves along the north coast of Rio Grande do Sul**: case study of a renewable energy hybrid system (in Portuguese). 2012. 117 p. Dissertation (Master in Water Resources and Environmental Sanitation) – Instituto de Pesquisas Hidráulicas. Universidade Federal do Rio Grande do Sul, Porto Alegre, Brazil.
- [14] Tramandaí. Available at: <<https://goo.gl/maps/Ly8MKQbt6G92>>.
- [15] Laguna. Available at: <<https://goo.gl/maps/GtCA6sJh84x>>.
- [16] Chuí river. Available at: <<https://goo.gl/maps/FdoAq5Wn2h12>>.
- [17] Quintão beach. Available at: <<https://goo.gl/maps/XsH8dJ6U7412>>.
- [18] São José do Norte. Available at: <<https://goo.gl/maps/ZXtkh8jDofo>>.
- [19] HOMER Legacy Software, version 2.68 Beta. The Micropower Optimization Model. HOMER Energy, 2009. Available at: <<https://www.homerenergy.com/>>.
- [20] LAMBERT, T.; GILMAN, P.; LILIENTHAL, P. Micropower system modeling with HOMER. In: FARRET, F. A.; SIMÕES, M. G. (Eds.). **Integration of Alternative Sources of Energy**. Hoboken, New Jersey: John Wiley & Sons, Inc., 2006. Ch. 15, p. 379-418. <https://doi.org/10.1002/0471755621.ch15>.
- [21] LILIENTHAL, P.; LAMBERT, T.; GILMAN, P. Computer Modeling of Renewable Power Systems. In: CLEVELAND, C. J. (Ed.). **Encyclopedia of Energy**. Elsevier, 2004. Vol. 1, p. 633-647. <https://doi.org/10.1016/B0-12-176480-X/00522-2>.
- [22] SILVA, J. S.; BELUCO, A.; ALMEIDA, L. E. B. Simulating an ocean wave power plant with HOMER. **International Journal of Energy and Environment**, v. 5, n. 5, p. 619-630, 2014. <https://doi.org/10.5935/2076-2909.20140001>.

6. Artigo 2

A 'feasibility space' as a goal to be achieved in the development of new technologies for converting renewable energies

Jones S. Silva^a, Fausto A. Canales^b and Alexandre Beluco^a

^a Instituto de Pesquisas Hidráulicas (IPH), Universidade Federal do Rio Grande do Sul (UFRGS), Porto Alegre, Rio Grande do Sul, Brazil

^b Department of Civil and Environmental, Universidad de la Costa, Barranquilla, Atlantico, Colombia

Journal: MethodsX

Published online: 12 June, 2020

DOI: 10.1016/j.mex.2020.100960

ABSTRACT

This method article proposes the establishment of a feasibility space as an objective to be achieved during the development of new technologies to convert energy from renewable resources. The feasibility space can also be a reference when designing an energy system based on renewable resources. The feasibility space is a set of parameter values for the design stage that define the economic and technical feasibility of an energy system or a new technology, which must be satisfied when the energy system comes into operation or when the new technology for converting power goes into operation. The study of possible feasibility spaces allows characterizing energy systems or new technologies as attractive investments, or, on the other hand, as unfeasible ventures.

- The method proposes to establish a goal to achieve during the development of technologies for energy conversion.
- The method provides a benchmark for both the stages of design and development of generation systems and new technologies.
- The feasibility space constitutes a planning tool for power systems based on renewable resources of any size.

ARTICLE INFO

Method Name: Feasibility space method, for determining the feasibility limits for the implementation of a generating plant based on renewable energy.

Keywords: renewable energy; feasibility space; hybrid energy systems; new technologies.

Specifications table

Subject Area	<i>Energy</i>
More specific subject area	<i>Renewable Energy – Hybrid Energy Systems</i>
Method name	<i>Feasibility space method, for determining the feasibility limits for the implementation of a generating plant based on renewable energy</i>
Name and reference of the original method	<i>Characterization of a feasibility space for a new technology – a case study of wave energy in southern Brazil. Silva et al. [1]. Current Alternative Energy (2018), v. 2, n. 2, p. 112-122.</i>
Resource availability	<i>N/A</i>

Method details

Background

Among the various sources of renewable energy, hydroelectric, solar and wind energy have reached technical and economic maturity for their exploitation over the past decades. The exploitation of other renewable resources is still under development, such as wave energy and tidal energy. The work of Silva and Beluco [1] aimed at identifying attractive investments for the development of appropriate technology for the energy exploration of ocean waves on the northern coast of the State of Rio Grande do Sul, in southern Brazil. Previous studies [2] had indicated a potential for energy in ocean waves that can be considered attractive for investors from the energy sector.

However, the attractiveness level of this investment depends on the characteristics of the energy system in which the devices for converting wave energy are connected. Based on this context, the concept of feasibility space [1] was developed. This space of optimal solutions can change over time and depends on the energy system to which the hybrid system under study or the new technology under development is connected.

The feasibility space establishes a limit for parameters related to the project and which must be reached so that the investment in the energy system or in the technology under development is attractive. The feasibility space must be seen as an objective to be achieved with an adequate project for an energy system or with the

development of a new technology, under penalty of not making the enterprise viable.

The notion of feasibility space is a tool intended to contribute to greater agility in the evaluation of the technical and economic viability of investments in projects involving renewable energy resources. New technologies can easily be included in studies, for example, of systems that take advantage of complementarity between variable renewable sources [3]. Attention to the issue of 'complementarity' has grown considerably in recent years [4].

Method

The method for determining the feasibility space consists of the following five steps. Figure 6.1 shows a flow chart associated with these steps. The notes presented after each step below are related to the application example presented in the following section.

1. Establish the characteristics of the study to be carried out and the feasibility space to be configured, characterizing the hybrid energy system to be designed or the new technology to convert energy from renewable resources to be developed.

Note. As an important first step in any study of this kind, the example in the next section corresponds to a feasibility study for a technology that is under development, in the case related to the use of ocean wave energy.

2. Establish the parameters that can define the feasibility space of the energy system under analysis or the new technology under development and set the range of values for those parameters that may contain the feasibility limits.

Note. Usually, these parameters can be the initial capital cost, the grid power price, the efficiency, among others. The example below involves these variables and the ranges of values for each variable appear on the axes of the graph in Figure 6.2.

3. Perform simulations of the energy system under analysis or the new technology under development (with software such as HOMER) to determine optimal solutions, within the intervals established for the feasibility analysis.

Note. The example below corresponds to a study that was carried out with HOMER and Ref. [1] shows the results obtained and the construction of the corresponding feasibility space.

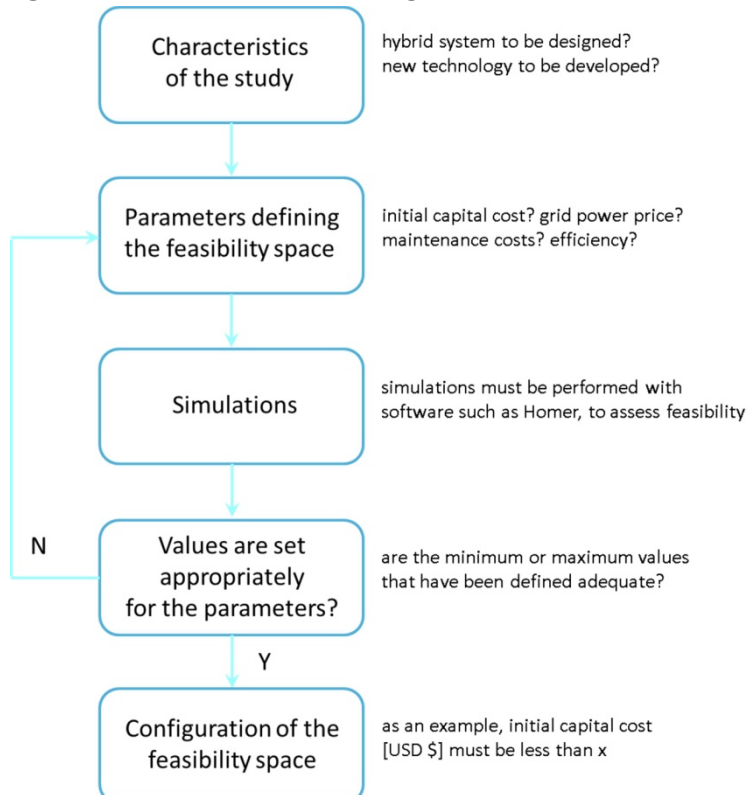
4. If the results of the simulations indicate that some of the optimal solutions correspond to some value outside the ranges established in item 2 above, return to item 2 and reformulate the estimates for the ranges that define the feasibility space.

Note. The study corresponding to the example below started from relatively wide intervals and there was no need for a feedback process to obtain better precision in the intervals to be considered in the results.

5. Considering the final results of item 3 above, configure the feasibility space for the hybrid energy system to be designed or the new technology for converting energy from renewable resources to be developed.

Note. The results can then be used to configure the feasibility space. In the case of the example below, the space is configured below the surface shown in Figure 6.2. In projects involving more than three variables, a study should show the most appropriate way to present the results, with several graphs showing the variables in two and in three dimensions.

Figure 6.1: Flowchart showing the steps of the method.



Application example

The original article [1] presenting the concept of feasibility space studied the investment viability for the development of devices for converting ocean wave energy on the southern coast of Brazil. The study carried out for the configuration of the feasibility space was based on simulations with the well-known [5] HOMER Legacy software [6].

Following step 1 of the method described above, the work to be done in this case consists in determining a feasibility space for a new developing technology for converting ocean wave energy on the coast of southern Brazil. Following step 2, the variables that define the feasibility of the project, in this case, are the initial capital cost, the grid power price and the conversion efficiency.

This design problem involves only three variables, according to the analysis presented in Ref. [1], and for that reason the results can be presented more simply in a single graph (shown in Figure 6.2). A problem involving more variables should have its results presented in several graphs, with two and three variables each graph, seeking to better characterize the feasibility space.

The ranges of variation established for these variables, intending to delimit the feasibility space, are as follows: initial capital cost ranging between USD\$ 50,000,000 and USD\$ 450,000,000; grid power price ranging between USD\$ 0.05 per kWh and USD\$ 0.15 per kWh; and the efficiency ranging between 20% and 40%. These values appear as limits in the figure below.

The next step consists of simulations performed with HOMER Legacy software. This software simulates hybrid systems [7-8] over a year and selects as optimal solutions those with the lowest total net present cost over the analysis time, which is equal to 25 years in this case. The paper of Silva and Beluco [1] describes the simulations and shows how the feasibility space was built.

The results of the simulations indicated that the ranges of variation of the variables, as established above, were adequate. The results were then used to configure the feasibility space, as shown in Table 6.1 and Figure 6.2. The simulated system is a PV-wind hybrid system operating near the coast and receiving energy from this hypothetical ocean wave power plant.

Then, the fulfillment of step 4 occurs when the results of the simulations are evaluated. If the results are considered adequate for configuring the feasibility space, then proceed to step 5. If the results are not sufficient, then it is necessary to return to step 2, define new intervals for the variables necessary to establish the feasibility space, and then go to step 3 and redo the simulations.

With the simulations completed and the results considered adequate, then step 5 can be achieved. The results must be presented in the most appropriate way to configure the feasibility limits of the system under study. An appropriate combination of two and three-dimensional graphics, if the problem involves a large number of variables, may be necessary.

Table 6.1 indicates the results for the initial capital cost, in USD\$, as a function of the cost of energy of the grid, in USD\$ per kWh, and the projected efficiency for the wave energy conversion system. The values for the cost of energy from the grid and efficiency correspond to the intervals established above. The values obtained for the initial cost, as can be seen, also appeared within the range established above. These values establish an upper limit for the feasibility of investing in ocean wave energy in the studied area. The table also shows the investment amounts, in USD\$, per installed kW.

Table 6.1: Results delimiting the feasibility space for ocean wave power plants in southern Brazil.

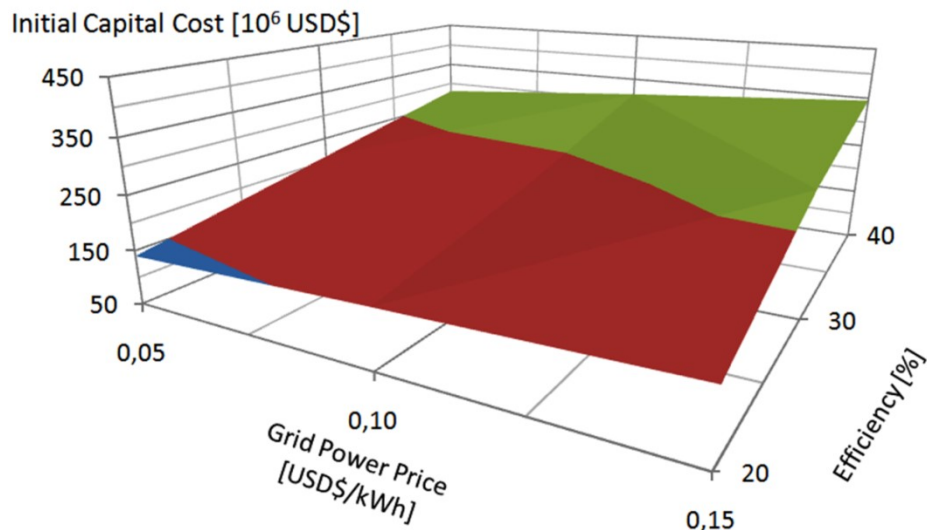
COE [USD\$]	Eff. [%]	Limit of feasibility [USD\$]	COEg [USD\$/kW]	COEg [USD\$]
0.15	40	429,805,626.60	2,865.37	0.120
	30	335,401,534.53	2,236.01	0.118
	20	232,905,370.84	1,552.70	0.118
0.10	40	311,922,569.29	2,079.48	0.094
	30	241,871,975.36	1,612.48	0.093
	20	166,476,022.88	1,109.84	0.093
0.05	40	195,247,807.46	1,301.65	0.048
	30	135,148,356.91	900.99	0.048
	20	92,401,361.27	616.01	0.047

Legend: COE is the cost of grid energy, Eff is the efficiency, and COEg is the cost of energy generated.

Figure 6.2 shows the limits that appear in Table 6.1, and they correspond to

average wind speed in the case study region set as 7.62 m/s in the simulation. The three different colors used to fill the surface that appears in this figure correspond to three different bands for the initial capital cost. The highest values for the initial capital cost associated with the highest values for the grid power price and the highest efficiency values, as can be observed.

Figure 6.2: Upper limit of feasibility for the system of Ref. [1], considering the initial capital cost of the hybrid system as a function of grid power price and efficiency of the ocean wave power plant, with average wind speed equal to 7.62 m/s.



This surface shows how the feasibility can be improved with equipment that has better efficiency in converting ocean wave energy, but this improvement comes at the expense of a higher initial investment cost for the acquisition of energy conversion devices. This surface can vary its position over time, both by the evolution of technologies for converting wave energy and by the evolution of other technologies involved in the hybrid system that includes a connection to the wave energy power plant connected.

Thus, an investment in a plant for converting energy from ocean waves on the southern coast of Brazil will be viable if the initial capital cost of the project, as a function of the grid power price and the final efficiency of the developed equipment, is lower than the values establishing the viability limit, as established in Table 6.1 and Figure 6.2. Thus, the feasibility space is an objective, a goal, to be achieved.

The data from this case study were cited in Ref. [9] and are available in the Mendeley data repository [10], specifically in Ref. [11].

Declaration of competing interest

The authors declare that they have no known competing financial interests or personal relationships that could have appeared to influence the work reported in this paper.

Acknowledgments

This work was developed as a part of research activities on renewable energy developed at the Instituto de Pesquisas Hidráulicas (IPH), Universidade Federal do Rio Grande do Sul (UFRGS). The authors acknowledge the support received by the institution. The last author acknowledges the financial support received from CNPq for his research work (proc. n. 312941/2017-0).

REFERENCES

- [1] SILVA, J. S.; BELUCO, A. Characterization of a Feasibility Space for a New Technology – A Case Study of Wave Energy in Southern Brazil. **Current Alternative Energy**, v. 2, n. 2, p. 112-122, 2018. <http://doi.org/10.2174/1570178615666180830102336>.
- [2] ASSIS, L. E.; BELUCO, A.; ALMEIDA, L. E. B. On the wave energy potential along the southern coast of Brazil. **International Journal of Energy and Environment**, v. 5, n. 1, p. 59-66, 2014. <http://doi.org/10.5935/2076-2909.20140002>.
- [3] BELUCO, A.; SOUZA, P. K.; LIVI, F. P.; CAUX, J. Energetic complementarity [of solar energy] with hydropower and the possibility of storage in batteries and water reservoirs. In: Sørensen, B. (Ed.). **Solar Energy Storage**. Academic Press, 2015. Ch. 7, p. 155-188. <https://doi.org/10.1016/B978-0-12-409540-3.00007-4>.
- [4] JURASZ, J.; CANALES, F. A.; KIES, A.; GUEZGOUZ, M.; BELUCO, A. A review on the complementarity of renewable energy sources: concept, metrics, application and future research directions. **Solar Energy**, v. 195, p. 703-724, 2020. <https://doi.org/10.1016/j.solener.2019.11.087>.
- [5] CONNOLLY, D.; LUND, H.; MATHIESEN, B. V.; LEAHY, M. A review of computer tools for analyzing the integration of renewable energy into various energy systems. **Applied Energy**, v. 87, n. 4, p. 1059-1082, 2010. <https://doi.org/10.1016/j.apenergy.2009.09.026>.
- [6] HOMER Legacy Software, version 2.68 Beta. The Micropower Optimization Model. HOMER Energy, 2009. Available at: <<https://www.homerenergy.com/>>.
- [7] LAMBERT, T.; GILMAN, P.; LILIENTHAL, P. Micropower System Modeling with HOMER. In: FARRET, F. A.; SIMÕES, M. G. (Eds.). **Integration of Alternative Sources of Energy**. Hoboken, New Jersey: John Wiley & Sons, Inc., 2006. Ch. 15, p. 379-418. <https://doi.org/10.1002/0471755621.ch15>.
- [8] LILIENTHAL, P.; LAMBERT, T.; GILMAN, P. Computer Modeling of Renewable Power Systems. In: CLEVELAND, C. J. (Ed.). **Encyclopedia of Energy**. Elsevier, 2004. Vol. 1, p. 633-647. <https://doi.org/10.1016/B0-12-176480-X/00522-2>.
- [9] BELUCO, A.; DURING FILHO, F. A.; SILVA, L. M. R.; SILVA, J. S.; TEIXEIRA, L. E.; VASCO, G.; CANALES, F. A.; ROSSINI, E. G.; SOUZA, J.; DARONCO, G. C.; RISSO, A. Dataset after Seven Years Simulating Hybrid Energy Systems with HOMER Legacy. **Data Science Journal**, v. 19, n. 1, art. 14, p. 1-8, 2020. <http://doi.org/10.5334/dsj-2020-014>.
- [10] BELUCO, A.; DURING FILHO, F. A.; SILVA, L. M. R.; SILVA, J. S.; TEIXEIRA,

- L. E.; VASCO, G.; CANALES, F. A.; ROSSINI, E. G.; SOUZA, J.; DARONCO, G. C.; RISSO, A. Seven years simulating hybrid energy systems with HOMER Legacy. **Mendeley Data**, v. 2, 2020. <http://doi.org/10.17632/ybxsttf2by.2>.
- [11] BELUCO, A.; DURING FILHO, F. A.; SILVA, L. M. R.; SILVA, J. S.; TEIXEIRA, L. E.; VASCO, G.; CANALES, F. A.; ROSSINI, E. G.; SOUZA, J.; DARONCO, G. C.; RISSO, A. Seven years simulating hybrid energy systems with HOMER Legacy. **Mendeley Data**, v. 2, 2020, file #09-silva-beluco-2018.hmr. Available at: <<https://data.mendeley.com/datasets/ybxsttf2by/2/files/32bddcad-0930-481f-a38e-19640b3d0863>>.

7. Artigo 3

A hydro PV hybrid system with hybrid storage in a water reservoir and compressed air – a case study in Southern Brazil

Jones S. Silva and Alexandre Beluco

Instituto de Pesquisas Hidráulicas (IPH), Universidade Federal do Rio Grande do Sul (UFRGS), Porto Alegre, Rio Grande do Sul (RS), Brazil

Journal:

Submission:

ABSTRACT. An alternative to improve the feasibility of energy generation projects based on renewable resources is the use of energy storage systems to reduce the effects of typical intermittency of these resources on the costs and performance of the generation system. This article is dedicated to the study of alternatives for the repowering of a dam in southern Brazil, called Laranjeiras. This dam was built in the 1960s and the original project for hydroelectric power generation was abandoned, for economic and financial reasons. A recent study proposed the implementation of a photovoltaic hybrid hydroelectric system, with less installed hydroelectric power and with photovoltaic modules installed on floating structures on the water surface, allowing the dam to be put back into operation. A subsequent study suggested using the reservoir for energy storage, with an even better feasibility result. Previous studies suggest the installation of a hydroelectric plant with a power house at the base of the dam, with a height of 20 m, operating at a flow rate of 9171 L/s, with a reservoir operating as an energy storage system, with a photovoltaic system of 360 kW and serving a load with demand of 40 MWh per day. This article studies the operation of the suggested generation system for the Laranjeiras dam operated with a hybrid storage system. This study was carried out with HOMER Legacy software and considers the use of the reservoir in conjunction with a compressed air storage system. The solution considered optimal operates with an energy cost of US\$ 0.021 per kWh and an implementation cost of US\$ 3,023,688.00.

Keywords: hybrid systems; energetic complementarity; hybrid energy systems; hydro PV hybrid systems; hybrid storage systems; PV modules on floating structures.

1. INTRODUCTION

This article has five chapters, in addition to this Introduction. The next chapter presents a review of the literature on energy storage in compressed air. The next chapter describes the Laranjeiras dam, where a hybrid system with hybrid storage including a compressed air storage system was designed. The fourth chapter is dedicated to simulations with HOMER software, describing the simulation of compressed air storage systems and describing the simulations performed for this paper. The subsequent two chapters present the results and discussions and the final conclusions.

2. COMPRESSED AIR ENERGY STORAGE (CAES)

Uncontaminated atmospheric air is composed of a mixture of gases, mainly nitrogen (N_2) and oxygen (O_2), which make up approximate percentages of 78 and 21%, respectively, at sea level [1]. The remainder, 1%, is mainly composed of the inert gas Argon (Ar) and also Carbon Dioxide (CO_2), in addition to several other gases [2]. The air is also composed of water, in the form of vapor, and may also contain pollutants, dust, ash, microorganisms, etc.

As it is a gas, air can be stored in a reservoir through a thermodynamic transformation called compression. Thus, for energy to be stored, it is necessary for the air to do work, that is, the air must be subjected to a pressure greater than atmospheric pressure. In this condition, there is an increase in the number of molecules per unit of volume, and an increase in the internal pressure in the reservoir. This compression process requires the use of an external energy source, and part of this energy is stored and returned to the system during the air expansion process. Therefore, energy storage systems in the form of large compressed air have basically two stages: compression and expansion. However, in both stages, energy losses are inevitable [1, 3, 4].

Compressed air energy storage (CAES) involves the conversion of electrical energy into high-pressure compressed air, which can be released at a time to drive a turbine generator to produce electricity, and, behind pumped hydroelectricity storage (PHS), is the second biggest form of energy storage currently [5].

One of the most promising mature energy storage technologies is compressed air energy. Some advantages are: fast response, high economic performance and small environmental impacts [6].

Different types of underground cavern can be exploited. Rock cavern excavated in hard rock or created by expanding existing underground mine workings is the most expensive. Salt caverns have been the ones usually used for gas storage, and this type of storage site occurs in many parts of the world. Underground porous rock formation offers the cheapest underground storage facility, but it is only suitable for gas storage if there is an impervious rock barrier covering the layer of porous rock. The pressure of the air in rock or salt caverns will vary as more air is added or released, considering a constant volume storage system. In contrast, water-bearing aquifers, or porous underground strata, from which oil or gas has been extracted, can be very attractive because the compressed air will displace water within the porous rock, creating a constant pressure storage system. These three types of structure require sound rock formations to prevent the air from escaping, and they also need to be sufficiently deep and strong to withstand the pressures imposed on them [7].

Two large-scale installations (Hunstorf, Germany and McIntosh, Alabama, United States) have proved the technical feasibility of CAES, but no plants have been constructed in recent years, and some planned large-scale CAES projects have been terminated/canceled or postponed, because of low round-trip efficiency and economics [8]. Both plants use underground salt caverns for storing the air, and also are classified as diabatic CAES systems [9].

To improve the CAES performance, Venkataramani and Ramalingam [6] introduced the concept of Poly-generation, in which there is simultaneous generation of hot energy from heat of compression, cool energy from expansion, and power from an alternator.

Hybrid systems composed by the integration of CAES systems with other energy systems have increasingly been analyzed in the literature in recent years, and the association of CAES installations with compact gas turbines has become the canon in this area of hybrid systems [10]. Hybridization is an appropriate solution to overcome renewable energy sources challenges such as intermittency nature [11].

Approaches where different renewable energy sources will operate under a synergetic approach need to be explored. Optimizing the complementarity among renewable energy systems both over time and spatially is a straightforward way to achieve that [12]. According to Gbadegesin *et al.* [13], the goal is to exploit the complementary characteristics of hybrid storage systems.

The main function of energy storage in renewable energy systems is to ensure power generation when renewable energy sources are unable to meet the load demand and make sure of energy generation when demand is low i.e. time-shifting and load leveling [14]. To replace completely conventional energy with renewable energy will require storage systems with very large capacities [10].

3. A HYDRO PV HYBRID SYSTEM IN LARANJEIRAS DAM, IN SOUTHERN BRAZIL

The focus of this work is the Laranjeiras dam, located in the municipality of Canela³, in the southernmost State⁴ of Brazil. The Laranjeiras dam was built in the 1960s and the corresponding hydroelectric power generation project was not completed, due to the national economic scenario, having been used for many years for tourism purposes. The dam was built on Paranhana⁵ river with 280 meters long and 10 meters high. Figure 7.1 shows a side view of the spillway, on the left, and the top of the dam and the water surface near the body of the dam, on the right.

In the original project, carried out by the extinct DNOS (National Department of Works and Sanitation), the Laranjeiras hydroelectric plant would be the third stage of the Salto System (which uses the waters of the Santa Maria⁶ River), downstream from the Bugres⁷ and Canastra⁸ hydropower plants, already in operation. The Laranjeiras reservoir is fed with the discharge flow from the Canastra hydroelectric plant [15]. The original project suggested the construction of a 5900 m channel up to an engine room, obtaining a total height of about 100 meters, providing about 7.5 MW, with a channel and pipe designed for a flow of 10 m³/s.

³ goo.gl/maps/z96fDJ7MxWtN8BFP6.

⁴ goo.gl/maps/XrGopSTTHUqwsQmq8.

⁵ goo.gl/maps/9iMY2kH8DpLmsHda7.

⁶ goo.gl/maps/rL18x9KSejv9EZoM6.

⁷ goo.gl/maps/wFgJsRWxEbKXjTiG9.

⁸ goo.gl/maps/PSnMbx4j3MJCP9JH9.

Figure 7.1: a) Lateral view of the spillway, on the left; b) water surface near the dam, on the right.



Vasco *et al.* [16] proposed a hydroelectric photovoltaic hybrid system to re-power the dam, now with a much lower generation target. Figure 7.2 shows the region of the dam shown in the link above, indicating a projection of the area occupied by the floating structures carrying the photovoltaic modules. This projection shows a relatively small area compared to the area occupied by the dam's surroundings, and may even receive a much larger number of photovoltaic modules.

Figure 7.2: Image of the Laranjeiras Dam and comparison of the dimensions of the PV panels placed on floating structures with the region near the dam.



The optimal solution consists of a hybrid energy system, implementing a hydroelectric plant at the base of the dam, with 1497 kW of installed capacity, operating simultaneously with a set of photovoltaic modules, on the water surface of the reservoir, with an installed capacity of 180 kW and connection to the grid with 400 kW of capacity, to meet the demand for consumer loads of up to 40 MWh per day. This hybrid system would result in a capital cost of US\$ 3,984.885 per kW and an energy cost of US\$ 0.026 per kWh.

Figure 7.3 shows the water resources available for hydroelectric generation in Laranjeiras. This is the flow released by the Canastra Hydroelectric Plant, which is the plant immediately downstream in the Salto System. This flow was considered the flow available for Laranjeiras hydroelectric plant, even though there is a contribution of a tributary of the river Paranhana which should correspond to approximately 10% of the released flow in Canastra.

Figure 7.3: Flow discharged by the Canastra Hydro Power Plant. Above, monthly minimum, average and maximum stream flow; below, the hourly distribution of stream flow throughout the year.

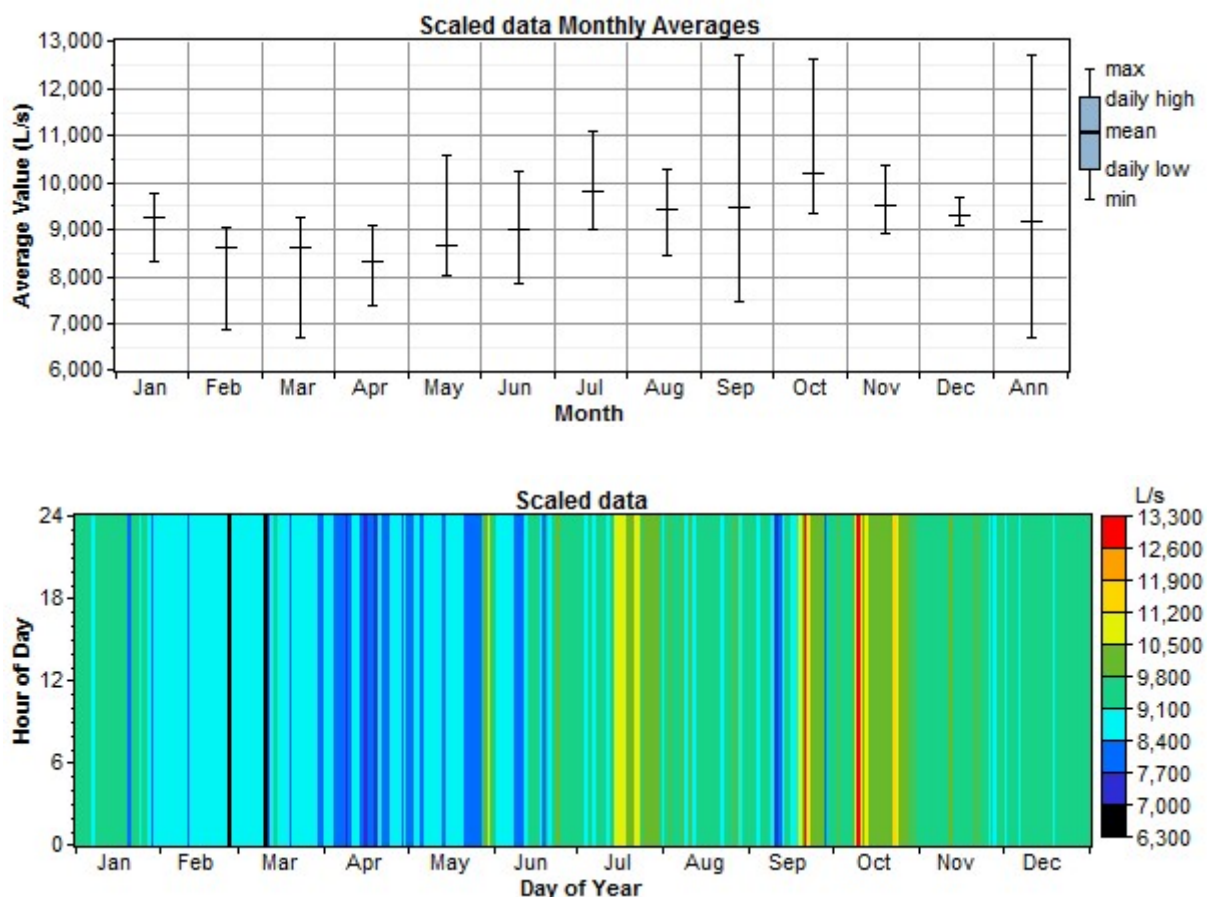
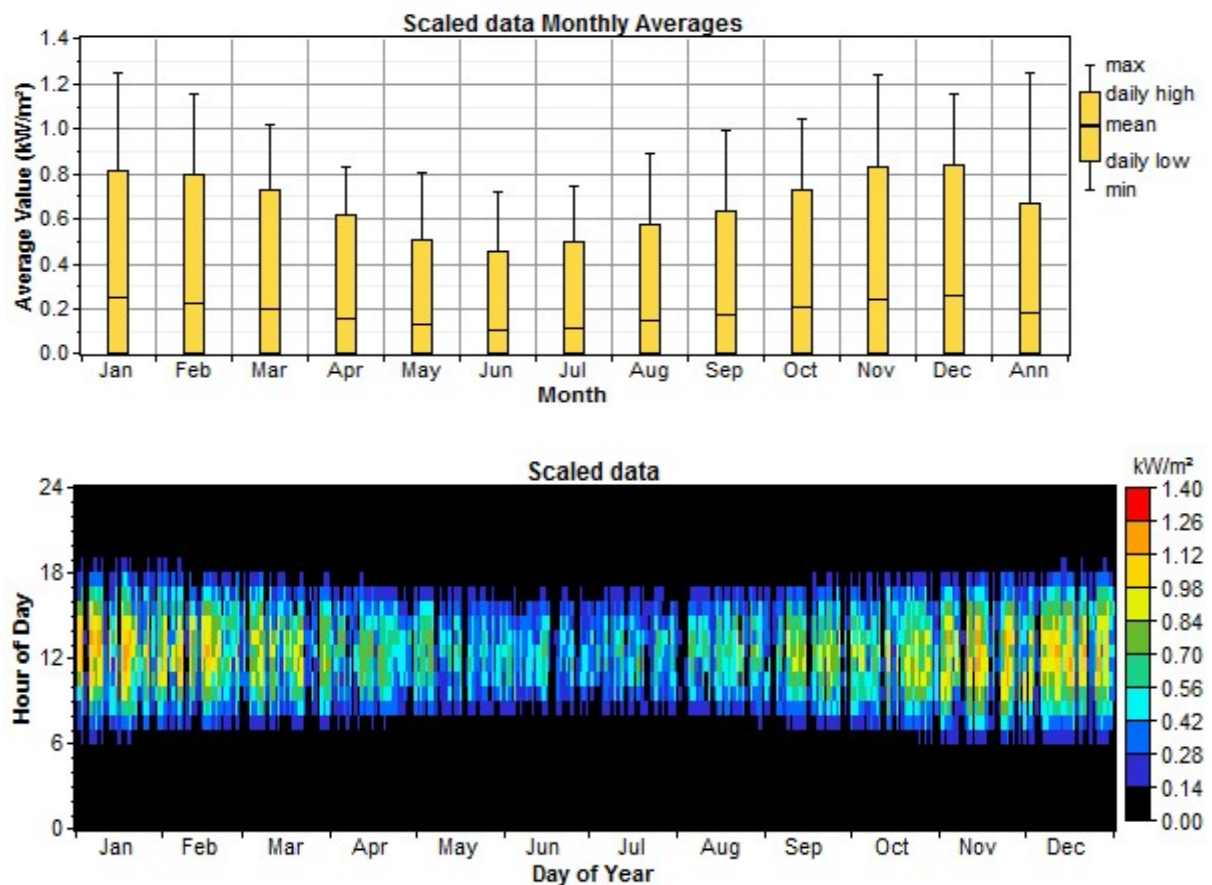


Figure 7.4 shows the solar radiation incident on a horizontal surface located at the Laranjeiras dam. This figure and the previous figure both show two graphs; above, a graph with minimum, average and maximum monthly values for the energy resource on screen; below, the hourly distribution over the days of the year of the monthly values of the energy resource on screen.

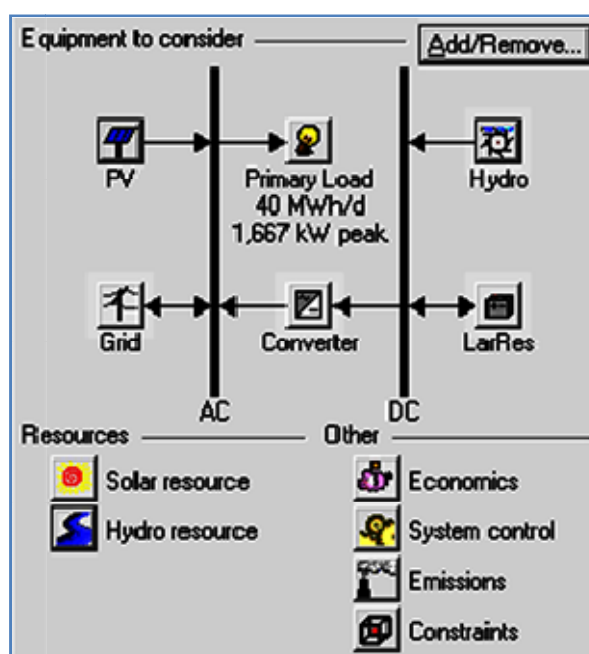
The paper of Vasco *et al.* [16] shows in its fourth figure a schematic diagram of the hydro PV hybrid system that was proposed. This hybrid system includes a hydroelectric power plant at the base of the Laranjeiras dam and photovoltaic modules, as well as a diesel support system and the possibility of storing energy in batteries. The diesel gen set and batteries did not appear in the optimal solutions obtained by HOMER Legacy.

Figure 7.4: Solar radiation incident on a horizontal plane, obtained with HOMER, for the location of the Laranjeiras Dam Power Plant. Above, monthly minimum, average and maximum solar radiation; below, the hourly distribution of solar radiation throughout the year.



Vasco *et al.* [17], in turn, proposed a system with energy storage in the water reservoir formed by the dam. Figure 7.5 shows a schematic diagram of the hydro PV hybrid system, showing the photovoltaic modules connected to the AC bus and the hydroelectric plant connected to the DC bus. The DC bus was actually used together with the batteries and the converter, to simulate a hydroelectric plant operating with energy storage in the form of water accumulated in the reservoir.

Figure 7.5: Schematic diagram of the hydro PV hybrid system proposed by Vasco *et al.* (2019b).



Energy storage in the reservoir was simulated as suggested by Canales *et al.* [18]. Figure 7.6 shows areas and volumes as a function of the water level in the reservoir. Figure 7.7 shows a screen of HOMER Legacy with information for reservoir simulation using the rechargeable battery model.

Figure 7.6: Areas and volumes as a function of height for the Laranjeiras dam.

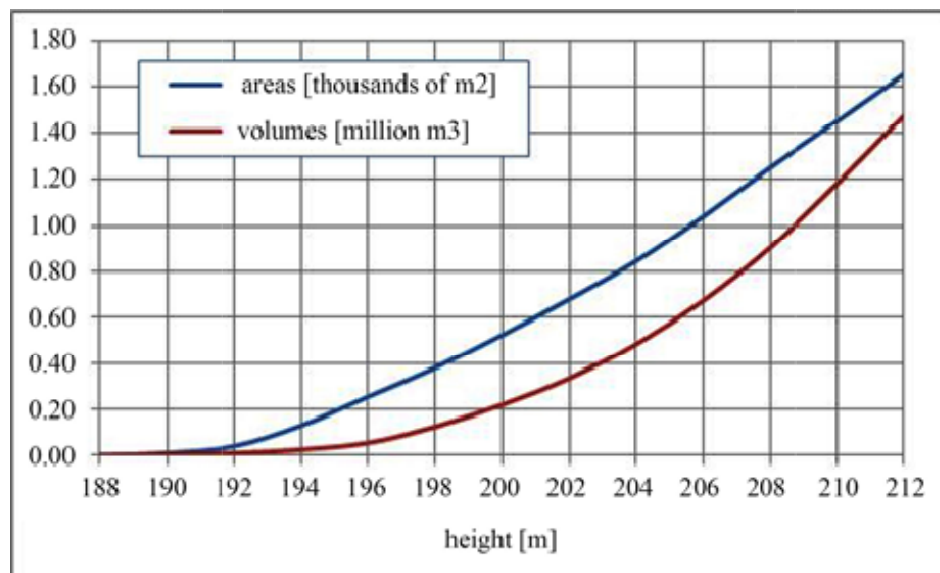
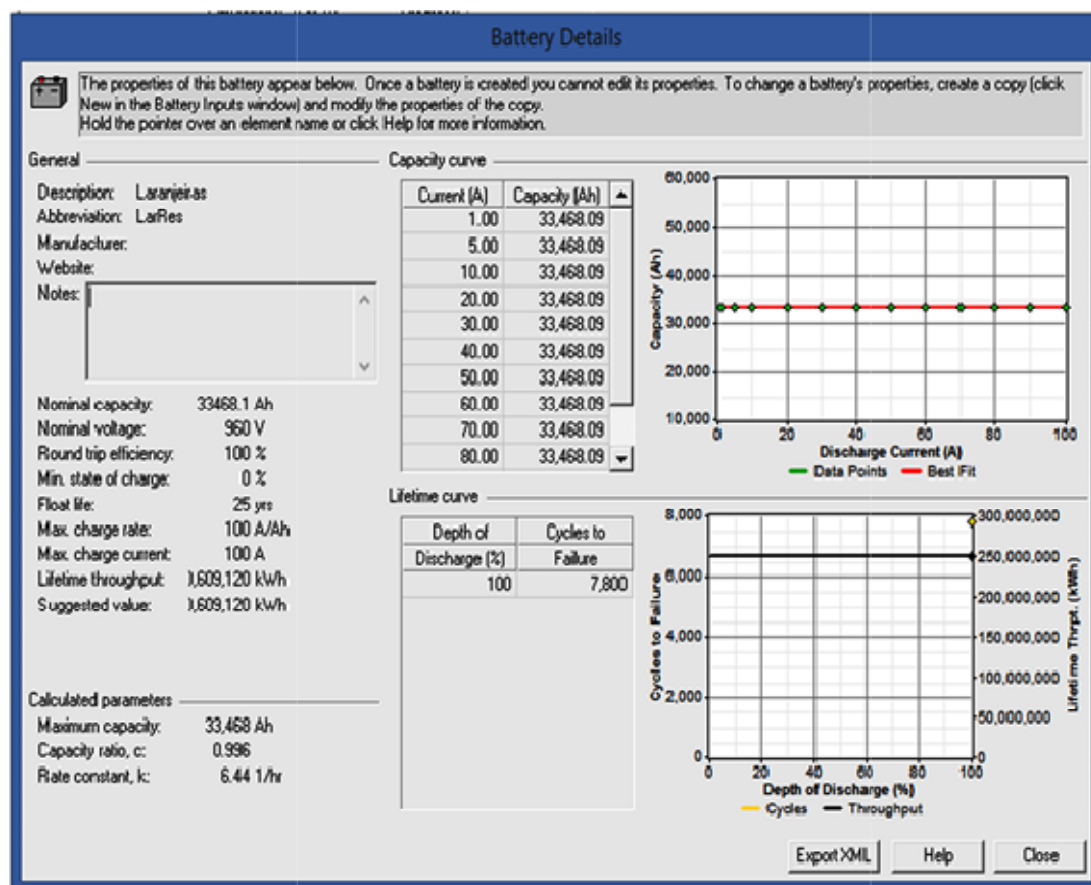


Figure 7.7: Configuration details of the rechargeable battery model, to simulate water reservoir.



4. SIMULATION WITH HOMER

This chapter briefly describes HOMER Legacy software and its application in this article to design a hybrid storage system and to achieve a better understanding of the performance of that system. The first section of this chapter briefly describes HOMER Legacy software and how it can be obtained and operated. The next section deals with the simulation of compressed air storage systems. HOMER Legacy does not present original packages that allow this direct simulation and the authors performed this simulation adapting one of the software models. The subsequent section describes the simulations performed for this work.

4.1. HOMER, The Micropower Optimization Model

HOMER Legacy [19] is a well-known software [20, 21] for simulation and optimization of small and micro hybrid energy systems, developed by NREL [22, 23] and then improved by HOMER Energy company. HOMER Legacy has been used extensively for several years [24, 25, 26, 27].

HOMER simulates hybrid systems over one year, with energy balance calculations performed every hour, performing discounted cash flow analysis for the lifetime of the project. The dimensions of the system components are determined so that the total net present cost over the life of the project, installation costs and maintenance and operating costs, in addition to replacement costs, reach a minimum value. HOMER also performs sensitivity studies.

HOMER Legacy includes models for hydroelectric plants, photovoltaic modules and wind turbines, as well as generators based on renewable fuels and fossil fuels. HOMER also allows you to simulate different consuming loads, including consumers of electricity and thermal energy, among others. The software also allows the simulation of rechargeable batteries, among other devices for storage and energy, as well as inverters and rectifiers, allowing the inclusion of DC and AC buses.

A recently published data article [28] presents the collection of results obtained after seven years of work involving the application of HOMER Legacy for simulating hybrid systems in different circumstances. This paper presents some details about how HOMER Legacy works, presents some instructions for obtaining the software

and describes the basic means so that its operation can be quickly learned.

4.2. Simulating compressed air energy storage systems

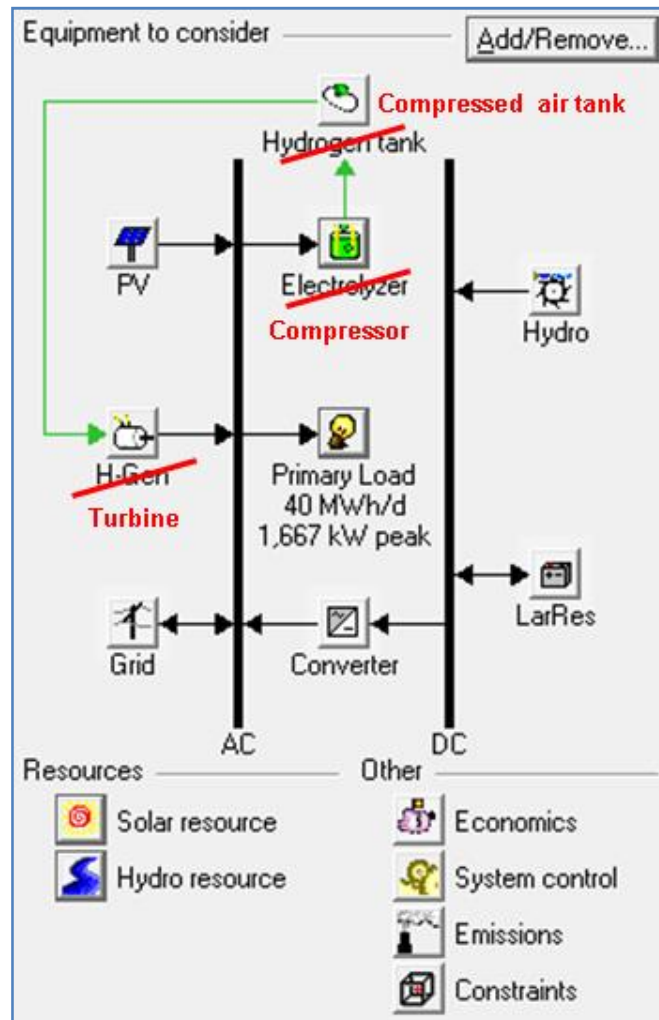
HOMER Legacy does not offer a ready-made model for simulating compressed air energy storage systems. However, it is possible to adapt existing models to simulate new components. For example, Canales *et al.* [18] showed how to simulate hydroelectric power plants with energy storage in the water reservoir formed by the dam. Canales and Beluco [29] also showed how to simulate reversible hydroelectric power plants.

Among the models available in HOMER Legacy, it would be possible to simulate a compressed air storage system by adapting a rechargeable battery model or by adapting the hydrogen storage model. The intention in this work is the simulation of a hybrid storage system, in which the compressed air storage system will operate in parallel with storage in a water reservoir. Thus, it will remain to adapt the hydrogen storage model.

Figure 7.8 presents a schematic diagram of the system simulated in this work, with a hydroelectric plant and photovoltaic modules forming a hybrid energy system, supplying energy to the interconnected system. The consumer load simulates the energy dispatch established by the energy system operator. The hydroelectric plant and the 'battery' on the DC bus follow instructions from Canales *et al.* [18] to simulate a hydroelectric plant with storage in its reservoir.

The components of the hydrogen storage system appear with their names adapted to the simulations performed in this work. The electrolyzer actually simulates an air compressor, the hydrogen tank actually simulates a compressed air reservoir and the hydrogen generator simulates a turbine to convert stored mechanical energy in the form of compressed air into electrical energy. The new names for the components of the compressed air storage system appear in this figure in red.

Figure 7.8: Schematic diagram of the hydro PV hybrid system with hybrid storage in water reservoir and compressed air studied in this paper.



The electrolyzer, then, is used to simulate the compressor and allows informing useful life time [years], efficiency [%] and minimum load ratio [%], all of which can be considered as variables for sensitivity analysis. The 'electrolyzer' also allows the insertion of capital costs, maintenance and operation costs and replacement costs, as for other components of HOMER Legacy. The sizes of the 'electrolyzer' to be considered in the simulations is the variable for optimization.

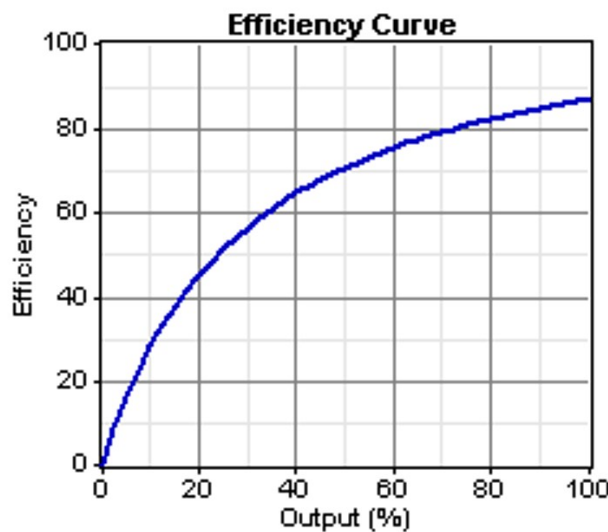
The hydrogen tank, in turn, is used to simulate the reservoir for compressed air and allows to inform life time [years] and the initial level of charge in the tank, as a percentage of the total [%] or as an absolute value [kg], allowing them to be considered as variables in sensitivity analysis, also allowing the requirement that the load at the end of the year is equal to or greater than the initial load. The storage tank also allows insertion of costs, as for electrolyzer, and tank sizes to be considered in

the simulations as the variable for optimization.

The generator is used to simulate the air turbine and allows to inform the lifetime [years] and the minimum load ratio [%], also allowing them to be considered in the sensitivity analysis. The generator also allows the insertion of costs, as in the electrolyzer and in the tank, and the sizes of the generators to be considered in the simulations as the variable for optimization. The generator in this case must operate connected to the AC bus.

The information described in the previous paragraph appears in the 'cost' folder of the generator, and in the 'fuel' folder, information related to efficiency must be inserted. The efficiency curve of the generator should reproduce the efficiency curve of turbines usually used to convert mechanical energy stored in compressed air into electrical energy. Figure 7.9 shows the efficiency curve adopted in the simulations of this work, which was built based on the content of Annex A "*How HOMER Creates the Generator Efficiency Curve*", and also following the efficiency results (70-80%) for adiabatic CAES obtained by Elmegaard and Brix [30].

Figure 7.9: Efficiency as a function of the percentage of power supplied by the generator, simulating a compressed air turbine.



4.3. Simulations with HOMER Legacy

HOMER Legacy was then applied to simulate the system shown in Figure 7.8, with the hydrogen components properly characterized for simulating a compressed

air system, with the optimization variables shown in Table 7.1 and with the sensitivity values in Table 7.2. As explained below, the costs of the reservoir, linked together, are also linked to other costs of the hydroelectric system.

The simulations were carried out for a project time life of 25 years, with an annual interest rate of 8%. The calculations were made every hour of simulation time, with the conversion equipment operating without requirements for annual or hourly energy reserves in relation to the available energy resources. The simulations pursued optimal solutions without capacity shortage, but without establishing minimum values for the renewable fraction.

The simulations considered that the photovoltaic modules had initial costs were US\$ 3200 per kW for the systems with the lowest power and US\$ 2560 per kW for the highest powers, with optimization values presented in Table 7.1. Replacement costs were considered equal to 80% of capital costs, while maintenance and operating costs were 5% of capital costs per year. Costs were the subject of a specific sensitivity study, with the three variables linked together.

The hydroelectric system was simulated considering three values of capital costs, replacement costs and costs of operation and maintenance, as shown in Table 7.2. These three values were equally divided among the three components of the hydroelectric system, as simulated for this study. As mentioned above, the hydroelectric system was designed by Vasco *et al.* [16, 17], simulated according to the instructions of Canales *et al.* [18].

Table 7.1: Optimization variables for the simulations performed with HOMER Legacy.

PV array [kW]	Grid [kW]	Lar Res	
0	0	1.25	17.50
180	200	2.50	20.00
360	400	5.00	25.00
540		7.50	30.00
720		10.00	40.00
900		12.50	50.00
		15.00	60.00

Table 7.2: Sensitivity variables for the simulations performed with HOMER Legacy.

Primary load [kWh/d]	Stream Flow [L/s]	Hydro Capital [\$]	Lares Capital Multiplier	PV Capital Multiplier
38,000.0	9,171.0	250,000.00	1.00	1.00
38,500.0	10,088.1	300,000.00	1.20	0.50
39,000.0	11,005.2	350,000.00	1.40	0.25
39,500.0		<i>linked to</i>	<i>linked to</i>	<i>linked to</i>
40,000.0		Hydro Repl. [\$]	Lares Repl. Multiplier	PV Repl. Multiplier
		200,000.00	1.00	1.00
		240,000.00	1.20	0.50
		280,000.00	1.40	0.25
		<i>linked to</i>	<i>linked to</i>	<i>linked to</i>
		Hydro O&M [\$]	Lar Res O&M Multiplier	PV O&M Multiplier
		12,500.00	1.00	1.00
		15,000.00	1.20	0.50
		17,500.00	1.40	0.25

5. RESULTS AND DISCUSSION

This section presents the results obtained with the simulations carried out with HOMER Legacy. First, the simulations with the hybrid storage system, including the Laranjeiras reservoir and the compressed air system. Then, the simulations with the possibility of the Laranjeiras reservoir not being included and, finally, the simulations only with the compressed air system.

For the first set of results, corresponding to the simulations carried out with the system in Figure 7.8, Figure 7.10 shows the solution space obtained for 10,088 liters per second and for excess energy sold to the interconnected system up to a peak of 400 kW. Figure 7.10 shows that all results include the compressed air energy storage system and Figure 7.11 indicates that the optimal system delivers energy at a cost of \$0.019 per kWh.

Figure 7.11 shows the result considered optimal for this system, with 1497 kW installed in the Laranjeiras dam for hydroelectric power generation, with 360 kW in photovoltaic panels on the surface of the reservoir, with the reservoir used for energy storage and with the system of compressed air with a capacity of 0.15 hours of storage. Figure 7.12 shows the results of Figure 7.11, with the non-mandatory use of the Laranjeiras reservoir as an energy store.

Figure 7.11 shows the results with systems simulated with both storage systems. Figure 7.12 shows results in which the use of the reservoir as an energy store depended on each system and its respective feasibility. The possibility of selling excess energy to the system up to a power of 400 kW enables the inclusion of photovoltaic panels in the optimal systems. When this possibility is discarded, the optimal systems fail to include them.

Figure 7.10: Optimization space for the system of Figure 7.8.

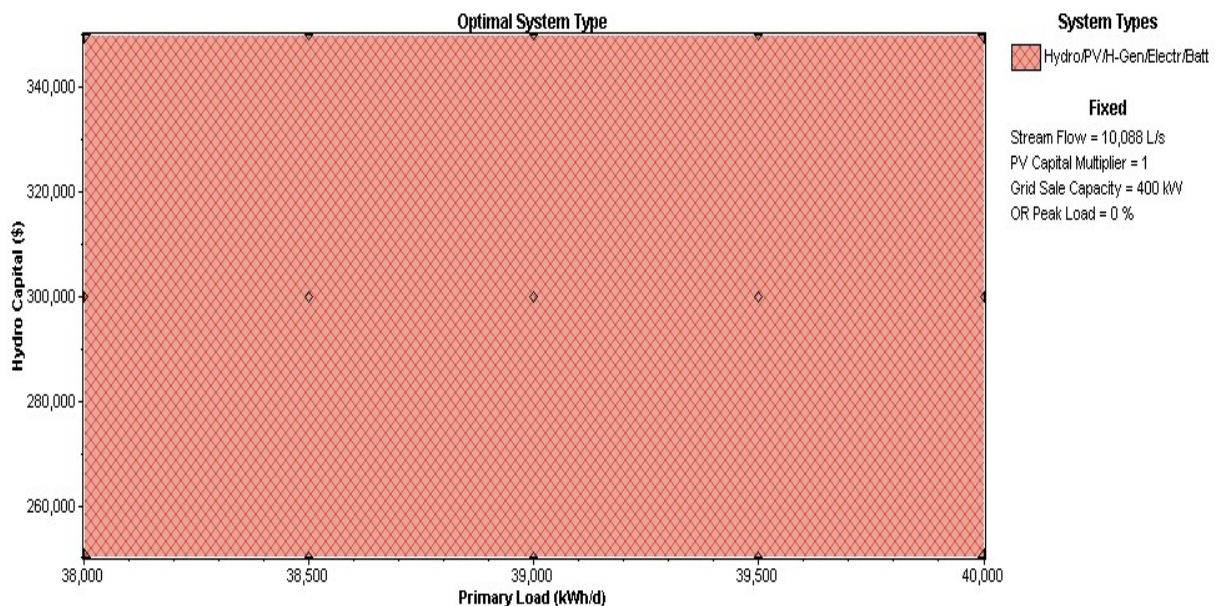


Figure 7.11: Optimization results obtained by HOMER Legacy for the system of Figure 7.8, for grid sale capacity equal to 4400 kW (above) and 0 kW (below).

The screenshot shows the HOMER Legacy software interface with two simulation results displayed side-by-side.

Top Simulation (Grid Sale Capacity 4400 kW):

PV (kW)	Hydro (kW)	H-Gen (kW)	LarRes	Conv. (kW)	Elec. (kW)	H2 Tank (kg)	Grid (kW)	Initial Capital	Operating Cost (\$/yr)	Total NPC	COE (\$/kWh)	Ren. Frac.	H-Gen (hrs)
360	1497	30	1	1800	30	7.50	400	\$ 1,864,580	108,537	\$ 3,023,183	0.019	0.98	35

Bottom Simulation (Grid Sale Capacity 0 kW):

PV (kW)	Hydro (kW)	H-Gen (kW)	LarRes	Conv. (kW)	Elec. (kW)	H2 Tank (kg)	Grid (kW)	Initial Capital	Operating Cost (\$/yr)	Total NPC	COE (\$/kWh)	Ren. Frac.	H-Gen (hrs)
180	1497	30	1	1800	30	25.00	400	\$ 1,059,000	93,354	\$ 2,055,536	0.013	0.98	47
360	1497	30	1	1800	30	5.00	400	\$ 1,461,080	113,324	\$ 2,670,792	0.017	0.99	23

Figure 7.12: Optimization results obtained by HOMER Legacy for the system of Figure 7.8, for grid sale capacity equal to 4400 kW (above) and 0 kW (below), with the non-mandatory use of the Laranjeiras reservoir as an energy store.

The screenshot shows the HOMER Legacy software interface with two simulation results displayed side-by-side.

Top Simulation (Grid Sale Capacity 4400 kW):

PV (kW)	Hydro (kW)	H-Gen (kW)	LarRes	Conv. (kW)	Elec. (kW)	H2 Tank (kg)	Grid (kW)	Initial Capital	Operating Cost (\$/yr)	Total NPC	COE (\$/kWh)	Ren. Frac.	H-Gen (hrs)
360	1497	30	1	1800	30	1.25	400	\$ 1,513,830	92,011	\$ 2,496,032	0.016	0.98	7
360	1497	30	1	1800	30	7.50	400	\$ 1,864,580	108,584	\$ 3,023,688	0.019	0.98	35

Bottom Simulation (Grid Sale Capacity 0 kW):

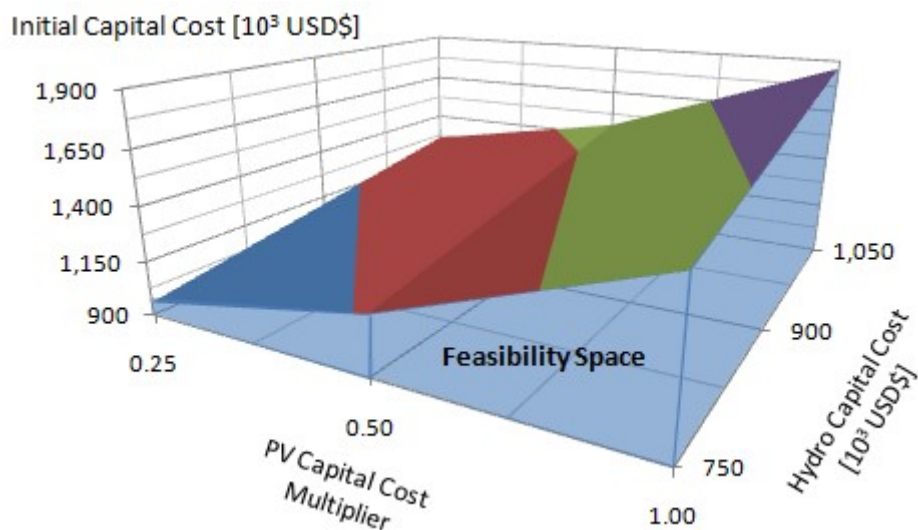
PV (kW)	Hydro (kW)	H-Gen (kW)	LarRes	Conv. (kW)	Elec. (kW)	H2 Tank (kg)	Grid (kW)	Initial Capital	Operating Cost (\$/yr)	Total NPC	COE (\$/kWh)	Ren. Frac.	H-Gen (hrs)
180	1497	30	1	1800	30	25.00	400	\$ 709,000	86,623	\$ 1,633,683	0.010	0.97	109
180	1497	30	1	1800	30	5.00	400	\$ 1,059,000	93,361	\$ 2,055,612	0.013	0.98	47
360	1497	30	1	1800	30	7.50	400	\$ 1,111,380	108,965	\$ 2,274,552	0.015	0.98	223
360	1497	30	1	1800	30	12.50	400	\$ 1,461,080	113,331	\$ 2,670,866	0.017	0.99	23

Based on the concept of feasibility space [31, 32], the feasibility space (

Figure 7.13) for the hybrid system of Figure 7.8, considering the initial capital cost of the system as a function of PV Capital Cost Multiplier and Initial Capital Cost, was possible to be constructed with the results of Table 7.3.

Table 7.3: Results for the construction of the feasibility space of**Figure 7.13.**

		PV Capital Cost Multiplier		
		0.25	0.50	1.00
Hydro Capital Cost [10 ³ USD\$]	Initial Capital Cost [10 ³ USD\$]			
		750	958.820	1,160.740
900	1,108.820	1,310.740	1,714.580	
1,050	1,258.820	1,460.740	1,864.580	

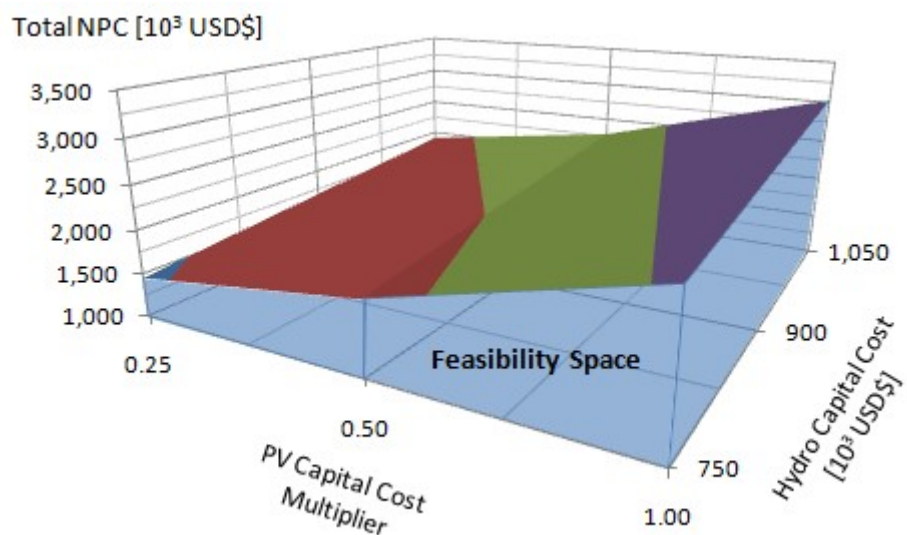
Figure 7.13: Upper limit of feasibility and feasibility space for the system of Figure 7.8, considering the initial capital cost of the hybrid system as a function of PV Capital Cost Multiplier and Hydro Capital Cost.

Other studies involving energetic complementarity [33, 34, 35] must be carefully studied so that the construction of the feasibility space can be improved.

And, finally, the feasibility space (Figure 7.14) for the hybrid system of Figure 7.8, considering the Total NPC of the system as a function of PV Capital Cost Multiplier and Hydro Capital Cost, was possible to be constructed with the results of Table 7.4.

Table 7.4: Results for the construction of the feasibility space of Figure 7.14.

		PV Capital Cost Multiplier		
		0.25	0.50	1.00
Hydro Capital Cost [10 ³ USD\$]		Total NPC [10 ³ USD\$]		
		750	1,448.804	1,820.223
900		900	1,678.865	2,050.284
1,050		1,050	1,908.926	2,280.345

Figure 7.14: Upper limit of feasibility and feasibility space for the system of Figure 7.8, considering the Total NPC of the hybrid system as a function of PV Capital Cost Multiplier and Hydro Capital Cost.

6. CONCLUSIONS

This work presents the main results of a pre-feasibility study of a hydro PV hybrid system for the repowering of the Laranjeiras dam, in southern Brazil, considering the use of the reservoir formed by the dam for energy storage in conjunction with a system of storage in compressed air. The optimal solution achieved with HOMER Legacy includes a 1497 kW hydroelectric power plant installed at the base of the dam, operating in conjunction with 360 kW PV modules, operating on floating structures on the surface of the water reservoir. This system was simulated with the possibility of buying 400 kW and not selling excess energy to the grid, providing 40 MWh per day, with an energy cost of US\$ 0.019 per kWh and a capital cost of US\$ 3,023,688.00.

The comparison of the results of this paper with the results previously presented by Vasco *et al.* [16, 17] which studied the design of this hybrid system without the use of the reservoir for energy storage, indicated some benefits of the hybrid storage. The energy storage also allowed reducing the total net present cost and the cost of energy. Feasibility of the optimal solution with a higher average stream flow rate contributed to these results, both technically and financially. In general, the use of two energy stores with different storage cycles allowed a better use of available energy, with a reduction in system costs.

ACKNOWLEDGEMENTS

This work was developed as part of the research activities on renewable energy supported by the *Instituto de Pesquisas Hidráulicas, Universidade Federal do Rio Grande do Sul*, from southern Brazil. The research work of the second author is supported by CNPq (proc. n. 312941/2017-0).

REFERENCES

- [1] FAHY, F. **Air: the excellent canopy**. Cambridge: Woodhead Publishing, 2010.
- [2] GRIMM, A. M. Notas de aula da Disciplina Meteorologia Básica. Universidade Federal do Paraná, 1999. Disponível em: <<http://fisica.ufpr.br/grimm/aposmeteo/cap1/cap1-2.html>>. Acesso em: 14 abr. 2019.
- [3] BARROS, B. F.; BORELLI, R.; GEDRA, R. L. **Eficiência energética**: técnicas de aproveitamento, gestão de recursos e fundamentos. São Paulo: Érica, 2015.
- [4] SALVADOR, M. A.; LAZZARIN, T. B.; COELHO, R. F. Panorama das estratégias de armazenamento de energia sob forma de ar comprimido. **Eletrônica de Potência**, Campo Grande, v. 21, n. 3, p. 169-178, jul./set. 2016. <http://doi.org/10.18618/REP.2016.3.2589>.
- [5] LETCHER, T. M. Storing electrical energy. In: _____. **Managing Global Warming**. Academic Press, 2019. Ch. 11, p. 365-377. <https://doi.org/10.1016/B978-0-12-814104-5.00011-9>.
- [6] VENKATARAMANI, G.; RAMALINGAM, V. Performance analysis of a small capacity compressed air energy storage system for renewable energy generation using TRNSYS. **Journal of Renewable and Sustainable Energy**, v. 9, n. 4, art. 044106, 17 p., 2017. <http://dx.doi.org/10.1063/1.5000287>.
- [7] BREEZE, P. Compressed air energy storage. In: _____. **Power System Energy Storage Technologies**. Academic Press, 2018. Ch. 3, p. 23-31. <https://doi.org/10.1016/B978-0-12-812902-9.00003-1>.
- [8] DING, Y.; LI, Y.; LIU, C.; SUN, Z. Solar electrical energy storage. In: Sørensen, B. (Ed.). **Solar Energy Storage**. Academic Press, 2015. Ch. 2, p. 7-25. <https://doi.org/10.1016/B978-0-12-409540-3.00002-5>.
- [9] GARVEY, S. D.; PIMM, A. Compressed air energy storage. In: Letcher, T. M. (Ed.). **Storing Energy: with Special Reference to Renewable Energy Sources**. Elsevier, 2016. Ch. 5, p. 87-111. <https://doi.org/10.1016/B978-0-12-803440-8.00005-1>.
- [10] BARTELA, Ł. A hybrid energy storage system using compressed air and hydrogen as the energy carrier. **Energy**, v. 196, art. 117088, 13 p., 2020. <https://doi.org/10.1016/j.energy.2020.117088>.
- [11] HAJIAGHASI, S.; SALEMNIA, A.; HAMZEH, M. Hybrid energy storage system for micro grids applications: a review. **Journal of Energy Storage**, v. 21, p. 543-570, 2019. <https://doi.org/10.1016/j.est.2018.12.017>.
- [12] KOUGIAS, I.; SZABÓ, S.; MONFORTI-FERRARIO, F.; HULD, T.; BÓDIS, K. A

- methodology for optimization of the complementarity between small-hydropower plants and solar PV systems. **Renewable Energy**, v. 87, pt. 2, p. 1023-1030, 2016. <https://doi.org/10.1016/j.renene.2015.09.073>.
- [13] GBADEGESIN, A. O.; SUN, Y.; NWULU, N. I. Techno-economic analysis of storage degradation effect on levelised cost of hybrid energy storage systems. **Sustainable Energy Technologies and Assessments**, v. 36, art. 100536, 8 p., 2019. <https://doi.org/10.1016/j.seta.2019.100536>.
 - [14] JAVED, M. S.; ZHONG, D.; MA, T.; SONG, A.; AHMED, S. Hybrid pumped hydro and battery storage for renewable energy based power supply system. **Applied Energy**, v. 257, art. 114026, 16 p., 2020. <https://doi.org/10.1016/j.apenergy.2019.114026>.
 - [15] CEEE (Companhia Estadual de Energia Elétrica). State Electric Energy Company. Re-evaluation of the design of Laranjeiras hydropower plant. ELC [in Portuguese]: Electroconsult, São Paulo. 1970.
 - [16] VASCO, G.; SILVA, J. S.; BELUCO, A.; ROSSINI, E. G.; SOUZA, J. A hydro PV hybrid system as a new concept for an abandoned dam in Southern Brazil. **Computational Water, Energy and Environmental Engineering**, v. 8, n. 2, p. 41-56, 2019a. <https://doi.org/10.4236/cweee.2019.82003>.
 - [17] VASCO, G.; SILVA, J. S.; CANALES, F. A.; BELUCO, A.; SOUZA, J.; ROSSINI, E. G. A hydro PV hybrid system for the Laranjeiras dam (in Southern Brazil) operating with storage capacity in the water reservoir. **Smart Grid and Renewable Energy**, v. 10, n. 4, p. 83-97, 2019b. <https://doi.org/10.4236/sgre.2019.104006>.
 - [18] CANALES, F. A.; BELUCO, A.; MENDES, C. A. B. Modelling a hydropower plant with reservoir with the micropower optimization model (HOMER). **International Journal of Sustainable Energy**, v. 36, n.7, p. 654-667, 2017. <https://doi.org/10.1080/14786451.2015.1080706>.
 - [19] HOMER Legacy Software, version 2.68 Beta. The micropower optimization model. HOMER Energy, 2009. Available at: <<https://www.homerenergy.com/>>.
 - [20] CONNOLLY, D.; LUND, H.; MATHIESEN, B. V.; LEAHY, M. A review of computer tools for analysing the integration of renewable energy into various energy systems. **Applied Energy**, v. 87, n. 4, p. 1059-1082, 2010. <https://doi.org/10.1016/j.apenergy.2009.09.026>.
 - [21] SINHA, S.; CHANDEL, S. S. Review of software tools for hybrid renewable energy systems. **Renewable and Sustainable Energy Reviews**, v. 32, p. 192-205, 2014. <https://doi.org/10.1016/j.rser.2014.01.035>.
 - [22] LILIENTHAL, P.; LAMBERT, T.; GILMAN, P. Computer modeling of renewable power systems. In: CLEVELAND, C. J. (Ed.). **Encyclopedia of Energy**. Elsevier, 2004. Vol. 1, p. 633-647. <https://doi.org/10.1016/B0-12-176480-X/00522-2>.

- [23] LAMBERT, T.; GILMAN, P.; LILIENTHAL, P. Micropower system modeling with HOMER. In: FARRET, F. A.; SIMÕES, M. G. (Eds.). **Integration of Alternative Sources of Energy**. Hoboken, New Jersey: John Wiley & Sons, Inc., 2006. Ch. 15, p. 379-418. <https://doi.org/10.1002/0471755621.ch15>.
- [24] BELUCO, A.; COLVARA, C. P.; TEIXEIRA, L. E.; BELUCO, A. Feasibility study for power generation during peak hours with a hybrid system in a recycled paper mill. **Computational Water, Energy and Environmental Engineering**, v. 2, n. 2, p. 43-53, 2012. <http://doi.org/10.4236/cweee.2013.22005>.
- [25] STIEL, A.; SKYLLAS-KAZACOS, M. Feasibility study of energy storage systems in wind/diesel applications using the HOMER model. **Applied Sciences**, v. 2, n. 4, p. 726-737, 2012. <http://doi.org/10.3390/app2040726>.
- [26] CANALES, F. A.; BELUCO, A.; MENDES, C. A. B. A comparative study of a wind hydro hybrid system with water storage capacity: conventional reservoir or pumped storage plant? **Journal of Energy Storage**, v. 4, p. 96-105, 2015. <https://doi.org/10.1016/j.est.2015.09.007>.
- [27] TEIXEIRA, L. E.; CAUX, J.; BELUCO, A.; BERTOLDO, I.; LOUZADA, J. A. S.; EIFLER, R.C. Feasibility study of hydro PV hybrid system operating at a dam for water supply in southern Brazil. **Journal of Power and Energy Engineering**, v. 3, n. 9, p. 70-83, 2015. <http://doi.org/10.4236/jpee.2015.39006>.
- [28] BELUCO, A.; DURING FILHO, F. A.; SILVA, L. M. R.; SILVA, J. S.; TEIXEIRA, L. E.; VASCO, G.; CANALES, F. A.; ROSSINI, E. G.; SOUZA, J.; DARONCO, G. C.; RISSO, A. Dataset after seven years simulating hybrid energy systems with HOMER Legacy. **Data Science Journal**, v. 19, n. 1, art. 14, p. 1-8, 2020. <http://doi.org/10.5334/dsj-2020-014>.
- [29] CANALES, F. A.; BELUCO, A. Modeling pumped hydro storage with the micropower optimization model (HOMER). **Journal of Renewable and Sustainable Energy**, v. 6, art. 043131, 2014. <http://doi.org/10.1063/1.4893077>.
- [30] ELMEGAARD, B.; BRIX, W. Efficiency of compressed air energy storage. In: The 24th International Conference on Efficiency, Cost, Optimization, Simulation and Environmental Impact of Energy Systems, 13 p., 2011. Available at: <https://backend.orbit.dtu.dk/ws/portalfiles/portal/6324034/prod21323243995265.ecos2011_paper%5B1%5D.pdf>.
- [31] SILVA, J. S.; BELUCO, A. Characterization of a feasibility space for a new technology – a case study of wave energy in Southern Brazil. **Current Alternative Energy**, v. 2, n. 2, p. 112-122, 2018. <http://doi.org/10.2174/1570178615666180830102336>.
- [32] SILVA, J. S.; CANALES, F. A.; BELUCO, A. A ‘feasibility space’ as a goal to be achieved in the development of new technologies for converting renewable energies. **MethodsX**, v. 7, art. 100960, 2020. <https://doi.org/10.1016/j.mex.2020.100960>.

- [33] BELUCO, A.; SOUZA, P. K.; LIVI, F. P.; CAUX, J. Energetic complementarity [of solar energy] with hydropower and the possibility of storage in batteries and water reservoirs. In: Sørensen, B. (Ed.). **Solar Energy Storage**. Academic Press, 2015. Ch. 7, p. 155-188. <https://doi.org/10.1016/B978-0-12-409540-3.00007-4>.
- [34] JURASZ, J.; BELUCO, A.; CANALES, F. A. The impact of complementarity on power supply reliability of small scale hybrid energy systems. **Energy**, v. 161, p. 737-743, 2018. <https://doi.org/10.1016/j.energy.2018.07.182>.
- [35] JURASZ, J.; CANALES, F. A.; KIES, A.; GUEZGOUZ, M.; BELUCO, A. A review on the complementarity of renewable energy sources: concept, metrics, application and future research directions. **Solar Energy**, v. 195, p. 703-724, 2020. <https://doi.org/10.1016/j.solener.2019.11.087>.

8. Conclusão geral

Esta Tese desenvolveu o conceito de espaço de viabilidade como uma ferramenta para o desenvolvimento de tecnologias de energias renováveis. Primeiramente, foi apresentado um novo estudo de caso para o litoral Norte do RS, com a simulação de um sistema híbrido no qual o foco foi a construção do espaço de viabilidade para uma tecnologia de geração de energia de ondas do mar. Após, foi apresentado um método para simulação de sistemas híbridos de energias renováveis e foi apresentado o conceito de espaço de viabilidade. Por último, realizou-se um estudo de um sistema híbrido de geração interligado a um sistema híbrido de armazenamento de energia composto por reservatório de água e dispositivo de ar comprimido, apresentando o espaço de viabilidade para todo o sistema.

Para a energia de ondas, foram realizadas simulações para custo de energia da rede de distribuição com os seguintes valores: USD\$ 0,05; USD\$ 0,10 e USD\$ 0,15. Para o custo de energia a USD\$ 0,10, os resultados apontaram que a usina de ondas seria viável com custos entre USD\$ 1.109,84/kW e USD\$ 2.079,48/kW, respectivamente para eficiências entre 20% e 40%.

Para o armazenamento com ar comprimido, a solução ótima encontrada com o HOMER inclui um sistema híbrido composto por uma usina hidrelétrica de 1.497 kW instalada ao pé da barragem de Laranjeiras, operando em conjunto com módulos fotovoltaicos de 360 kW, instalados em estruturas flutuantes sobre a superfície do reservatório. Este sistema foi simulado com a possibilidade de compra de até 400 kW de energia da rede e sem a possibilidade de venda de energia excedente, com a finalidade de atender uma carga de 40 MWh/dia, com custo de energia de USD\$ 0,019/kW e um custo de capital de USD\$ 3.3023.688,00. Em comparação com estudos anteriores, o armazenamento de energia proposto indicou alguns benefícios, como a redução do custo total presente líquido de todo o sistema de energia e do custo da energia gerada pelo sistema.

Durante o desenvolvimento de tecnologias de energias renováveis, os limites que devem ser satisfeitos para se atingir viabilidade são ferramentas importantes para gestores de tecnologias. O espaço de viabilidade é um conjunto de valores-

chave de parâmetros de viabilidade que devem ser satisfeitos por dispositivos em desenvolvimento. Os parâmetros variam ao longo do tempo, dependem da matriz energética e da demanda de energia na qual o recurso em desenvolvimento deve estar inserido.

As principais variáveis a serem consideradas em um espaço de viabilidade são os custos iniciais de instalação da tecnologia, o custo da energia gerada pelo dispositivo, a eficiência total do processo de conversão de energia e o preço para a venda de energia pelo sistema ao qual a usina está conectada;

A definição de um espaço de viabilidade é importante para o estabelecimento de novas políticas de incentivo à transição para soluções sustentáveis. O espaço de viabilidade pode estimular a competição entre tecnologias em desenvolvimento, possivelmente levando a melhores resultados tecnológicos, como dispositivos mais eficientes.

9. Recomendações

Para estudos futuros, recomendamos:

- criação de um *software* que simule armazenamento de energia com ar comprimido;
- definição de um modelo com mais opções de componentes/tecnologias de geração e armazenamento de Hidrogênio;
- desenvolvimento de um programa de energias renováveis de código aberto, para que trocas de conhecimentos possam acontecer entre pesquisadores do mundo, visando ao desenvolvimento de um programa mais completo, iterativo e eficiente;
- concepção de um programa que seja claro quanto aos limites/tamanhos máximos que podem ser projetados com cada componente do sistema de energia;
- proposição de um modelo que apresente a opção para o espaço de viabilidade para tecnologias de energias renováveis;
- apresentação de novas variáveis para construção de diferentes espaços de viabilidade 3D, como o caso da localização espacial, ou seja, da localização geográfica.

ANEXO A – HOMER

Conteúdos obtidos no menu de ajuda do programa.

How HOMER Calculates the Hydro Power Output



In each time step, HOMER calculates the electrical power output of the hydro turbine using the following equation:

$$P_{hyd} = \frac{\eta_{hyd} \cdot \rho_{water} \cdot g \cdot h_{net} \cdot \dot{Q}_{turbine}}{1000 W/kW}$$

where:

P_{hyd} = power output of the hydro turbine [kW]

η_{hyd} = **hydro turbine efficiency** [%]

ρ_{water} = density of water [1000 kg/m³]

g = acceleration due to gravity [9.81 m/s²]

h_{net} = **effective head** [m]

$\dot{Q}_{turbine}$ = **hydro turbine flow rate** [m³/s]

See also

[Nominal hydro power](#)

Written by: Tom Lambert (tom@homerenergy.com)

Last modified: December 27, 2007

How HOMER Calculates the PV Array Power Output



HOMER uses the following equation to calculate the output of the PV array:

$$P_{PV} = Y_{PV} f_{PV} \left(\frac{\bar{G}_T}{\bar{G}_{T,STC}} \right) [1 + \alpha_p (T_c - T_{c,STC})]$$

where:

Y_{PV} is the rated capacity of the PV array, meaning its power output under **standard test conditions** [kW]

f_{PV} is the **PV derating factor** [%]

\bar{G}_T is the **solar radiation incident on the PV array** in the current time step [kW/m²]

$\bar{G}_{T,STC}$ is the incident radiation at **standard test conditions** [1 kW/m²]

α_p is the **temperature coefficient of power** [%/°C]

T_c is the **PV cell temperature** in the current time step [°C]

$T_{c,STC}$ is the PV cell temperature under **standard test conditions** [25 °C]

If on the PV Inputs window you choose not to model the effect of temperature on the PV array, HOMER assumes that the temperature coefficient of power is zero, so that the above equation simplifies to:

$$P_{PV} = Y_{PV} f_{PV} \left(\frac{\bar{G}_T}{\bar{G}_{T,STC}} \right)$$

See also

[PV Inputs window](#)

[PV derating factor](#)

[PV temperature coefficient of power](#)

[Calculating the radiation incident on the PV array](#)

[Calculating the PV cell temperature](#)

[Standard test conditions](#)

[Can HOMER model a maximum power point tracker?](#)

Written by: Tom Lambert (tom@homerenergy.com)

Last modified: November 15, 2007

How HOMER Calculates Wind Turbine Power Output



To calculate the output of the wind turbine in a particular hour, HOMER follows a three-step process:

1. It takes that hour's wind speed from the wind resource data and adjusts it to the hub height using either the logarithmic profile or the power law profile, as described in [Wind Shear Inputs](#).
2. It refers to the wind turbine's power curve to calculate the power output under standard conditions of temperature and pressure.
3. It multiplies that value by the air density ratio. It calculates the air density ratio using the method described in the article on [altitude](#).

Written by: Tom Lambert (tom@homerenergy.com)

Last modified: October 26, 2004

Wind Shear Inputs



Use this window to describe the way the wind speed increases with height above ground. HOMER uses this information to calculate the wind speed at the hub height of the wind turbine.

Ground-level obstacles such as vegetation, buildings, and topographic features tend to slow the wind near the surface. Since the effect of these obstacles decreases with height above ground, wind speeds tend to increase with height above ground. This variation of wind speed with height is called *wind shear*. Wind energy engineers typically model wind shear using one of two mathematical models, the logarithmic profile or the power law profile.

Logarithmic profile

The logarithmic profile (or log law) assumes that the wind speed is proportional to the logarithm of the height above ground. The following equation therefore gives the ratio of the wind speed at hub height to the wind speed at anemometer height:

$$\frac{v(z_{hub})}{v(z_{anem})} = \frac{\ln(z_{hub}/z_0)}{\ln(z_{anem}/z_0)}$$

where:

- z_{hub} = the hub height of the wind turbine [m]
- z_{anem} = the **anemometer height** [m]
- z_0 = the surface roughness length [m]
- $v(z_{hub})$ = wind speed at the hub height of the wind turbine [m/s]
- $v(z_{anem})$ = wind speed at anemometer height [m/s]
- $\ln(..)$ = the natural logarithm

The surface roughness length is a parameter that characterizes the roughness of the surrounding terrain. The table below contains representative surface roughness lengths taken from [Manwell, McGowan, and Rogers](#):

Terrain Description	z_0
Very smooth, ice or mud	0.00001 m
Calm open sea	0.0002 m
Blown sea	0.0005 m
Snow surface	0.003 m
Lawn grass	0.008 m
Rough pasture	0.010 m
Fallow field	0.03 m
Crops	0.05 m
Few trees	0.10 m
Many trees, few buildings	0.25 m
Forest and woodlands	0.5 m
Suburbs	1.5 m
City center, tall buildings	3.0 m

Power law profile

The power law profile assumes that the ratio of wind speeds at different heights is given by the following equation:

$$\frac{v(z_{hub})}{v(z_{anem})} = \left(\frac{z_{hub}}{z_{anem}} \right)^\alpha$$

where:

- z_{hub} = the hub height of the wind turbine [m]
- z_{anem} = the **anemometer height** [m]
- α = the power law exponent
- $v(z_{hub})$ = wind speed at the hub height of the wind turbine [m/s]
- $v(z_{anem})$ = wind speed at anemometer height [m/s]

The power law exponent is a dimensionless parameter. Foundational research in fluid mechanics showed that its value is equal to 1/7 for turbulent flow over a flat plate. Wind speed researchers, however, have found that in practice the power law exponent depends on temperature, season, terrain roughness, and several other factors.

See also:

- Wind resource inputs**
- Anemometer height**
- Wind turbine hub height**

Written by: Tom Lambert (tom@homerenergy.com)
Last modified: August 11, 2004

Hydrogen Outputs



The Hydrogen tab of the Simulation Results window contains the following output variables:

Variable	Description
Electrolyzer production	The total amount of hydrogen produced by the electrolyzer, in kg/yr
Reformer production	The total amount of hydrogen produced by the reformer, in kg/yr
Total hydrogen production	The total amount of hydrogen produced by the system, in kg/yr
Unmet hydrogen load	The total hydrogen demand that the system was unable to supply, in kg/yr
Electrolyzer capacity factor	The average hourly production of the electrolyzer divided by its rated hourly production capacity
Reformer capacity factor	The average hourly production of the reformer divided by its rated hourly production capacity

Written by: Tom Lambert (tom@homerenergy.com)

Last modified: October 27, 2004

Hydrogen Tank Outputs



The Hydrogen Tank tab of the Simulation Results window contains the following output variables:

Variable	Description
Hydrogen production	The total amount of hydrogen produced annually by the system
Hydrogen consumption	The total amount of hydrogen consumed annually by the system
Hydrogen tank autonomy	The energy capacity of the hydrogen tank divided by the average electrical load

This page also contains three graphs showing the amount of hydrogen in the tank over the year.

Written by: Tom Lambert (tom@homerenergy.com)

Last modified: June 21, 2004

Hydrogen Tank Autonomy



Type: Output Variable

Units: hr

Symbol: A_{htank}

The hydrogen tank autonomy is the ratio of the energy capacity of the hydrogen tank to the electric load. HOMER calculates the hydrogen tank autonomy using the following equation:

$$A_{htank} = \frac{Y_{htank} \text{LHV}_{H_2} (24 \text{ h/d})}{L_{prim,ave} (3.6 \text{ MJ/kWh})}$$

where:

Y_{htank} = capacity of the hydrogen tank [kg]

LHV_{H_2} = energy content (lower heating value) of hydrogen [120 MJ/kg]

$L_{prim,ave}$ = average primary load [kWh/d]

Written by: Tom Lambert (tom@homerenergy.com)

Last modified: June 21, 2004

Electrolyzer Efficiency



Type: Input Variable

Units: %

Symbol: $\eta_{electrolyzer}$

The efficiency with which the electrolyzer converts electricity into hydrogen. This is equal to the energy content (based on higher heating value) of the hydrogen produced divided by the amount of electricity consumed.

Example: The higher heating value of hydrogen is 142 MJ/kg, which is equal to 39.4 kWh/kg. So an electrolyzer that consumes 50 kWh of electricity to produce one kilogram of hydrogen has an efficiency of 39.4 kWh/kg divided by 50 kWh/kg, which is 79%.

Written by: Tom Lambert (tom@homerenergy.com)

Last modified: May 6, 2004



Generator Fuel Curve Intercept Coefficient

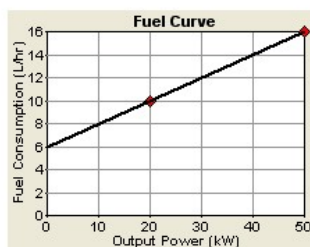
Type: Input Variable

Units: fuel units/hr/kW_{rated}

Symbol: F_0

The fuel curve intercept coefficient is the no-load fuel consumption of the generator divided by its rated capacity. If you were to plot a straight line of fuel consumption versus the power output of the generator, the y-intercept of that line divided by the generator size is equal to the fuel curve intercept coefficient.

For example, if a 50 kW generator consumes 10 L/hr at 20 kW output and 16 L/hr at rated output, the slope of the fuel curve would be $(16-10)/(50-20) = 0.2 \text{ L/hr/kW}$. So the y-intercept would be $10 - (0.2 * 20) = 6 \text{ L/hr}$. Dividing by 50 kW (the size of the generator) gives the fuel curve intercept coefficient of 0.12 L/hr/kW. This fuel curve is plotted below:



The **Fuel Curve Calculator** window helps calculate the fuel curve slope and intercept coefficient.

If the generator is running in a particular hour, HOMER calculates the fuel consumption for that hour using the following equation:

$$F = F_0 \cdot Y_{gen} + F_1 \cdot P_{gen}$$

where:

F = fuel consumption this hour [L]

F_0 = generator fuel curve intercept coefficient [L/hr/kW_{rated}]

F_1 = **generator fuel curve slope** [L/hr/kW]

Y_{gen} = rated capacity of the generator [kW]

P_{gen} = output of the generator in this hour [kW]

If the generator is not running in a particular hour, then the fuel consumption for that hour is zero.

See also

Fuel curve slope

Written by: Tom Lambert (tom@homerenergy.com)

Last modified: October 29, 2004



Generator Fuel Curve Slope

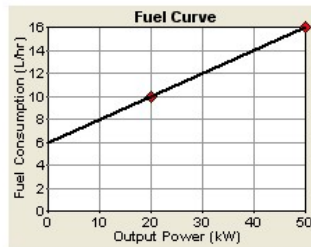
Type: Input Variable

Units: fuel units/hr/kW

Symbol: F_I

The fuel curve slope is the marginal fuel consumption of the generator, in units of fuel per hour per kW of output. If you were to plot a straight line of fuel consumption versus the power output of the generator, the slope of that line is the fuel curve slope.

For example, if a 50 kW generator consumes 10 L/hr at 20 kW output and 16 L/hr at rated output, its fuel curve slope $(16-10)/(50-20) = 0.2 \text{ L/hr/kW}$. This fuel curve is plotted below:



The **Fuel Curve Calculator** window helps calculate the fuel curve slope and intercept coefficient.

If the generator is running in a particular hour, HOMER calculates the fuel consumption for that hour using the following equation:

$$F = F_0 \cdot Y_{gen} + F_I \cdot P_{gen}$$

where:

F = fuel consumption this hour [L]

F_0 = **generator fuel curve intercept coefficient** [L/hr/kW_{rated}]

F_I = generator fuel curve slope [L/hr/kW]

Y_{gen} = rated capacity of the generator [kW]

P_{gen} = output of the generator in this hour [kW]

If the generator is not running in a particular hour, then the fuel consumption for that hour is zero.

See also

[Fuel curve intercept coefficient](#)

Written by: Tom Lambert (tom@homerenergy.com)
Last modified: October 29, 2004

How HOMER Creates the Generator Efficiency Curve



On the Generator Inputs window, when you enter the fuel curve inputs HOMER draws the corresponding efficiency curve. This article explains how HOMER creates that graph from the fuel curve inputs.

Fuel units

You may have noticed that the units of the fuel curve inputs sometimes change when you select a different fuel from the drop-down box. That's because in HOMER, fuels can be denominated in units of kg, L, or m³. When you create a new fuel, you choose which units you want to use for that fuel. For example, you may choose to denominate liquid fuels (e.g. diesel, gasoline, ethanol) in L, and gaseous fuels (e.g. natural gas, hydrogen) in m³. Once you have created a fuel, all the inputs that relate to that fuel will use the specified units. For example, if diesel fuel is denominated in L, then the price of diesel fuel will be in \$/L and the fuel curve inputs for a diesel generator will be in L/hr/kW. Similarly, if natural gas is denominated in m³ then its price will be in \$/m³ and the fuel curve inputs for a natural gas engine will be in m³/hr/kW. This article uses the term "units" to mean the units specified for the particular fuel, whether kg, L, or m³. For example, "units/hr" means L/hr for a fuel denominated in L, and kg/hr for a fuel denominated in kg.

Fuel curve

The fuel curve describes the amount of fuel the generator consumes to produce electricity. HOMER assumes that the fuel curve is a straight line. The following equation gives the generator's fuel consumption in units/hr as a function of its electrical output:

$$F = F_0 \cdot Y_{gen} + F_1 \cdot P_{gen}$$

where F_0 is the fuel curve intercept coefficient in units/hr/kW, F_1 is the fuel curve slope in units/hr/kW, Y_{gen} is the rated capacity of the generator in kW, and P_{gen} is the electrical output of the generator in kW.

Efficiency curve

In HOMER, we define the generator's electrical efficiency as the electrical energy coming out divided by the chemical energy of the fuel going in. The following equation gives this relationship:

$$\eta_{gen} = \frac{3.6 \cdot P_{gen}}{\dot{m}_{fuel} \cdot LHV_{fuel}}$$

where P_{gen} is the electrical output in kW, \dot{m}_{fuel} is the mass flow rate of the fuel in kg/hr and LHV_{fuel} is the lower heating value (a measure of energy content) of the fuel in MJ/kg. The factor of 3.6 arises because 1 kWh = 3.6 MJ.

The mass flow rate of the fuel is related to F , the generator's fuel consumption, but the exact relationship depends on the units of the fuel. If the fuel units are kg, then \dot{m}_{fuel} and F are equal, so the equation for \dot{m}_{fuel} is as follows:

$$\dot{m}_{fuel} = F = F_0 \cdot Y_{gen} + F_1 \cdot P_{gen}$$

If the fuel units are L, the relationship between \dot{m}_{fuel} and F involves the density. The equation for \dot{m}_{fuel} is as follows:

$$\dot{m}_{fuel} = \rho_{fuel} \left(\frac{F}{1000} \right) = \frac{\rho_{fuel} (F_0 \cdot Y_{gen} + F_1 \cdot P_{gen})}{1000}$$

where ρ_{fuel} is the fuel density in kg/m³. If the fuel units are m³ the factor of 1000 is unnecessary, and the equation for \dot{m}_{fuel} is as follows:

$$\dot{m}_{fuel} = \rho_{fuel} F = \rho_{fuel} (F_0 \cdot Y_{gen} + F_1 \cdot P_{gen})$$

Let us further develop the efficiency equation for the case where the fuel units are L. In this case, the efficiency equation becomes:

$$\eta_{gen} = \frac{3600 \cdot P_{gen}}{\rho_{fuel} (F_0 + F_1 \cdot p_{gen}) \cdot LHV_{fuel}}$$

If we divide numerator and denominator by Y_{gen} , the capacity of the generator, and define a new symbol p_{gen} for the relative output of the generator ($p_{gen} = P_{gen}/Y_{gen}$) then the efficiency equation becomes:

$$\eta_{gen} = \frac{3600 \cdot p_{gen}}{\rho_{fuel} (F_0 + F_1 \cdot p_{gen}) \cdot LHV_{fuel}}$$

That equation gives the efficiency of the generator as a function of its relative output. It is this relation that HOMER plots in the efficiency curve on the Generator Inputs window when the fuel units are L.

If the fuel units are m³, the efficiency equation becomes:

$$\eta_{gen} = \frac{3.6 \cdot p_{gen}}{\rho_{fuel} (F_0 + F_1 \cdot p_{gen}) \cdot LHV_{fuel}}$$

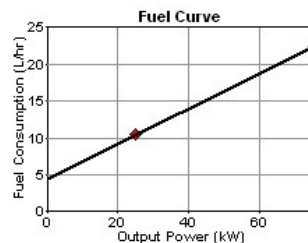
Finally, if the fuel units are kg, the efficiency equation becomes:

$$\eta_{gen} = \frac{3.6 \cdot p_{gen}}{(F_0 + F_1 \cdot p_{gen}) \cdot LHV_{fuel}}$$

Example

For an example, let's analyze a 75 kW generator that burns diesel. Assume diesel has a density of 820 kg/m³ and a lower heating value of 43.2 MJ/kg. If the generator consumes 22.5 L/hr at full load and 10.5 L/hr at 25 kW, what does its efficiency curve look like?

First we need to calculate the fuel curve slope and intercept coefficient. We assume (as we must in HOMER) that the fuel curve is a straight line passing through the two given points, as shown in the graph below.



Note that if we were given more than two points on this curve, we could calculate the line of best fit, using a linear regression technique for example. But since we are given only two points, we can directly calculate the slope and intercept of the line that passes through those points.

We can find the slope and intercept of that line as follows:

$$\text{slope} = \frac{22.5 \text{ L/hr} - 10.5 \text{ L/hr}}{75 \text{ kW} - 25 \text{ kW}} = 0.24 \text{ L/hr/kW}$$

$$\text{intercept} = 10.5 \text{ L/hr} - (25 \text{ kW})(0.24 \text{ L/hr/kW}) = 4.5 \text{ L/hr}$$

Note that HOMER's first fuel curve input is not the intercept itself, but rather the intercept coefficient, defined as the intercept divided by the rated capacity of the generator. (This is so that HOMER can apply the fuel curve inputs to each generator size that you specify in the Sizes to consider table.) So the two fuel curve inputs are:

$$F_0 = \frac{\text{intercept}}{\text{rated output}} = \frac{4.5 \text{ L/hr}}{75 \text{ kW}} = 0.06 \text{ L/hr/kW}$$

$$F_1 = \text{slope} = 0.24 \text{ L/hr/kW}$$

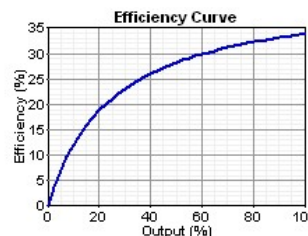
Since this is a liquid fuel denominated in L, the appropriate efficiency equation is:

$$\eta_{gen} = \frac{3600 \cdot p_{gen}}{\rho_{fuel}(F_0 + F_1 \cdot p_{gen}) \cdot \text{LHV}_{fuel}}$$

So we can substitute our values of density, lower heating value, and fuel curve as follows:

$$\eta_{gen} = \frac{3600 \cdot p_{gen}}{820(0.06 + 0.24 \cdot p_{gen}) \cdot 43.2}$$

Therefore the efficiency is 33.9% at full load ($p_{gen} = 1$), 28.2% at 50% load, 18.8% at 20% load, and 7.0% at 5% load. The efficiency curve is shown below:



Written by: Tom Lambert (tom@homerenergy.com)

Last modified: May 6, 2004

Levelized Cost of Energy



Type: Output Variable

Units: \$/kWh

Symbol: COE

HOMER defines the leveled cost of energy (COE) as the average cost per kWh of useful electrical energy produced by the system. To calculate the COE, HOMER divides the annualized cost of producing electricity (the total annualized cost minus the cost of serving the thermal load) by the total useful electric energy production. The equation for the COE is as follows:

$$COE = \frac{C_{ann,tot} - c_{boiler} E_{thermal}}{E_{prim,AC} + E_{prim,DC} + E_{def} + E_{grid,sales}}$$

where:

- $C_{ann,tot}$ = **total annualized cost** of the system [\$/yr]
- c_{boiler} = **boiler marginal cost** [\$/kWh]
- $E_{thermal}$ = total thermal load served [kWh/yr]
- $E_{prim,AC}$ = **AC primary load served** [kWh/yr]
- $E_{prim,DC}$ = **DC primary load served** [kWh/yr]
- E_{def} = **deferrable load served** [kWh/yr]
- $E_{grid,sales}$ = total grid sales [kWh/yr]

The second term in the numerator is the portion of the annualized cost that results from serving the thermal load. In systems that do not serve a thermal load ($E_{thermal}=0$) this term will equal zero.

The COE is a convenient metric with which to compare systems, but HOMER does not rank systems based on COE. For an explanation, please refer to [Why does HOMER rank systems by total NPC?](#)

Written by: Tom Lambert (tom@homerenergy.com)

Last modified: May 16, 2005

Economic Inputs



This window gives access to the following variables:

Variable	Description
Annual real interest rate	The discount rate used to convert between one-time costs and annualized costs.
Project lifetime	The number of years over which the net present cost of the project should be calculated.
System fixed capital cost	The fixed capital cost that occurs regardless of the size or architecture of the system.
System fixed O&M cost	The fixed annual costs that occur regardless of the size or architecture of the system.
Capacity shortage penalty	A penalty applied to the system for any capacity shortage .

To the right of each input is a sensitivity button which allows you to do a **sensitivity analysis** on that variable.

Written by: Tom Lambert (tom@homerenergy.com)

Last modified: May 28, 2004

Simulation Results



Double click a row in the **optimization results** to open the simulation results window for that system. The top of the window displays the components of the system and three outputs: the total net present cost, levelized cost of energy, and operating cost.

This window contains the following tabs:

- The **Cost Summary** tab displays the total cash flow, categorized either by component or by cost type.
- The **Cash Flow** tab shows the year-by-year cash flows and provides access to the **detailed cash flow** table.
- The **Electrical** tab displays details about the production and consumption of electricity by the system.
- The **Thermal** tab shows details about the production and consumption of thermal energy by the system (if the system contains a thermal load).
- The **PV** tab shows details about the operation of the PV array if the system contains one.
- The **Wind Turbine** tab shows details about the operation of the wind turbine if the system contains one.
- The **Hydro** tab shows details about the operation of the hydro turbine if the system contains one.
- The **Generator** tab shows details about the operation of the generator if the system contains one.
- The **Grid** tab shows details about the purchases from and sales to the grid if the system is grid-connected, or about the **breakeven grid extension** if the system is not grid-connected.
- The **Battery** tab shows details about the use and expected lifetime of the battery.
- The **Converter** tab shows details about the operation of the inverter and rectifier, including capacity, electrical input and output, hours of operation, and losses.
- The **Emissions** tab displays the annual pollutants emitted by the system.
- The **Hourly Data** tab allows you to analyze those variables that are stored for each hour of the year.
- For a system with a hydrogen fuel cell, the FC tab displays fuel cell output. When the system includes an electrolyzer and storage tank, the **Hydrogen**, and **H2 Tank** tabs display hydrogen production and storage details respectively.

Written by: Tom Lambert (tom@homerenergy.com)

Last modified: June 5, 2008

Optimization Results



For each **sensitivity case** that it solves, HOMER simulates every system in the **search space** and ranks all the **feasible** systems according to increasing **net present cost**. The **Optimization Results** tab of HOMER's main window displays that list of systems.

You can get to the **Optimization Results** tab by clicking directly on it, or by clicking on a row in the tabular **sensitivity outputs**. Sensitivity variables appear in drop-down boxes at the top of the tab. Choose the sensitivity case by selecting a value from each drop-down box. HOMER updates the list of systems each time you make a selection from one of the drop-down boxes.

The radio buttons at the top of the list of optimization results let you filter the list of feasible systems according to system type. The two choices, **Overall** and **Categorized**, are explained below.

Overall

If you choose to display the overall system rankings, HOMER shows the top-ranked **system configurations** according to net present cost. (You can set the maximum size of this list in the **Preferences** window.) An example is shown below. If you look closely, you'll see that the icons indicate the presence of each type of component under consideration. In this example the icons indicate the presence of, from left to right: PV panels, wind turbines, the diesel generator, batteries, and the converter. To the right are several columns that indicate the sizes and quantities of the components, plus a few summary values drawn from the simulation results of the least-cost system, such as the total capital cost, total net present cost, and levelized cost of energy.

Tip: Double click any system in the list to see detailed **Simulation Results**.

	PV	G3	Dsl	Batt.	Inv.	Total Capital	Total NPC	COE (\$/kWh)	Ren. Frac.	Diesel (L)	Dsl (hrs)	
	1	8	24	3	\$ 25,508	\$ 75,536	0.388	0.25	5,176	2,724		
	1	8	48	3	\$ 28,628	\$ 76,236	0.391	0.24	5,023	2,458		
	1	1	8	24	3	\$ 32,508	\$ 77,865	0.400	0.34	4,580	2,447	
	1	1	8	48	3	\$ 35,628	\$ 78,672	0.404	0.34	4,423	2,198	
	1	8	12	3	\$ 23,948	\$ 79,732	0.409	0.26	5,605	3,485		
	1	8	48	6	\$ 30,815	\$ 80,765	0.415	0.18	5,076	2,101		
	2	8	48	6	\$ 44,015	\$ 81,591	0.419	0.53	2,916	1,214		
	2	1	8	24	3	\$ 39,508	\$ 81,592	0.419	0.42	4,106	2,270	
	1	8	24	6	\$ 27,695	\$ 82,101	0.421	0.22	5,343	2,803		
	1	1	8	12	3	\$ 30,948	\$ 82,536	0.424	0.34	5,041	3,184	
	2	1	8	48	3	\$ 42,628	\$ 82,558	0.424	0.42	3,958	2,042	
	1	1	8	48	6	\$ 37,815	\$ 82,798	0.425	0.29	4,382	1,814	
	2	8	48	6	\$ 44,015	\$ 83,299	0.428	0.68	2,738	1,995		

Categorized

The overall rankings are typically dominated by two or three **system types**. In the above example, the top systems are all either wind/generator/battery or PV/wind/generator/battery systems. For a broader comparison, click the ratio button labeled **Categorized**. The categorized rankings show the least-cost system of each type. In the example shown below, the top-ranked system corresponds to the top-ranked system in the overall rankings shown above. But the second system listed corresponds to the third-place system in the overall rankings, because the second-place system in the overall rankings was of the same type as the first-place system. The fifth and ninth systems in the categorized rankings are interesting for comparison because they represent the least-cost pure diesel and completely renewable-powered systems, respectively. They would both appear so far down the overall rankings that they would be hard to see. But the categorized rankings makes it easy to compare these systems with the other alternatives.

Tip: Double click any system in the list to see detailed **Simulation Results**.

Sensitivity Results Optimization Results											
Sensitivity variables											
Wind Speed (m/s)		6	Diesel Price (\$/L)		0.4						
Double click on a system below for simulation results.											
			PV (kW)	G3 (kW)	Dsl. (kW)	Batt. (kW)	Inv. (kW)	Total Capital	Total NPC	COE (\$/kWh)	Ren. Frac.
				1	8	24	3	\$ 25,508	\$ 75,536	0.388	0.25
				1	1	8	24	\$ 32,508	\$ 77,865	0.400	0.34
				1	8	24	3	\$ 19,308	\$ 84,268	0.433	0.00
					8	24	3	\$ 12,308	\$ 84,728	0.435	0.00
					8			\$ 7,000	\$ 115,832	0.595	0.00
				1	8		3	\$ 22,388	\$ 124,183	0.637	0.00
				1	8		3	\$ 16,188	\$ 126,450	0.649	0.00
				1	1	8	3	\$ 29,388	\$ 128,491	0.660	0.00
				12	1	96	9	\$ 116,243	\$ 142,374	0.731	1.00
				16		128	9	\$ 135,203	\$ 163,612	0.840	1.00

See also

Sensitivity results

Written by: Tom Lambert (tom@homereenergy.com)

Last modified: May 6, 2004

Sensitivity Results



A **sensitivity analysis** can result in a huge amount of output data. Every simulation that HOMER performs results in several dozen summary outputs (like the annual fuel consumption and the total capital cost) plus about a dozen arrays of hourly data (like the hourly output of the wind turbine). HOMER typically performs hundreds or thousands of these simulations per **sensitivity case**, and a sensitivity analysis can easily involve hundreds of sensitivity cases. We designed HOMER's graphic and tabular output capabilities to let you efficiently analyze all that data.

Tabular

The tabular sensitivity results consist of a list showing the least-cost **system** for each sensitivity case. In the example shown below, the first two columns display the values of the two sensitivity variables: the wind speed and the diesel fuel price. The next five columns contain icons indicating the presence in the least-cost system of the five components under consideration. From left to right, they are PV panels, wind turbines, the diesel generator, batteries, and the converter. Following are several columns that indicate the sizes and quantities of the components under consideration, plus a few summary values drawn from the simulation results of the least-cost system, such as the total capital cost, total net present cost, and levelized cost of energy.

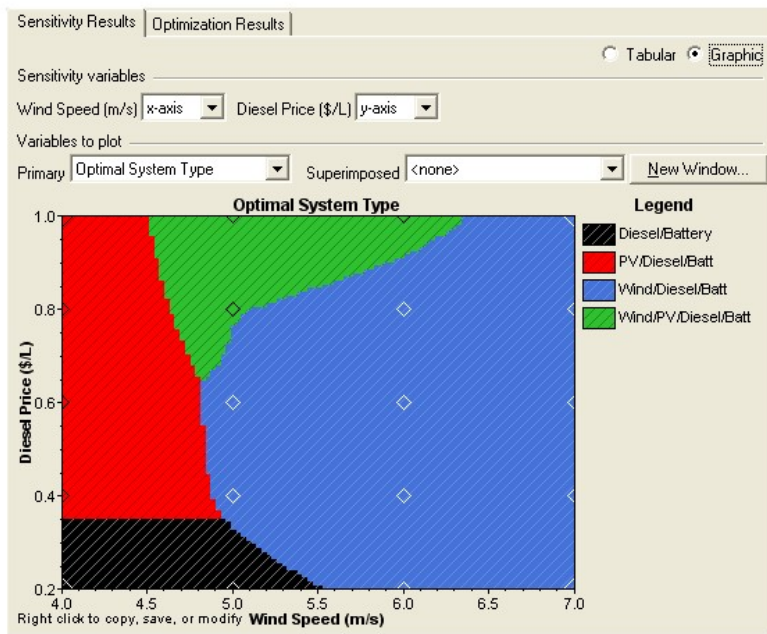
		Sensitivity Results Optimization Results										<input checked="" type="radio"/> Tabular		<input type="radio"/> Graphic	Export		
		Double click on a system below for optimization results.															
Wind (m/s)	Diesel (\$/L)						PV (kW)	G3 (kW)	Dsl (kW)	Batt. (kW)	Inv. (kW)	Disp. Strgy	Total Capital	Total NPC	COE (\$/kWh)		
4.000	0.20						8	24	3	CC	\$ 12,308	\$ 67,117	0.345				
4.000	0.40						1	8	24	3	CC	\$ 19,308	\$ 84,268	0.433			
4.000	0.60						4	8	48	6	CC	\$ 45,615	\$ 106,088	0.545			
4.000	0.80						4	8	48	6	CC	\$ 45,615	\$ 117,135	0.601			
4.000	1.00						8	8	48	6	CC	\$ 73,615	\$ 126,538	0.650			
5.000	0.20							8	24	3	CC	\$ 12,308	\$ 67,117	0.345			
5.000	0.40						1	8	24	3	CC	\$ 25,508	\$ 83,156	0.427			
5.000	0.60							1	8	48	6	CC	\$ 30,815	\$ 104,154	0.535		
5.000	0.80						4	1	8	48	6	CC	\$ 58,815	\$ 113,628	0.583		
5.000	1.00						4	1	8	48	6	CC	\$ 58,815	\$ 120,890	0.621		
6.000	0.20							1	8	24	3	CC	\$ 25,508	\$ 64,486	0.331		
6.000	0.40							1	8	24	3	CC	\$ 25,508	\$ 75,536	0.388		
6.000	0.60							2	8	48	6	CC	\$ 44,015	\$ 89,273	0.458		
6.000	0.80							2	8	48	6	CC	\$ 44,015	\$ 95,629	0.491		
6.000	1.00						2	2	8	48	6	LF	\$ 59,015	\$ 101,056	0.519		
7.000	0.20							1	8	24	3	CC	\$ 25,508	\$ 60,168	0.309		
7.000	0.40							1	8	24	3	CC	\$ 25,508	\$ 69,749	0.358		
7.000	0.60							2	8	48	6	LF	\$ 44,015	\$ 76,929	0.395		
7.000	0.80							2	8	48	6	LF	\$ 44,015	\$ 80,308	0.412		
7.000	1.00							2	8	48	6	LF	\$ 44,015	\$ 83,687	0.430		

You can double click on any row in the table to jump to the **optimization results** for that sensitivity case. That lets you see the sub-optimal systems (the ones that were not least cost) and view the **simulation results** for any of the ranked systems.

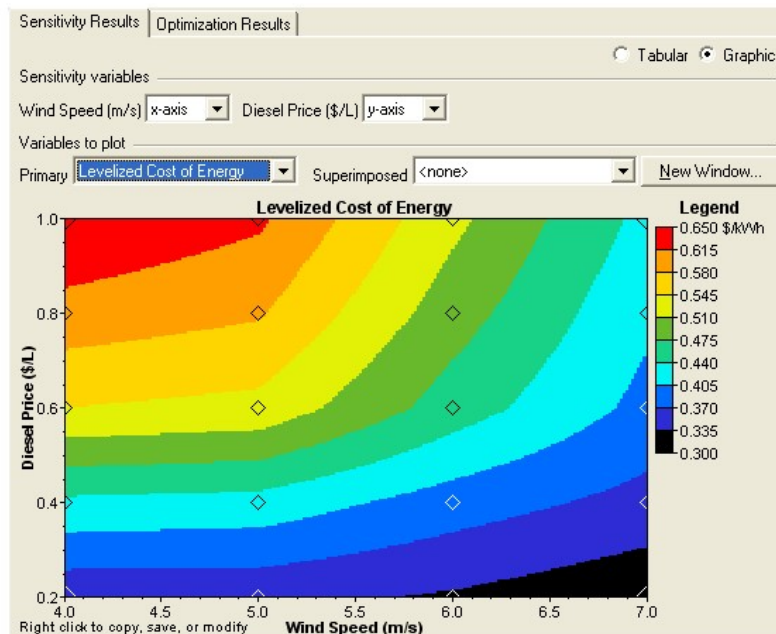
Graphic

When the analysis involves more than one **sensitivity variable**, a graph often conveys the results in a more meaningful way than a table can. You can create three types of graphs: optimal system type charts, surface plots, and line graphs. These graphs are drawn right on the **Sensitivity Results** tab, but you can also create them in their own resizable windows by clicking the button labeled **New Window**. A right-click on any graph allows you to change its properties, copy it to the clipboard, or save it as an image file.

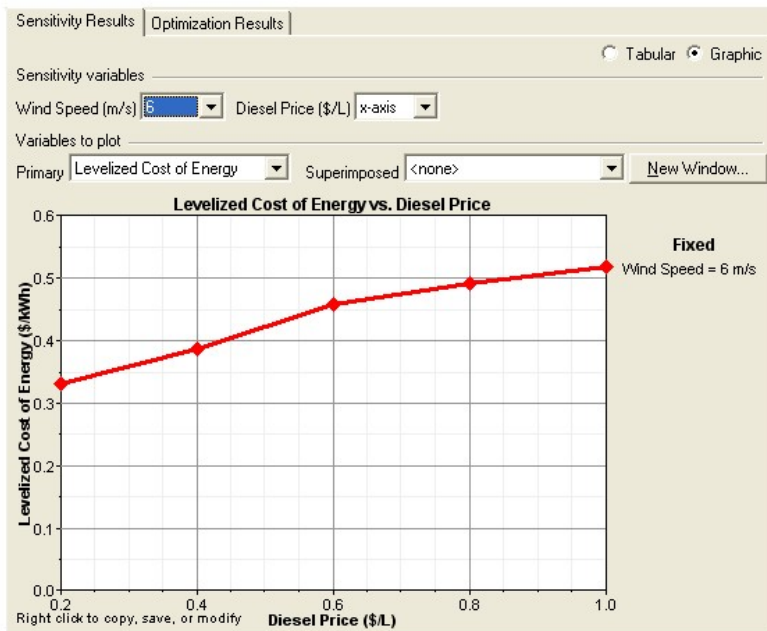
The optimal system type (OST) graph gives the highest-level view of the sensitivity results. It shows the least-cost type of system (diesel-battery is one type of system, wind-diesel-battery is another) versus two sensitivity variables. The example below shows the same information we just saw in the tabular display above. The graphic format makes it easier to see under which conditions the different types of systems are optimal. Diamonds indicate points where HOMER actually solved for the least-cost system. All other points are colored using interpolation.



If you choose to plot any variable other than the optimal system type versus two sensitivity variables, HOMER creates a surface plot. The example shown below plots the leveled cost of energy versus the same axes used in the optimal system type graph shown above. As in the OST graph, diamonds indicate points where HOMER actually solved for the least-cost system. The leveled cost of energy at all other points is inferred by interpolation.



HOMER creates line graphs to plot one output variable versus one single sensitivity variable. The example shown below plots the leveled cost of energy versus the diesel fuel price. This is a subset of the results shown in the above surface plot, with the wind speed fixed at 6 m/s. The diamonds indicate points where HOMER actually solved for the least-cost system.



Written by: Tom Lambert (tom@homereenergy.com)

Last modified: May 6, 2004

ANEXO B – CEEE

Projeto da Barragem de Laranjeiras – volumes acumulados e áreas inundadas.

